*SRESA's International Journal of*

# LIFE CYCLE RELIABILITY AND SAFETY ENGINEERING

**Vol.2** **Issue No.4** **October–December 2013** **ISSN – 2250 0820**

***Special Issue :***
***On***

## Reliability Analysis Using Soft Computing

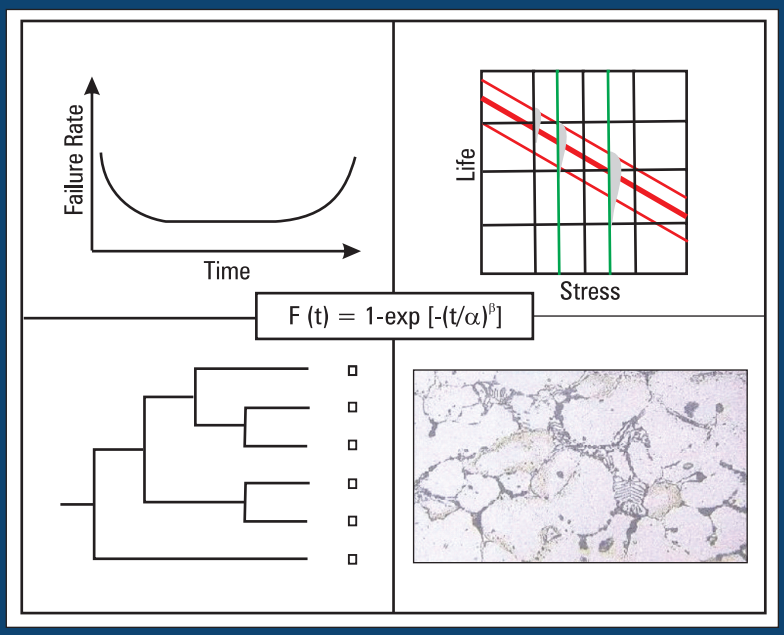


**Guest-Editor**
**Dr. D. Datta**



**Society for Reliability and Safety**
**website: http://www.sresa.org.in**

# SRESA Journal of Life Cycle Reliability and Safety Engineering

Extensive work is being performed world over on assessment of Reliability and Safety for engineering systems in support of decisions. The increasing number of risk-based / risk-informed applications being developed world over is a testimony to the growth of this field. Here, along with probabilistic methods, deterministic methods including Physics-of-Failure based approach is playing an important role. The International Journal of Life Cycle Reliability and Safety Engineering provides a unique medium for researchers and academicians to contribute articles based on their R&D work, applied work and review work, in the area of Reliability, Safety and related fields. Articles based on technology development will also be published as Technical Notes. Review articles on Books published in the subject area of the journal will also form part of the publication.

Society for Reliability and Safety has been actively working for developing means and methods for improving system reliability. Publications of quarterly News Letters and this journal are some of the areas the society is vigorously pursuing for societal benefits. Manuscript in the subject areas can be communicated to the Chief Editors. Manuscript will be reviewed by the experts in the respective area of the work and comments will be communicated to the corresponding author. The reviewed final manuscript will be published and the author will be communicated the publication details. Instruction for preparing the manuscript has been given on inside page of the end cover page of each issue. The rights of publication rest with the Chief-Editors.

## SCOPE OF JOURNAL

| System Reliability analysis | Structural Reliability | Risk-based applications |
|---|---|---|
| Statistical tools and methods | Remaining life prediction | Technical specification optimization |
| Probabilistic Safety Assessment | Reliability based design | Risk-informed approach |
| Quantitative methods | Physics-of-Failure methods | Risk-based ISI |
| Human factor modeling | Probabilistic Fracture Mechanics | Risk-based maintenance |
| Common Cause Failure analysis | Passive system reliability | Risk-monitor |
| Life testing methods | Precursor event analysis | Prognostics & health management |
| Software reliability | Bayesian modeling | Severe accident management |
| Uncertainty modeling | Artificial intelligence in risk and reliability modeling | Risk-based Operator support systems |
| Dynamic reliability models | Design of Experiments | Role of risk-based approach in Regulatory reviews |
| Sensitivity analysis | Fuzzy approach in risk analysis | Advanced electronic systems reliability modeling |
| Decision support systems | Cognitive framework | Risk-informed asset management |

## SRESA AND ITS OBJECTIVES

a) To promote and develop the science of reliability and safety.
b) To encourage research in the area of reliability and safety engineering technology & allied fields.
c) To hold meetings for presentation and discussion of scientific and technical issues related to safety and reliability.
d) To evolve a unified standard code of practice in safety and reliability engineering for assurance of quality based professional engineering services.
e) To publish journals, books, reports and other information, alone or in collaboration with other organizations, and to disseminate information, knowledge and practice of ensuring quality services in the field of Reliability and Safety.
f) To organize reliability and safety engineering courses and / or services for any kind of energy systems like nuclear and thermal power plants, research reactors, other nuclear and radiation facilities, conventional process and chemical industries.
g) To co-operate with government agencies, educational institutions and research oganisations

*SRESA's International Journal of*

# LIFE CYCLE RELIABILITY AND SAFETY ENGINEERING

Vol.2 Issue No.4 October–December 2013 ISSN – 2250 0820

***Special Issue* :**

**On**

## Reliability Analysis Using Soft Computing

**Chief-Editors**

P.V. Varde
A.K. Verma
Michael G. Pecht

**SOCIETY FOR RELIABILITY AND SAFETY**

*Typeset & Printed*

**EBENEZER PRINTING HOUSE**
Unit No. 5 & 11, 2nd Floor, Hind Services Industries,
Veer Savarkar Marg,
Dadar (west), Mumbai -28
Tel.: 2446 2632/ 3872
E-mail: outwork@gmail.com

# Guest Editorial

This is the special issue on reliability analysis using soft computing. Reliability analysis in the probabilistic framework is very common and standard. Monte carlo simulation technique in various configurations such as static, dynamic and Bayesian can be used to estimate the reliability of a model. However, if model contains only imprecise uncertain parameters or if uncertainty of the model parameters is subjective, traditional Monte Carlo method fails. Soft computing based reliability analysis overcomes this situation. In fact, imprecise based model uncertainty rather reliability is evaluated using soft computing methods such as fuzzy set theory, evidence theory etc. Reliability analysis using such soft computing techniques is challenging and some of these challenges are addressed in this issue.

The first paper of this issue is by C. Corey Fischer and Ramana V. Grandhi on 'A Comparison of Model-Form Uncertainty Quantification Techniques for Thermal-Structural Modeling'. This paper addresses the model form uncertainty as the uncertainty that arises as a result of the lack of confidence in knowing which model within a model set used to predict a system response is the best approximating model. Basically, the work in this paper presents a design scenario in which multiple computer models, defining the physical behavior of one single configuration, are used for predicting the same system response, and thus representing the presence of model-form uncertainty. Four different model-form uncertainty quantification (UQ) techniques are presented through an application of prediction of transient temperature response at different locations within a corrugated-core sandwich panel. It is worth to mention that as far as model form uncertainty quantification is concerned, the effectiveness of each technique presented in this work is an innovative concept and each one is weighted against those of the other techniques in conjunction with the applicability of each model-form UQ technique.

The second paper is by Abhirup Bandyopadhyay and Samarjit Kar on 'Long-term assessment of Health Risk under Uncertain Environment of Contaminated Sites using Spatiotemporal Modelling'. The authors have proposed a novel system dynamics model that particularly addresses the presence of multi-compound non aqueous phase liquids in porous media and estimates the current and future risks from water-body, soil and groundwater contamination. Stochastic and partial dynamic modelling technique have been adopted to estimate the spatiotemporal risk in presence of both probabilistic and possibilistic uncertain environment. The *paper* provides a probabilistic as well as a possibilistic framework for long term assessment of human health risk of being infected by contamination

The third paper in this issue is by D. Datta and Debanshee Datta on 'Reliability Evaluation of Weibull and Exponentiated Weibull Distribution Estimates for Wind Speed Data through Uncertainty Analysis'. In this paper, authors have introduced a modified Weibull distribution named as Exponentiated Weibull distribution in fitting wind speed data. It may be mentioned that modified Weibull distribution is a better fit compared to the fitting of traditional or classical Weibull distribution. Authors have proved this with reference to a standard data set by QQ-plot. As far as reliability of both the models is concerned with respect to fitting the wind speed data, a new measure 'Akaike Information Criterion (AKC)' has been applied. Mean and variance of the wind speed data with respect to the best fitted Exponentiated Weibull distribution are estimated and a comparison of the representative estimates is also presented in this study. Shannon entropy of classical Weibull distribution and Exponentiated Weibull distribution has been computed to account the uncertainty associated with the random variable sampled from these two distributions.

The paper by S.V. Shrikhande, P.V. Varde and D. Datta is on 'Review on Prognostics and Health Management of Digital Systems and its Application to Nuclear Plants'. The thrust of this paper is on review of prognostics of electronic component, its related issues and mathematical techniques useful for prognostic algorithms. Review on modelling of accumulated damage based on measured life-cycle loads is presented in this paper. The paper introduces use of fuses and canary devices and presents the current state-of-research in the area of prognostic and health management for electronics and its implementation challenges. This paper mentions various applications where prognostics are successfully deployed. It covers different approaches and methodologies for prognostics and RUL estimation. It describes data reduction and simplification techniques, various techniques for intelligent algorithms including Machine Learning and also sensors for Prognostics and Health Management (PHM) of Complementary Metal Oxide Semiconductor (CMOS) Integrated Circuits (ICs).

'Fuzzy Arithmetic form Credibility Theory', by Rituparna Chutia and Tapan Kumar Chutia deals with the credibility distribution of triangular fuzzy variable. The work is focused on a very simple alternative method of finding the membership function for functions of triangular fuzzy variable by credibility theory. Authors study prove that this concept of credibility theory also facilititate in finding an alternative method of computing basic arithmetic operations of triangular fuzzy variables and generalised membership function for the root of triangular fuzzy variable.

Guest editor, Dr. D. Datta is very thankful to his all colleagues associated with Society for Reliability and Safety. The guest editor is very thankful to the Chief-editors in general and, Dr. Varde and Dr. Gopika Vinod in particular. I am very thankful to all the authors who have responded to my invitation, some of them at a short notice, and the publishers who have done a good job of bringing out this special issue.

**Dr. D. Datta** completed his M.Sc. (Nuclear Physics), M. Phil (High Energy Nuclear Physics) from University of Kolkata and Saha Institute of Nuclear Physics, Kolkata in the year 1983 and 1984. He joined in the orientation course of nuclear engineering in 28$^{th}$ batch of BARC Training School in Physics discipline in the year 1984-85. After his graduation from BARC training school, he joined in the Health Physics Division of BARC at Tarapur. He worked for a period of 17 years over there at various health physics units at Tarapur. During this long period he has developed software for use at different facilities of radiation protection including waste immobilization, fuel reprocessing for radiation shielding and criticality safety for safe handling of fissile material, advanced fuel fabrication, radiation dose database management laser based communication system for radiological data transfer and Tarapur Atomic Power Station for radiological emergency. He has completed his Ph D from Mumbai University in the year 2000. Currently he is a senior scientist, Professor of Homi Bhabha National Institute and heading the "Computational Radiation Physics Section" of Health Physics Division at BARC. His research interests include mathematical & statistical modeling, artificial intelligence, soft computing, sensitivity analysis, uncertainty analysis, Data mining and radiological risk analysis. He has contributed in uncertainty and sensitivity analysis in the field of atmospheric dispersion and groundwater modeling using fuzzy mathematics, interval mathematics and evidence theory as principal collaborator of BRNS sponsored R&D projects. He has published four book chapters, a number of research papers in the peer-reviewed journal and in the international/national conferences. He was deputed to IAEA, Vienna in the year 2004 by the department of atomic energy to validate the software developed by the agency on radiation protection. He is the recipient of "Millennium Plaques of Honour", an eminent scientist award from the Indian Science Congress Association, in the year 2010. He is the guest faculty of following Institutes: IIT- BHU, IIT-Rajasthan, IISC-Bangalore, NIT-Durgapur (W.B), NIT-Rourkela, Kolkata University, Dibrugarh University and Guwahati University. He has guided a number of B.Tech / M.Tech students of various Engineering Institutes including Homi Bhabha National Institute. Presently he is guiding four PhD candidates of Homi Bhabha National Institute. He is a member of the Editorial board of the following journals: International Journal of Energy, Information and Communication, International journal of Fuzzy Computation and Modelling, International Journal of Environmental Modelling and Software. He is currently working in the field of uncertainty modelling using evidence theory, exploratory data analysis using wavelets and data mining.

*Life Cycle Reliability and Safety Engineering*
*Vol.2 Issue 4 (2013) 01-14*

# A Comparison of Model-Form Uncertainty Quantification Techniques for Thermal-Structural Modeling

**C. Corey Fischer[1] and Ramana V. Grandhi[2]**
[1]*Graduate Research Assistant, Department of Mechanical and Materials Engineering, Wright State University, Russ Engineering Center 212, 3640 Colonel Glenn Hwy. Dayton, OH 45435, USA.*
[2]*Distinguished Professor, Department of Mechanical and Materials Engineering, Wright State University, Russ Engineering Center 210, 3640 Colonel Glenn Hwy. Dayton, OH 45435, USA.*
*email: fischer.36@wright.edu*

## Abstract

***Work in the field of uncertainty quantification has, in the past, focused primarily on parametric uncertainties naturally inherent in the design parameters of most engineering problems. However, current work has begun to incorporate model-form uncertainties into the uncertainty quantification process. Model-form uncertainty is the uncertainty that arises as a result of the lack of confidence in knowing which model within a model set used to predict a system response is the best approximating model. Thus, fostering the necessity to develop and utilize techniques for quantifying this uncertainty. This work presents a design scenario in which multiple computer models, defining the physical behavior of one single configuration, are used for predicting the same system response, and thus representing the presence of model-form uncertainty. Four different model-form uncertainty quantification (UQ) techniques are presented and applied to the physical problem, consisting of three mathematical models, each of which are used for predicting the transient temperature response at different locations within a corrugated-core sandwich panel used in thermal protection systems subject to thermal loading and boundary conditions, to demonstrate the challenges inherent in each of the quantification techniques. The effectiveness of each technique is weighted against those of the other techniques in conjunction with the applicability of each model-form UQ technique.***

***Keywords -Uncertainty Quantification; Model-Form Uncertainty; Bayesian Model Averaging; Adjustment Factor Approach; Structural Design***

## 1. Introduction

Any prediction of a system response obtained through the use of modeling processes can assume some type of uncertainty thought of taking on one or more of three forms: parametric, predictive, and model-form uncertainty [1]. The first of these three forms, parametric uncertainty, refers to the natural variability present within the input parameters the model of interest is dependent upon, while the latter two, predictive and model-form uncertainty, refer to the variability present within the modeling process itself. Uncertainty quantification work in the literature has primarily focused on the quantification of parametric uncertainty through the exploration, adaptation, and application of multiple approaches and methodologies. However, the majority of these approaches and methodologies fail to account for the presence of uncertainties that arise as a result of the modeling process itself.

When the solution approach for solving an engineering problem utilizes physics-based simulations, multiple models often arise as possibilities for representing the same physical situation. The presence of multiple models being available to simulate the same given situation can result from the use of different modeling packages utilizing various fidelities or even operating on differing assumptions of governing physics within the same level of fidelity as well as varying applications of boundary conditions and mesh sizes. In very rare situations, the phenomena being modeled has been explored extensively and is well enough understood that a "best" model can emerge from the set of possible models where in this work, the term "best" model refers to the model that most accurately represents the true physical scenario being modeled. However, in most physical scenarios multiple sets of differing physics can couple in different ways, there exists uncertainty in the selection of the "best" model as a result of a lack of knowledge

of the true physics governing the physical scenario. As a result of this uncertainty, a single "best" model will not emerge from the model set, and thus multiple models operating on assumptions of differing physics can produce different results for the prediction of the same physical problem. Therefore, in order to completely quantify the uncertainty present in the modeling process, it is necessary to not only quantify parametric uncertainties, but also the uncertainty inherent in selecting the "best" model– the model-form uncertainty.

In this work, multiple approaches for the quantification of model-form uncertainties are presented, discussed and applied to a nonlinear transient heat transfer problem. This work presents the application bounds of each approach such as requirements on the availability of experimental data and whether or not the approach can account for probabilistic model predictions–predictions including the quantification of parametric and/or predictive uncertainties. These approaches include the traditional adjustment factor approaches, probabilistic adjustment factor approach which is an adaptation of the prior, and the Bayesian model averaging (BMA) approach.

## 2. Uncertainty in Modeling Process

The process involved in modeling a physical scenario requires the construction of a mathematical model which entails discretization of the physical scenario as well as making assumptions on the physics governing the true scenario. It is however, often beyond the capability of the designer to fully understand the true engineering problem at hand and thus capture the full complexity and all aspects of the physical scenario. Therefore, as a result of the assumptions made during development of physics-based models, discrepancy inevitably exists between the physical scenario being modeled and the prediction of the response by the computational model. This discrepancy is referred to as the predictive uncertainty of a particular model [2], and is unique to each individual model within a set of models considered for predicting a system response.

As mentioned previously, in the solution of an engineering problem, it is common practice for multiple models to be constructed for the purpose of representing the same physical scenario. Such examples include models of varying fidelities, such as assumptions on linear, quasi-linear, or non-linearity within a model, or models that account for complex phenomenon or boundary conditions in different manners, using different simplification techniques. As a result, the predictions of each of these models, for the particular output of interest, can be different from one another. Guedes-Soares states that in situations where multiple models yield different responses, that there can exist only one correct model [3]. However, as stated earlier, it is often beyond the capability of the designer to select the "best" model within the design space, or even a subset of the design space, and arises as a result of the inability to completely understand the full complexity of the physics governing the problem. As is the case in many engineering problems, due to the physical complexity and multidisciplinary interactions, a correct model will often not exist, instead one merely seeks to identify the "best" model among the model set. For reasons mentioned above, there exists uncertainty in the selection of this "best model. This uncertainty in the identification of the model most accurately predicting the correct outcome is referred to as model-form uncertainty [4].

The definition of input parameters to each model within a model set, such as dimensions, material properties, environmental conditions, or modeling constants, are often defined as being deterministic. However, in nature, the parameters are rarely deterministic, or seldom able to be accurately represented as deterministic values, within the true physical scenario. As a result of this fact, there exists a third type of uncertainty in the modeling process–parametric uncertainty– which refers to the natural variability present in the values of parameters that a mathematical model is dependent upon [2]. Parametric uncertainties are often classified as either aleatory or epistemic uncertainty, dependent upon the degree of information known in regards to the form of their uncertainty [5]. Aleatory uncertainty refers to the form of uncertainty that arises from the natural unpredictable variation in the performance of a system [6], and can often be represented through distribution functions of a parameters variability. Epistemic uncertainty, on the other hand, is defined as uncertainty due to a lack of knowledge regarding the performance of a system that can, in theory, be reduced through the introduction of additional data or information [7].

All of the aforementioned uncertainties are present in nearly every physics-based modeling problem. A general representation for the modeling of an output of interest, $y$, is given in Eq. (1). As can be seen, this output of interest is a function of three terms: $\tilde{f}_k$, $\bar{x}_i$, and $\hat{\varepsilon}_k$.

$$y = \tilde{f}_k(\bar{x}_i) + \hat{\varepsilon}_k \quad (1)$$

Here, $\tilde{f}_k$ represents the result/prediction obtained using model $k$, to the set of input parameters, $\bar{x}_i$. The second term, $\hat{\varepsilon}_k$, represents the discrepancy between the result/prediction obtained from model $k$, and the true physical value of the output of interest. The selection of the appropriate model, $\tilde{f}_k(\bar{x}_i)$, given this representation of a modeling problem, is representative of the inherent model-form uncertainty whereas, the variation in $\tilde{f}_k(\bar{x}_i)$ due to the uncertainty present in the set of input parameters, $\bar{x}_i$, is representative of parametric uncertainty. Finally, the determination of a discrepancy between response/prediction of model $k$ and the true physical value of the output of interest, $\hat{\varepsilon}_k$, is representative of the predictive uncertainty present in model $k$. The breakdown of these three distinct types of uncertainty is demonstrated in Figure 1.

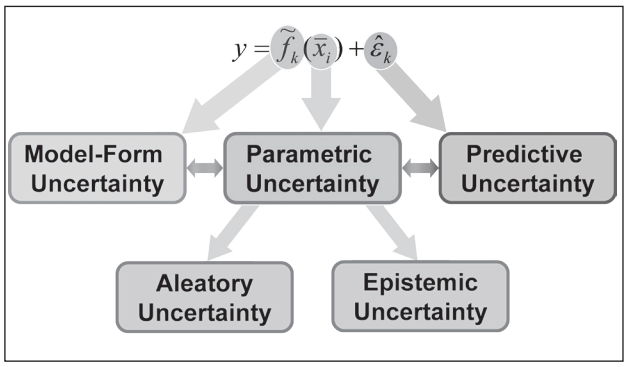


*Figure 1. Modeling Uncertainty Breakdown.*

### 2.1 Bayes' Theorem for Quantifying Model Probability

The first step for quantifying model-form uncertainty is to define model probabilities. Model probability is defined as the degree of belief that a model is the best approximating model from within a model set [8]. Original model probabilities can be assigned on one of two different concepts. Either expert opinion, if available, can be used to assign model probabilities based upon some prior knowledge of each model within the model set, or the more likely basis is to assign these probabilities based upon a uniform distribution of the probabilities assigned to each model within the model set. In the case of the uniformly distributed model probabilities where there exists $K$ models within the model set, each model is assigned a probability of $\Pr(M_k) = 1/K$. Note that the sum of model probabilities, as shown in Eq. (2), for a model set, must be equal to 1.

$$\sum_{k=1}^{K} \Pr(M_k) = 1, \quad k = 1, 2, \ldots, K \quad (2)$$

In the event that experimental data is available, Bayes' theorem can then be used to update these original (prior) probabilities into posterior probabilities. Applying Eq. (3) updates the model probability of model $k$.

$$\Pr(M_k|D) = \frac{\Pr(D|M_k)(M_k)}{\sum_{k=1}^{K} \Pr(D|M_k)\Pr(M_k)} \quad (3)$$

In Eq. (3), $\Pr(D|M_k)$, which is broadly known as $\mathrm{L}(M_k|D)$, is called the likelihood of model $M_k$ given experimental data $D$, or the likeliness that model $M_k$ will predict the known data $D$, because the first argument $D$ is known, while the second argument $M_k$ is not held fixed [9]. The numerical value of the likelihood, $\Pr(D|M_k)$ is not needed in the uncertainty quantification process; however, it is of importance in the evaluation of model probabilities given experimental data. Note that the denominator in Eq. (3) is common to all models, and this model likelihood value is calculated using Eq. (4) as shown by Park *et al* in [8].

$$\Pr(D|M_k) = \left(\frac{1}{2\pi(\hat{\sigma})^2_{mle}}\right)^{N/2} \exp\left(-\frac{N}{2}\right) \quad (4)$$

Model likelihood then becomes a function of the maximum likelihood estimator, $(\hat{\sigma})^2_{mle}$ a measure of the variation within model $k$, as calculated in Eq. (5), where $N$ in Eqs. (4-5) represents the number of experimental data points available for calculating the error term, $\epsilon$. This maximum likelihood estimator provides an estimate for the model's variance based upon given experimental data in which the error term is the difference between the given experimental data point $i$ and the prediction for that data point from model $k$. In Eq. (5) this error term is squared so as to eliminate the possibility of a positive and negative error canceling each other out.

$$(\hat{\sigma})^2_{mle} = \frac{\sum_{i=1}^{N} \epsilon^2_{k,i}}{N} \quad (5)$$

### 2.2 Model-Form Uncertainty Quantification Techniques

Many methods for the quantification of model-form uncertainty have recently arisen within the literature,

each one with its own pros and cons. Original work in model-form uncertainty quantification gave birth to methods requiring the presence of experimental data, such as Bayesian model averaging which requires the presence of experimental data in order to develop a maximum likelihood estimator of variance within a model prediction as is used in updating model probabilities through Bayes' theorem. Riley and Grandhi quantified the model-form and predictive uncertainty in the calculation of the flutter velocity of the AGARD 445.6 wing using BMA in [10]. Other methods requiring the availability of experimental data include the methods of Continuous Model Expansion explored by Drapert, which showed a reliance on experimental data points, as well as difficulty in handling asymmetric distributions of parametric uncertainties [11], and work done recently by Allaire and Willcox, which require a maximum entropy representation of the modeling uncertainty, an extra step that could be cost-intensive for a high simulation-cost model [12]. As previously mentioned, the common thread among these three methods is the dependence on the availability of experimental data. The adjustment actor approach, however, was demonstrated by Mosleh and Apostolakis as a possible method for model-form uncertainty quantification which operates on the utilization of expert opinion to assign model probabilities in the absence of empirical data [13]. Riley and Grandhi present an adaptation of this approach for use with non-deterministic model predictions, called the probabilistic adjustment actor approach [14]. This work will explore the adjustment factor approaches, probabilistic adjustment factor approach, and the Bayesian Model Averaging approach and apply these methods to a multi-physics problem.

### 2.2.1 Adjustment Factor Approach

As mentioned previously, the adjustment factor approach was first demonstrated by Mosleh and Apostolakis as a method for quantifying model-form uncertainty in the absence of experimental data by using an adaptation of Bayes' Theorem. This approach modifies the result of the "best" model–model within the model set being considered for use in solving the problem that obtains the highest model probability–by applying an adjustment factor to account for the uncertainty that exist in selection of the "best" model. The applicability of this approach to engineering problems has been well demonstrated in the literature. Zio and Apostolakis utilized an adjustment factor approach to quantify the uncertainty present in the selection of a "best" radioactive waste repository model in [15]. Reinert and Apostolakis also used this approach in the assessment of risk for decision-making processes in [16].

Multiple derivations of the adjustment factor approach exist in the literature. These derivatives all employ a similar technique of quantifying the model-form uncertainty through the use of expert opinion regarding a model's accuracy with respect to other models in the model set by assigning model probabilities, and updating those probabilities through the use of Bayes' theorem upon the availability of experimental data. In this approach, $\Pr(M_k)$ represents the model probability assigned to model $k$. Recall that this model probability is the probability that model $k$ is the "best" model among model set $M$ being considered, where Eq. (6) defines the model set $M$.

$$M = \{M_1, M_2, ...., M_k\} \tag{6}$$

Note that model probabilities for each of the $K$ individual models within the model set $M$ remain bounded by the laws of probability theory. Thus, constraints are applied to the model probability values, as shown in Eq. 7.

$$\sum_{k=1}^{K} \Pr(M_k) = 1 \quad \textit{such that} \quad 0 \le \Pr(M_k) \le 1 \tag{7}$$

The various derivations of the adjustment factor approach differ here, in the form of the adjustment factor being applied–used to adjust–the "best" model. In the additive adjustment factor approach, the adjusted model, $y$, is formed by adding an additive adjustment factor, $E^*_a$, to the "best" model from the model set being considered, as shown in Eq. (8).

$$y = y^* + E^*_a \tag{8}$$

This additive adjustment factor, $E^*_a$, is assumed to be a normally distributed factor representing the uncertainty present in the selection of the "best" model as being most accurate at predicting the true physical response. In assuming a Gaussian form for this factor, the first and second moments–expected value and variance–of the adjustment factor are calculated as shown in Eqs. (9-10).

$$\mathrm{E}[E^*_a] = \sum_{k=1}^{K} \Pr(M_k)(y_k - y^*) \tag{9}$$

$$\mathrm{Var}[E^*_a] = \sum_{k=1}^{K} \Pr(M_k)(y_k - \mathrm{E}[y])^2 \tag{10}$$

It is important to note that use of the adjustment factor approach is reliant on models within the model set to be deterministic; this is to say that the models cannot incorporate parametric uncertainty. Therefore, the expected value of the adjusted model, E[$y$], is calculated as shown in Eq. (11), as the sum of the prediction of the "best" model and the expected value of the additive adjustment factor, E[$E^*_a$], found using Eq. (9).

$$\mathrm{E}[y] = y^* + \mathrm{E}[E^*_a] \tag{11}$$

Similarly, due to each individual model being deterministic, the variance of the adjusted model, Var[$y$], assumes only the variance of the additive adjustment factor, Var[$E^*_a$], as shown in Eq. (12).

$$\mathrm{Var}[y] = \mathrm{Var}[E^*_a] \tag{12}$$

The first and second moments–expected value and variance–of the adjusted prediction, $y$, are calculated by Eqs. (11-12) which fully define a normal distribution representing the uncertainty inherent in the prediction of a system response as a result of model-form uncertainty.

Another derivative of the adjustment factor approach is that of a multiplicative adjustment factor. In the multiplicative adjustment factor approach, the adjusted model, $y$, is formed by multiplying the prediction of the "best" model, $y^*$ from the model set being considered by a multiplicative adjustment factor, $E^*_m$, as shown in Eq. (13).

$$y = y^* * E^*_m \tag{13}$$

This multiplicative adjustment factor, $E^*_m$, is assumed to be a log normally distributed factor representing the uncertainty present in the selection of the "best" model as being most accurate at predicting the true physical response. In assuming a log normally distributed form for this factor, the first and second moments–expected value and variance–of the adjustment factor are calculated as shown in Eqs. (14-15).

$$\mathrm{E}[\ln(E^*_m)] = \sum_{k=1}^{K} \Pr(M_k)(\ln(y_k) - \ln(y^*)) \tag{14}$$

$$\mathrm{Var}[\ln(E^*_m)] = \sum_{k=1}^{K} \Pr(M_k)(\ln(y_k) - \mathrm{E}[\ln(y)])^2 \tag{15}$$

As was the case with the additive adjustment factor approach, it is important to note that use of the adjustment factor approach is reliant on models within the model set to be deterministic. Therefore, the expected value of the adjusted model, E[ln($y$)], is calculated as shown in Eq. (16), as the sum of the natural logarithm of the prediction of the "best" model and the expected value of the multiplicative adjustment factor, E[ln($E^*_m$)], from Eq. (14).

$$\mathrm{E}[\ln(y)] = \ln(y^*) + \mathrm{E}[\ln(E^*_m)] \tag{16}$$

Much like the additive adjustment factor approach, due to each individual model being deterministic, the variance of the adjusted model, Var[ln(y)], assumes only the variance of the multiplicative adjustment factor, Var[ln($E^*_m$)], as shown in Eq. (17).

$$\mathrm{Var}[\ln(y)] = \mathrm{Var}[\ln(E^*_m)] \tag{17}$$

While these adjustment factor approaches have the benefit of being able to quantify model-form uncertainty in the absence of experimental data, they lack the ability to handle probabilistic model predictions, this is to say that the adjustment factor approach cannot quantify the model-form uncertainty present in the selection of a "best" model, from a model set, when the models within said model set contain quantified parametric uncertainty. This is a result of the assumption made during derivation of the approach that individual models are deterministic. Therefore, a rederivation of the approach, working on the assumption that individual models are probabilistic/stochastic in nature, would allow for the approach to be adapted to handle parametric uncertainty.

### 2.2.2 Probabilistic Adjustment Factor Approach

The probabilistic adjustment factor approach is an adaptation of the traditional adjustment factor approach in that it is capable of handling stochastic model, and thus parametric uncertainty. Note that this approach does not quantify the parametric uncertainty within each model of a model set, but it can handle parametrically uncertain models in its analysis [14]. As with the traditional adjustment factor approach, a distribution must first be assumed for each of the individual models within the model set for derivation of the probabilistic adjustment factor approach. In general there is no restriction on the on the form of this distribution; however, as was the case with the additive adjustment factor approach, this work will

focus on the approach derived from assumption of a normal distribution.

The first step to quantifying model-form uncertainty through the use of the probabilistic adjustment factor approach is the same as that of the traditional adjustment factor approach. Model probabilities are applied to each individual model within the model set using either expert opinion or uniformly distributed probabilities, and then updating through the application of Bayes' theorem given the availability of experimental data, such that constraints of Eq. (7) are satisfied. The adjusted model for the probabilistic adjustment factor approach can then be computed as shown in Eq. (18)

$$y = \mathrm{E}[y^*] + E^*_{pafa} \tag{18}$$

Eq. (18) is similar to Eq. (8) from the additive adjustment factor approach with the slight difference in the utilization of the expected value of the "best" model, $\mathrm{E}[y^*]$, rather than the deterministic "best" model prediction. Calculating the first and second moments–expected value and variance–of the probabilistic adjustment factor is also different for this new approach, as the approach had to be re-derived to handle the stochastic model set. The calculation of these two moments can be performed using Eqs. (19-20).

$$\mathrm{E}[E^*_{pafa}] = \sum_{k=1}^{K} \Pr(M_k)(\mathrm{E}[y_k] - \mathrm{E}[y^*]) \tag{19}$$

$$\mathrm{Var}[E^*_{pafa}] = \sum_{k=1}^{K} \Pr(M_k)(\mathrm{E}[y_k] - \mathrm{E}[y])^2 \tag{20}$$

After calculating the first and second moments of the probabilistic adjustment factor, the expected value and variance of the adjusted model can then be calculated using Eqs. (21-22).

$$\mathrm{E}[y] = \mathrm{E}[y^*] + \mathrm{E}[E^*_{pafa}] \tag{21}$$

$$\mathrm{Var}[y] = \mathrm{Var}[E^*_{pafa}] + \sum_{k=1}^{K} \Pr(\mathrm{M}_k)(\mathrm{Var}[y_k])^2 \tag{22}$$

As can be seen, there is only a slight difference in the formulations of the expected value equations for the traditional adjustment factor approach and the probabilistic adjustment factor approach, only in that of operating on the expected value of the "best" model prediction rather than the deterministic model prediction, as is the case for the traditional approach. The key difference in the two derivations comes in the formulation of the variance equation. The variance, shown in Eq. (22), includes the addition of the summation of weighted individual model variances–weighted by model predictions–to the variance of the adjustment factor calculated using Eq. (20), known as the between-model variance. The second term in the equation represents the variance in the adjusted model due to variances within each of the individual models–the within-model variance. Therefore, the first term in Eq. (22) can be thought of as representing the model-form uncertainty within the problem, whereas the second term represents the parametric uncertainty inherent to each model within the model set, and quantified using parametric uncertainty quantification techniques. In the event that individual models within the model set are deterministic, do not account for parametric uncertainties, and experimental data is available, the probabilistic adjustment factor approach can still be utilized by assuming the maximum likelihood estimator of variance for each individual model to be said model's variance in the evaluation of Eq. (22).

### 2.2.3 Bayesian Model Averaging (BMA)

The Bayesian model averaging technique is one that requires the availability of experimental data as mentioned previously; however, this technique can handle both stochastic and deterministic models. BMA is a technique for quantifying model-form uncertainty by averaging the predictions of each individual model within a model set using each model's corresponding model probability as a weighting factor. As is the case with the previous approaches, a distribution must be assumed for the averaged model, and the individual models, if stochastic, must follow this same distribution. For the purpose of this work, each model, if stochastic, must follow a normal distribution–defined by an expected value and variance–thus the averaged model assumes the form of a Gaussian distribution. The expected value of the averaged model, $\mathrm{E}[y \mid \mathrm{D}]$, is calculated by Eq. (23) as the summation of the model probabilities, $\Pr(M_k \mid D)$, multiplied by the corresponding model's expected value, $\mathrm{E}[y \mid M_k D]$.

$$\mathrm{E}[y|D] = \sum_{k=1}^{K} \Pr(M_k|D)\mathrm{E}[y|M_k, D] \tag{23}$$

Similarly, the equation for calculating the variance of the averaged model is shown in Eq. (24). This equation states that the variance of the averaged model, Var[$y|D$], is the summation of the model probabilities Pr($M_k|D$), multiplied by the corresponding model's variance, Var[$y|D$], plus the summation of the model probabilities multiplied by the squared difference between the corresponding model's expected value, E [$y|D$].

$$\mathrm{Var}[y|D] = \sum_{k=1}^{K} \Pr(M_k|D)\mathrm{Var}[y|M_k, D] + \sum_{k=1}^{K} \Pr(M_k|D)(\mathrm{E}[y|M_k, D] - \mathrm{E}[y|D])^2 \quad (24)$$

In the event that BMA is being applied to a deterministic model set, case in which uncertainties due to input parameters are not included, Eqs. (25-26) are used to calculate the averaged model expected value and variance. The difference in the formulation between Eq. (23) and Eq. (25) is that the latter used the individual model deterministic predictions, *yk*, rather than their expected values. The key difference in these two derivations is seen in the formulation of the equation for calculation of averaged model variance, where the first term of Eq. (24) changes by using the maximum likelihood estimator of variance, $(\hat{\sigma})^2_{mle}$ calculated using Eq. (5), in place of the individual stochastic model variances as well as substituting the individual deterministic model predictions, $y_k$, for the stochastic model expected values in the first term of Eq. (26), corresponding to the second term of Eq. (24) [17].

$$\mathrm{E}[y|D] = \sum_{k=1}^{K} \Pr(M_k|D)y_k \quad (25)$$

$$\mathrm{Var}[y|D] = \sum_{k=1}^{K} \Pr(M_k|D)(y_k - \mathrm{E}[y|D])^2 + \sum_{k=1}^{K} \Pr(M_k|D)(\hat{\sigma}_k)^2_{mle} \quad (26)$$

## 3. Thermal-Structural Modeling Demonstration

The model-form uncertainty inherent in the calculation of maximum temperature at various locations within an idealized thermal protection system (TPS) panel, using three different computational models, will be quantified using each of the model-form UQ techniques presented in this paper. This idealized TPS panel is taken to represent a corrugated-core sandwich panel from a space shuttle thermal protection system. Each of these computational models were constructed on differing assumptions of the geometric and material properties as well as differing approaches on capturing the true physics of the transient thermal problem subject to time dependent heat flux and boundary conditions. The problem of interest has been explored by Bapanapalli *et al* from an optimization point of view on geometry and material configurations [18]. This problem serves as a good baseline for exploring model-form uncertainty due to the modeling possibilities as well as the validity to different system responses. This work will focus on quantifying only model-form uncertainty present in selection of the "best" model among the following three models, used for the purpose described above:

1. Full geometric-material model (2-D heat transfer)
2. Homogenized core-material model (1-D heat transfer)
3. Thermal resistance network (TRN) model

The simplified geometry of the idealized TPS panel is shown in Figure 2, and can be completely described using 6 geometric variables: thickness of top face sheet (TFS), $t_t$, thickness of bottom face sheet (BFS), $t_b$, thickness of webs, $t_w$, angle of webs to BFS, $\theta$, height of sandwich panel (center-to-center distance between TFS and BFS), $d$, and length of a unit-cell of the sandwich panel, $2p$.

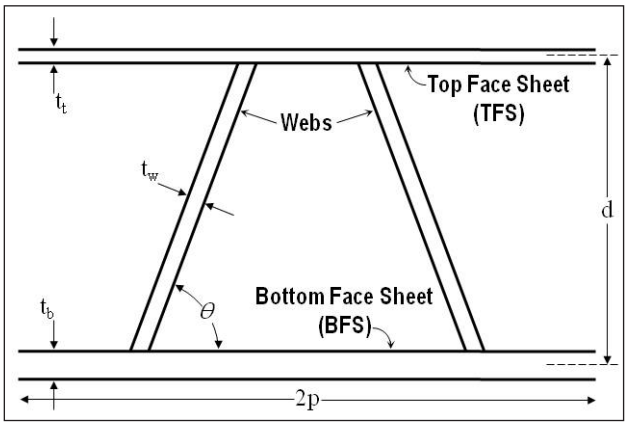


*Figure 2. Simplified Geometry of Corrugated-Core Sandwich Panel for Thermal Protection System.*

Note that the geometry is simplified due to an assumption that the corrugated-core structure is made of discrete web components which are not attached to each other by horizontal sections, as is the case in some

corrugated-core sandwich panels. These horizontal sections are typically included within the geometry of the system for the purpose of attaching the core to the top and bottom face sheets; however, from a design point of view, these sections are redundant.

### 3.1 Transient Loading and Boundary Conditions

Loading and boundary conditions are taken to simulate the operating conditions incident on a TPS panel located approximately 827 inches from the tip of a space shuttle during a reentry period. The initial temperature of the entire structure is assumed to be 295 K, while a linearly varying heat flux is incident on the top surface of the TFS of the TPS Panel. Heat is conducted through the structure as well as radiated to the ambient by the top surface during the entire transient process while convection occurs during the final reentry stage of the shuttle–while the shuttle sits on a landing pad–and is taken to be free convection. The bottom surface of the BFS is assumed to be perfectly insulated to represent a worst-case scenario where the BFS temperature would rise to a maximum as it cannot dissipate the heat.

During the initial reentry period–time period of 0 to 450 seconds–ambient temperatures are assumed to be 213 K. Radiation and conduction dissipate heat during this step, while heat flux is incident on the tops surface of the top face sheet. This incident heat flux ramps linearly during the 450 second time span from 0 to 3.0 $^{Btu}/_{ft^2 s}$. The second step of the analysis represents the second phase of reentry–time period of 450 to 1575 seconds–during which the ambient temperatures are assumed to be 243 K. While radiation to the ambient and conduction throughout the structure occur during this phase, heat flux is also incident on the top surface of the top face sheet. This heat flux is also ramped linearly during the 1125 second time span from 3.0 to 3.5 $^{Btu}/_{ft^2 s}$. The final phase of reentry–time period of 1575 to 2175 second–is represented by the third stage of this analysis in which ambient temperature is assumed to be 273 K. As with the first two phases, this phase consists of radiation to the ambient, conduction throughout the structure, and an incident heat flux. Heat flux decreases linearly from 3.5 to 0 $^{Btu}/_{ft^2 s}$ during this final reentry phase. The fourth and final stage of this transient analysis represents the period after touchdown–time period of 2175 to 5175 seconds–during which time the ambient temperature is assumed to be 295 K. During this period, along with radiation to ambient and conduction throughout the structure, convective heat transfer boundary conditions are imposed on the top surface to simulate the heat transfer to the surroundings while the vehicle is sitting on the runway. The value of the convective heat transfer coefficient, h, is taken to be 6.5 $^{W}/_{m^2 K}$ and the top surface of the top face sheet is assumed to have an emissivity, *e*, of 0.8. Another assumption to note is an assumption of a perfect conduction interface between the face sheets and webs, face sheets and insulation, and between the webs and insulation materials as illustrated in Figure 2, that is, there is no thermal contact resistance at the interface.

### 3.2 Analysis Models

As mentioned previously, the model set being considered for predicting temperature throughout the TPS panel consists of three models. The first of these three models is a full geometric representation of the cross-section of the corrugated-core sandwich panel as shown in Figure 3(a). Heat transfer in this model is two dimensional due to the geometry of the webs. As can be seen in Figure 3(a), the top face sheet of this model is composed of Inconel, the bottom face sheet is composed of aluminum, web constructed of titanium, and the core is an insulation material, typically Saffil but for the purposes of these models, the core takes on general material properties of insulation similar to that of Saffil. Figure 3(b) depicts the geometry and material composition of the homogenized core model in which heat transfer is considered to be one dimensional. The top and bottom face sheets are still composed of inconel and aluminum respectively; however, the core is modeled as one homogenized material having material properties calculated using Eqs. (27-29).

$$\rho^* = \frac{\rho_1 V_1 + \rho_2 V_2}{V^*} \tag{27}$$

$$C^* = \frac{C_1 \rho_1 V_1 + C_2 \rho_2 V_2}{\rho^* V^*} \tag{28}$$

$$k^* = \frac{k_1 A_1 + k_2 A_2}{A^*} \tag{28}$$

In these equations, *r* stands for density, *C* denotes specific heat, and *k* represents thermal conductivity. The subscripts 1 and 2 represent titanium (web) and insulation respectively, while the superscript '*' represents the homogenized core. Area of cross-section perpendicular to the flow of heat is given by

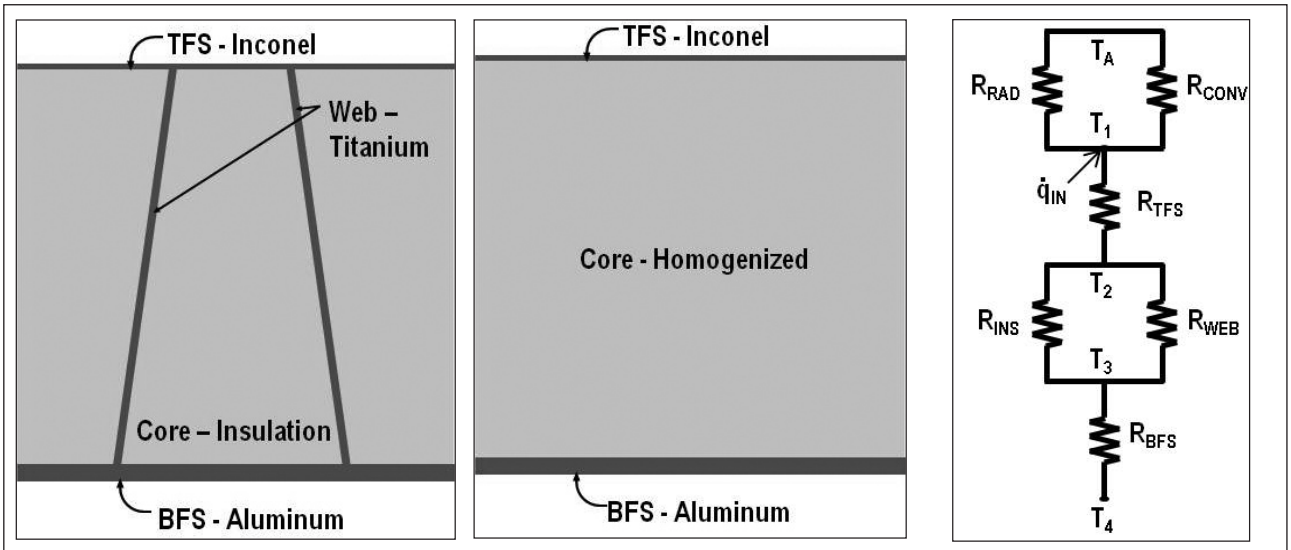


(a) Full geometric-material model (b) Homogenized core-material model (c) Thermal resistance network model

*Figure 3. Analysis Models*

$A$, where $A_1$ is determined using Eq. (30), which takes into account the angle of the web corrugations, $\theta$. The geometry of the 2-D as well as the 1-D models were defined within the Abaqus software package along with all loading and boundary condition steps in order to perform a nonlinear transient heat transfer analysis in which a 15 second time step was used for the first three stages and a 40 second time step for the final stage.

$$A_1 = \frac{2t_w}{\sin(\theta)} 2p \tag{30}$$

The values of the 6 geometric variables used to fully define the geometry of the idealized TPS panel are tabulated in Table 1, and are used to define the geometry of the first two Abaqus models within the model set, as well as used in determining thermal resistances for use within the thermal resistance network analysis. This thermal resistance network analysis was carried out following general heat transfer analysis of a thermal resistance network for the thermal resistance network of Figure 3(c). $R_{RAD}$, $R_{CONV}$, $R_{TFS}$, $R_{INS}$, $R_{WEB}$, *and* $R_{BFS}$ in Figure 3(c) represent the thermal resistance due to radiation, convection, conduction in the top face sheet, insulation, web and bottom face sheet respectively, $\dot{q}_{in}$ represents the rate of heat flow into the structure incident on the TFS. These calculations, solving for temperatures, $T_1$, $T_2$, $T_3$, and $T_4$, were performed using implicit methods and automated for each time step using Matlab.

This work focused on four different system responses corresponding to the maximum temperature during the transient response at four distinct locations within the geometry of the TPS panel, which are depicted in Figure 4. Note that the physical positions of these four locations remain the same for the homogenized core model; however, these locations are lost when it comes to the TRN model, rather they correspond to $T_1$, $T_2$, $T_3$, and $T_4$ in Figure 3(c) representing the temperatures on the top surface of the TFS, intersection of the TFS with the insulation and the web, intersection of the insulation and the web with the BFS, and the bottom surface of the BFS, respectively.

## 4. Model-Form UQ Results

The three models contained within the model set described previously and depicted in Figure 3, were

**Table 1. Corrugated-Core Sandwich Panel Geometric Values**

| $t_w$(mm) | $t_t$(mm) | $t_b$(mm) | $\theta$(degrees) | d(mm) | p(mm) |
|---|---|---|---|---|---|
| 3.0 | 2.0 | 6.0 | 82 | 140.0 | 75.0 |

**Table 2. Maximum Temperature. Experimental data points are fabricated for demonstration purposes only.**

| Location | Experimenta Data (K) | 2-D Model Prediction (K) | 1-D Model Prediction (K) | Thermal Resistance Network Prediction (K) |
|---|---|---|---|---|
| 1 | 961 | 963.942 | 951.353 | 956.393 |
| 2 | 931 | 929.049 | 950.905 | 956.393 |
| 3 | 418 | 415.044 | 425.946 | 434.256 |
| 4 | 417 | 415.039 | 425.946 | 434.256 |

performed using the transient analysis with loading and boundary conditions mentioned above for the temperature at the four locations shown in Figure 4. The results of these analyses, temperature with respect to time, can be seen in Figure 5, where Figure 5(a) corresponds to predicted temperature at location 1 within the TPS panel for the entire reentry period of a shuttle, and likewise for Figure 5(b) corresponding to location 2, etc. As can be seen in this figure, upon comparing the transient temperature response at location 1 to that at location 2, the 2-D Full Geometric model predicts higher temperatures than the TRN model. However, for most of the transient response, the TRN model predicts higher temperatures than the 1-D Homogenized Core model at location 1; whereas, this is only partially true at location 2. The TRN model still predicts higher temperatures than the 1-D Homogenized Core model; however, both predict higher temperatures than the 2-D Full Geometric model. Nevertheless, it can be noted that the temperature profiles for each of the three models have the same shape envelopes at all locations of interest. The maximum temperatures for each location, as predicted by each of the three models within the model set, are tabulated in Table 2.

Model-form uncertainty present in the selection of the "best" model from the model set was quantified using the additive adjustment factor, multiplicative adjustment factor, probabilistic adjustment factor, and Bayesian model averaging approaches for predicting the maximum temperature at each of the four locations described above. For this problem, the prior probabilities of the three models are assumed to be uniform, and then updated using Bayes' theorem, shown in Eq. (3). The experimental data points used in the calculation of the maximum likelihood estimator of variance, calculated using Eq. (5), are tabulated in Table 2. Note that these data points are not actual experimental results; they were fabricated for the sole purpose of demonstrating these model-form uncertainty quantification techniques, and should in no way be taken as experimental results for the configuration described–albeit not needed for quantification of model-form uncertainty in the adjustment factor approaches are utilized to demonstrate application of Bayes' theorem and consequently yield identical model probabilities for each of the UQ techniques. Upon updating model probabilities, and obtaining the maximum likelihood estimator needed for both quantification of model likelihood and applying probabilistic adjustment

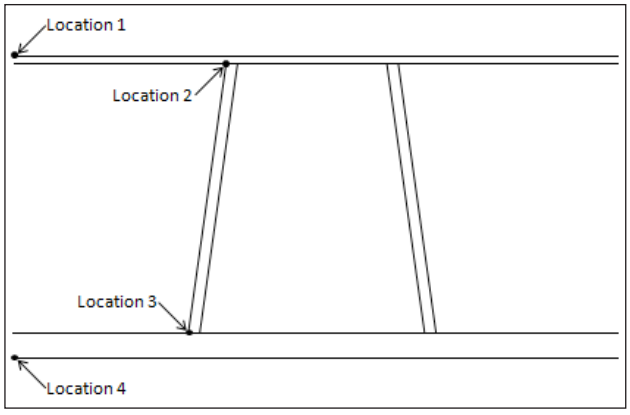


*Figure 4. Locations for the Response of Interest for Each Model.*

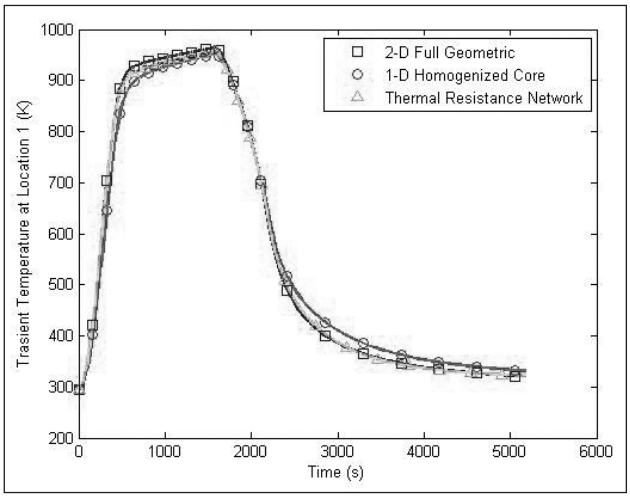


(a) Location 1

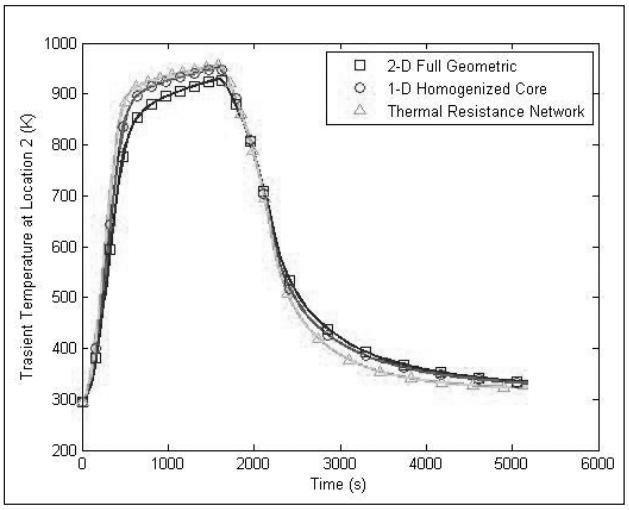


(b) Location 2

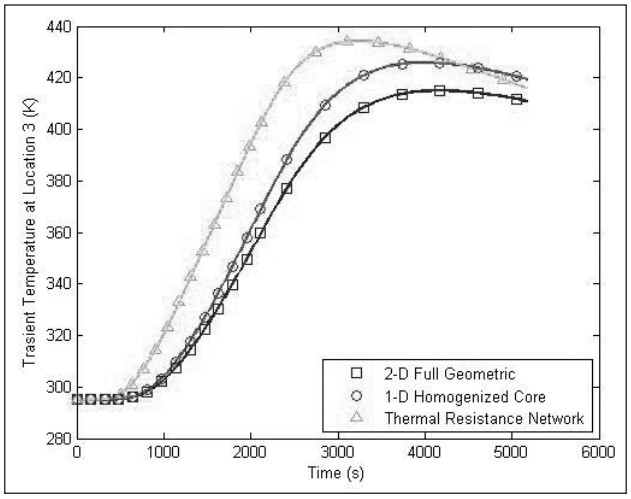


(c) Location 3

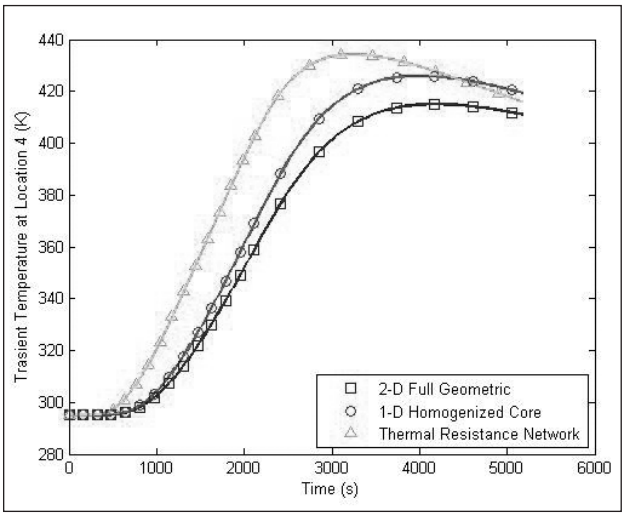


(d) Location 4

*Figure 5. Transient Temperature Response of Three models in Model Set.*

factor approach and Bayesian model averaging to quantify model-form uncertainty, the model-form uncertainty techniques were applied to the model set for each problem, maximum temperature at four different locations.

Table 3 and Figure 6 show the distribution of the prediction for maximum temperature at location 1, within the TPS panel, obtained using the four different model-form uncertainty quantification techniques discussed earlier. As can be seen, all four approaches generated the same mean value for the normal distribution of predicted maximum temperature at location 1. The difference between these four approaches is found in the standard deviation of the prediction distribution, it can be noted that the three adjustment factor approaches yielded standard deviations much closer in value, in comparison to the BMA approach. This can be attributed to the fact that the BMA approach inherently quantifies the average degree of uncertainty in each model prediction of the response, whereas the adjustment factor approaches do not, thus illustrating the necessity of the BMA approach on the availability of experimental data. From the point of view of size of confidence interval, it can be seen that the additive and multiplicative adjustment factor approaches yield nearly identical results being the least conservative prediction distributions, while the probabilistic adjustment factor approach yields the most conservative prediction distribution of the three adjustment factor approaches. This can be attributed to the fact that the maximum likelihood estimators were used as model variances in the quantification of model-form uncertainty using the probabilistic adjustment factor approach in this problem.

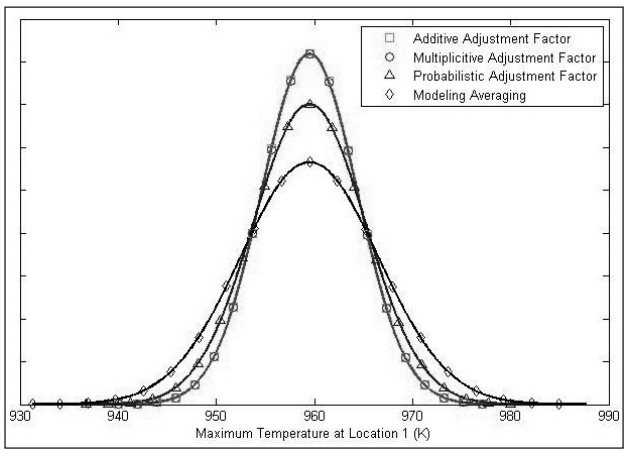


*Figure 6. Combined Model Prediction Distribution for Maximum Temperature at Location 1.*

**Table 3. Combined Model Prediction Parameters for Location 1.**

| Technique | Mean (K) | Standard Deviation (K) |
|---|---|---|
| Additive Adjustment Factor | 959.486 | 4.872 |
| Multiplicative Adjustment Factor | 959.486 | 4.878 |
| Probabilistic Adjustment Factor | 959.486 | 5.692 |
| Bayesian Model Averaging | 959.486 | 7.055 |

**Table 4. Combined Model Prediction Parameters for Location 2.**

| Technique | Mean (K) | Standard Deviation (K) |
|---|---|---|
| Additive Adjustment Factor | 932.659 | 8.669 |
| Multiplicative Adjustment Factor | 932.659 | 8.589 |
| Probabilistic Adjustment Factor | 932.659 | 8.885 |
| Bayesian Model Averaging | 932.659 | 12.371 |

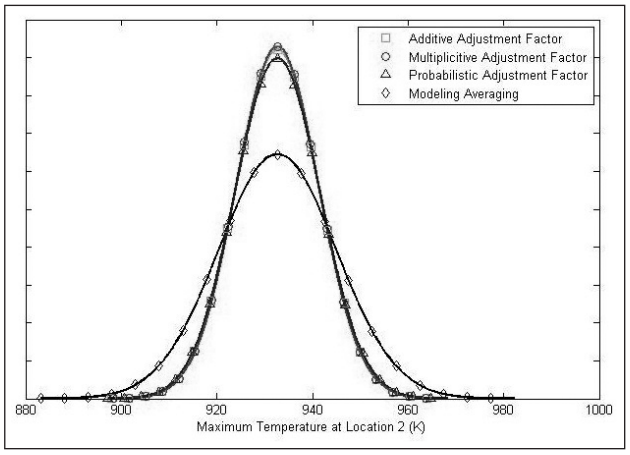


*Figure 7. Combined Model Prediction Distribution for Maximum Temperature at Location 2.*

Likewise, Table 4 and Figure 7 show the distribution of the prediction for maximum temperature at location 2, within the TPS panel. As was the case before, all four approaches generated identical mean values for the normal distribution of predicted maximum temperatures at location 2. The difference between these four approaches at this location is also found in the standard deviation of the prediction distributions. It can be noted that the three adjustment factor approaches once again yielded standard deviations much closer in value, in comparison to the BMA approach. It can be seen that the additive and multiplicative adjustment factor approaches, as with the quantification of maximum temperature at location 1, yielded nearly identical distributions that are less conservative predictions than the probabilistic adjustment factor approach, as was the case at location 1.

Finally, Table 5 and Figure 8 show the distribution of the prediction for maximum temperature at location 3, while Table 6 and Figure 9 show the prediction distribution for maximum temperature at location 4. As was the case with the previous two locations, all four approaches generated nearly identical mean values for the normal distribution of predicted maximum temperatures for each of the respective two remaining locations; whereas the difference, as before, lies in the standard deviation of the prediction distribution. It can be noted that the three adjustment factor approaches once again yielded standard deviations much closer in value, in comparison to the BMA approach. It can be seen that the additive and multiplicative adjustment factor approaches, as with the quantification of maximum temperature at location 1 and 2, yield nearly identical prediction distributions for locations 3 and 4, while the probabilistic adjustment factor approach yielded a slightly more conservative prediction distribution for both locations, as was the case at the previous two locations.

## 5. Conclusions

In this work, four methodologies were presented for the quantification of model-form uncertainty in physics-based simulations. These methodologies were the additive adjustment factor, multiplicative adjustment factor, probabilistic adjustment factor, and

**Table 5. Combined Model Prediction Parameters for Location 3.**

| Technique | Mean (K) | Standard Deviation (K) |
|---|---|---|
| Additive Adjustment Factor | 419.902 | 6.931 |
| Multiplicative Adjustment Factor | 419.902 | 6.878 |
| Probabilistic Adjustment Factor | 419.902 | 7.535 |
| Bayesian Model Averaging | 419.902 | 9.985 |

**Table 6. Combined Model Prediction Parameters for Location 4.**

| Technique | Mean (K) | Standard Deviation (K) |
|---|---|---|
| Additive Adjustment Factor | 418.471 | 6.267 |
| Multiplicative Adjustment Factor | 418.471 | 6.198 |
| Probabilistic Adjustment Factor | 418.471 | 6.566 |
| Bayesian Model Averaging | 418.471 | 8.984 |

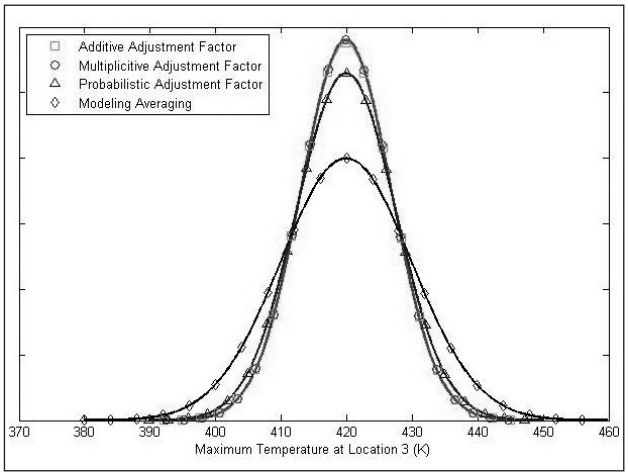


*Figure 8. Combined Model Prediction Distribution for Maximum Temperature at Location 3.*

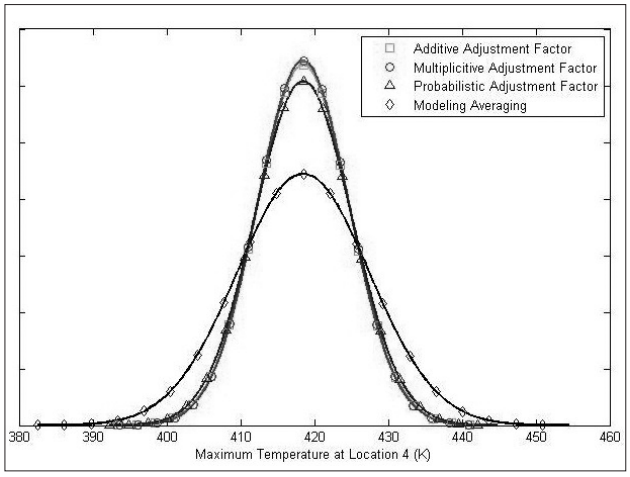


*Figure 9. Combined Model Prediction Distribution for Maximum Temperature at Location 4.*

Bayesian model averaging approaches. Limitations on these techniques include a constraint that experimental data points be available for Bayesian model averaging and that model predictions be deterministic for the additive and multiplicative adjustment factor approaches. The probabilistic adjustment factor approach, a novel derivation of the additive adjustment factor approach, can handle stochastic model predictions in contrast to that from which it was derived. It has been shown that in the presence of experimental data and deterministic model predictions, this probabilistic adjustment factor approach can be utilized by assuming each model's maximum likelihood estimator of variance be used as the model's variance. This results in a slightly more conservative prediction distribution than that of the additive or multiplicative adjustment factor approach.

The methodologies in this work were demonstrated on a transient heat transfer analysis of a corrugated-core sandwich panel for use in thermal protection systems, specifically use on a space shuttle. For this problem, three different heat transfer models, each with varying assumptions and complexity, were considered. Results concluded that the adjustment factor approaches yielded similar normal distribution parameters whereas Bayesian model averaging yielded more conservative distribution parameters as

a result of quantifying the average degree of predictive uncertainty in each model along with model-form uncertainty.

Recommendations on the best methodology to use for quantification of model-form uncertainty are dependent upon the nature of the problem. In the event that experimental data is available, it seems that Bayesian model averaging is the best technique in regards to most conservative prediction distribution, and is no more computational intensive than the other approaches. However, studies were not performed on quantifying the predictive and/or parametric uncertainty in combination with model-form uncertainty. Note that Bayesian model averaging does however inherently quantify the average degree of uncertainty in each model prediction of the response, whereas the adjustment factor approaches do not. In the absence of experimental data, and deterministic models, either the additive or the multiplicative adjustment factor approaches can be used due to the fact that they yield nearly identical results. Finally, given stochastic models and no experimental data, the probabilistic adjustment factor approach remains as the only viable option for quantifying model-form uncertainty from among the techniques presented in this work.

## Acknowledgements

The authors would like to acknowledge the support provided by the Air Force Research Laboratory through contract, FA8650-09-2-3938, for the Collaborative Center for Multidisciplinary Sciences.

## References

1. Kennedy, M. C. and O'Hagan, A., "Bayesian calibration of computer models," Journal of the Royal Statistical Society: Series B (Statistical Methodology), Vol. 63, No. 3, 2001, pp. 425–464.
2. Droguett, E. L. and Mosleh, A., "Bayesian methodology for model uncertainty using model performance data," Risk Analysis, Vol. 28, No. 5, 2008, pp. 1457–1476.
3. Soares, C. G., "Quantification of model uncertainty in structural reliability," Probabilistic Methods for Structural Design, Springer, 1997, pp. 17–37.
4. Zhang, R. and Mahadevan, S., "Model uncertainty and Bayesian updating in reliability-based inspection," Structural Safety, Vol. 22, No. 2, 2000, pp. 145–160.
5. Paté-Cornell, M. E., "Uncertainties in risk analysis: Six levels of treatment," Reliability Engineering & System Safety, Vol. 54, No. 2, 1996, pp. 95–111.
6. Hacking, I., The emergence of probability: a philosophical study of early ideas about probability, induction and statistical inference, Cambridge University Press, 1984.
7. Chernoff, H. and Moses, L. E., Elementary decision theory, Courier Dover Publications, 2012.
8. Park, I., Amarchinta, H. K., and Grandhi, R. V., "A Bayesian approach for quantification of model uncertainty," Reliability Engineering & System Safety, Vol. 95, No. 7, 2010, pp. 777–785.
9. Robert, C., The Bayesian choice: from decision-theoretic foundations to computational implementation, Springer Verlag, 2007.
10. Riley, M. E. and Grandhi, R. V., "Quantification of model-form and predictive uncertainty for multi-physics simulation," Computers & Structures, Vol. 89, No. 11, 2011, pp. 1206–1213.
11. Draper, D., "Assessment and propagation of model uncertainty," Journal of the Royal Statistical Society. Series B (Methodological), 1995, pp. 45–97.
12. Allaire, D. and Willcox, K., "Surrogate modeling for uncertainty assessment with application to aviation environmental system models," AIAA journal, Vol. 48, No. 8, 2010, pp. 1791–1803.
13. Mosleh, A. and Apostolakis, G., "The assessment of probability distributions from expert opinions with an application to seismic fragility curves," Risk Analysis, Vol. 6, No. 4, 1986, pp. 447–461.
14. Riley, M. E. and Grandhi, R. V., "A Method for the Quantification of Model-Form and Parametric Uncertainties in Physics-Based Simulations," 52nd AIAA/ASME/ASCE/AHS/ASC Structures, Structural Dynamics and Materials Conference, AIAA, Denver, Colorado, 2011.
15. Zio, E. and Apostolakis, G., "Two methods for the structured assessment of model uncertainty by experts in performance assessments of radioactive waste repositories," Reliability Engineering & System Safety, Vol. 54, No. 2, 1996, pp. 225–241.
16. Reinert, J. M. and Apostolakis, G. E., "Including model uncertainty in risk-informed decision making," Annals of nuclear energy, Vol. 33, No. 4, 2006, pp. 354–369.
17. Park, I. and Grandhi, R. V., "Quantifying multiple types of uncertainty in physics-based simulation using Bayesian model averaging," AIAA journal, Vol. 49, No. 5, 2011, pp. 1038–1045.
18. Bapanapalli, S. K., Martinez, O. M., Gogu, C., Sankar, B. V., Haftka, R. T., and Blosser, M. L., "Analysis and Design of Corrugated-Core Sandwich Panels for Thermal Protection Systems of Space Vehicles," AIAA Paper, Vol. 1942, 2006, pp. 2006.

*Life Cycle Reliability and Safety Engineering*
*Vol.2 Issue 4 (2013) 15-27*

# Long-term Assessment of Health Risk under Uncertain Environment of Contaminated Sites using Spatiotemporal Modelling

Abhirup Bandyopadhyay and Samarjit Kar
*National Institute of Technology Durgapur*
*Email: abhirupnit@gmail.com*

## Abstract

*For the design of sustainable and cost-effective management strategies for contaminated sites, decision makers need appropriate tools, i.e. environmental decision support systems to assist them in the planning, assessment, selection and optimisation of possible alternatives. We propose a novel system dynamics model which provides estimates of current and future risks originating from water-body, soil and groundwater contamination. The model particularly addresses the presence of multi-compound non aqueous phase liquids in porous media, which have been identified as major sources of groundwater and surface water contamination at many of these sites. Advection-Diffusion Equation is considered to describe the flow of concentration of the contaminant through space and model the system as an epidemic condition induced by the contaminant concentration. The spread of a disease through a population is inherently uncertain due to the unpredictability of person-to-person contacts. It is particularly important to include this randomness in models for emerging diseases, as in the early stages of an outbreak case numbers will be very small and so random variations alone can cause an epidemic to die out. Thus, through stochastic and partial dynamical modelling we estimate spatiotemporal risk of being infected by the contamination. Also the parameters of the model system are imprecise in nature, so the uncertainties of the input parameters were captured with fuzzy membership functions and simulate the model with vague parameters. Thus this paper provides a probabilistic as well as a possibilistic framework for long term assessment of human health risk of being infected by contamination.*

***Key words: Spatiotemporal, health risk, advection, diffusion, ground water***

## 1. Introduction

The human health risk assessment models are widely used in the decision-making process for industrial release of waste to soil, water or air. The complex nature of real life information used for risk assessment has guided the researchers to develop new approaches for better representation of human health risk. The risk assessment models consider parameters that are generally prone to uncertainty because of simplification and imprecise nature of the available information [1]. Uncertainty can be divided into two categories: (i) type A uncertainty, induced from natural variability, which cannot be reduced and (ii) type B uncertainty that resulted from lack of proper knowledge or partial ignorance of information [2]. Many techniques including probabilistic approach, mathematical and numerical modelling, interval analysis, convex modelling, fuzzy set theory, possibility theory and evidence theory are available to characterize the uncertainties in the natural processes [3,4]. There is no single method that offers comprehensive solutions to all the types of uncertainties. Each approach has its own set of advantages and disadvantages [5].

The environmental problems like risk assessment from contaminant discharges is associated with several parameters that is naturally variable and difficult to characterize by available statistical approaches [6]. Evaluation of parameter values in such cases is not precise. Moreover, health risk is evaluated on the basis of many simplified assumptions and extrapolations. These factors inherit uncertainties; thus an environmental evaluation is somewhat skewed from the exact solutions. Other than the mathematical precision-based exactness, fuzzy set theory is capable of describing uncertainties through the incorporation of possible parameter values. Fuzzy set theory can produce results with moderate acceptability [4,5,7].

Here in this paper we consider the problem of assessing risk of human health hazards from naturally or industrially produced contaminant; chemical, biological, radiological etc. waste create different

human health hazards for our consideration. When a new disease emerges and begins to cause infections and fatalities it is desirable for health authorities to be able to make predictions concerning the future behaviour of the epidemic. Since the disease is emerging, there is unlikely to be a previous outbreak or other existing data on which to base predictions. Also, if there is no immunity in the population to this new pathogen or contaminant there is a risk that a very large outbreak will occur, causing a large number of deaths. Mathematical modelling is one of the few available tools for predicting possible outcomes, and assessing the effectiveness of proposed control strategies.

For example we could consider the case of radioactive waste and human health risk of cancer and other infections from it. Produced water is the largest source of natural radioactive waste contamination. Produced water, discharged from offshore oil and gas operations, contains chemicals from formation water, condensed water, and any chemical added down hole or during the oil/water separation process. Although, most of the contaminants fall below the detection limits within a short distance from the discharge port, a few of the remaining contaminants including naturally occurring radioactive materials (NORM) are of concern due to their bioavailability in the media and bioaccumulation characteristics in finfish and shellfish species used for human consumption. In the past, several initiatives have been taken to model human health risk from NORM in produced water. Four different radioisotopes of radium (223Ra, 224Ra, 226Ra and 228Ra) exist in nature. The half-lives of 223Ra, 224Ra, 226Ra and 228Ra are 11.4 days, 3.7 days, 1600 years and 5.75 years, respectively [8]. Due to their short half-lives, 223Ra and 224Ra do not play significant role in risk assessment. Two isotopes of radium, 226Ra and 228Ra are of most concern as they are leachable and mobile because of their high solubility in water [9] and they may bio accumulate in marine organisms [10]. Stephenson [40] reported 226Ra and 228Ra in the ranges of 4 -- 584 pCi/l and 18 -- 586 pCi/l with the mean values of 262 and 277 pCi/l, respectively, for produced water outfalls in the Gulf of Mexico. Produced water in the Gulf of Mexico has a higher radium activity than that present in produced water from any known offshore oil platform [11]; thus higher risk to human health is expected from these produced waters [6]. Although few studies including in [9] demonstrated co-precipitation of radium with barium sulphate in seawater, all the produced waters may not contain barium and radium simultaneously. Vegueria [9] collected the sediment samples from varying distances of 250 -- 1000 m around the port and these samples contained radium as well. The presence of radium with barium sulphate in sediments might be an indication of radium's presence in the water column beyond the port. Moreover, the co-existence of barium and radium is necessary for co-precipitation. The probability of this co-existence is significantly reduced due to instantaneous dispersion of produced water upon discharge and also reported high concentrations of radium at the vicinity of produced water outfall. Chowdhury [6] performed human health cancer risk assessment through the ingestion of marine fish, in which they reported radium's presence in the water column.

We implement the developed computational approach to the specific case of a susceptible-infected-susceptible (SIS) infection dynamics. We show how it is possible to obtain a detailed study of the quantities customarily tracked in epidemiological studies and provide an analysis of the spatiotemporal evolution of the epidemic pattern. The rather heterogeneous spatiotemporal pattern emerging during the epidemic evolution might find its origin in one or more features of the underlying network as well as in the inherent stochastic dynamics of the disease transmission. We put forward a deterministic as well as a stochastic computational framework for the modelling of the spreading of infection by contaminant. The model is analyzed by using an information theory approach that allows the quantitative characterization of the heterogeneity level and the predictability of the spreading pattern in presence of stochastic fluctuations. In particular we are able to assess the reliability of numerical forecast with respect to the intrinsic stochastic nature of the disease (contamination) transmission. The epidemic pattern predictability is quantitatively determined and traced back to the occurrence of epidemic pathways defining a backbone of dominant connections for the disease spreading. The presented results provide a general computational framework for the analysis of containment policies and risk forecast of global human health risk from contaminants. The contamination spread appears to have a major effect in driving the epidemic evolution, therefore allowing the possibility of predicting an overall epidemic pattern on top of the stochastic fluctuations. Motivated by these findings, we investigate the predictability of the epidemic spread through the analysis of the statistical overlap of risk

pattern of outbreak of epidemic generated in different stochastic realizations of the spreading process. This overlap is quantitatively defined by using a statistical similarity analysis of the global distribution of infected individuals and spatiotemporal spread of concentration of contaminant. The assessment of human health risk is evaluated in terms of probability of being infected by contamination. The spatiotemporal distribution of risk probability provide a frame work for decision makers to identify equiprobable risk zones and employ heterogeneous plane for different zones. The imprecision of system parameter is introduced in terms of interval valued fuzzy number and we extend the model into a fuzzy boundary value problem (FBVP) under the same considerations. Fuzzy extension of the model provides a possibility; that is a fuzzy probability value and a frame work for risk assessment under uncertainty and natural fluctuations of parameter values.

### 1.1 The Basic SIS Model for Infection from Contaminant

In the basic standard compartmentalization of the SIS, each individual can only exist in one of the discrete states such as susceptible (S) and infected (I). The total population N is given by N =S (t) + I (t), where S(t) and I (t) represent the number of susceptible and infected individuals at time t, respectively (in the following we replace for simplicity the general notation X[m] by S , I ). The epidemic evolution is governed by the basic dynamical evolution of the SIR model where the probability of a susceptible individual acquiring the infection from any given infected individual in the time interval dt is proportional to βdt. Here β is the transmission parameter that captures the aetiology of the infection process. At the same time, infected individuals recover with a probability rdt, where $r^{-1}$ is the average duration of the infection. The relevant parameter describing the epidemic is the basic reproduction number $R_0 = \beta/r$ [12] given by the average number of secondary cases that each infected individual generates in a susceptible population. If $R_0 > 1$ and the initial density of susceptible are larger than $R_0^{-1}$, then an epidemic will develop.

In this paper we assume the human health hazard from contaminant spreads like an epidemic mainly induced by the present concentration of the contaminant in the environment and also by infectious individuals in lesser quantity. The contaminant is assumed to decay in a constant rate per unit mass and to be deposited in constant rate by some industrial or natural process. Thus we model the spread of contaminant induced health hazards by the epidemic Langevin equation for each class and obtain the following SIS model:

$$\begin{cases} \dfrac{dS}{dt} = AS(1-\dfrac{S}{k_1}) - eS\dfrac{C}{N+C} - eiSI - mS + rI \\ \dfrac{dI}{dt} = eS\dfrac{C}{N+C} + eiSI - (m+r+v)I \\ \dfrac{dC}{dt} = \dfrac{1}{V}\left[g - m_0 C - l(S+I)C\right] \end{cases} \quad (1)$$

Where S and I are the volume of susceptible and infected respectively and C is the concentration of the contaminant. Also A is the intrinsic growth rate of S, e is the rate of infection spread to S by contaminant C, ei is the rate of infection spread to S by infectious I, m is the natural mortality rate, r is the recovery rate of infectious, v is the infection induced death rate, g is the rate of deposition of contaminant, $m_0$ is the natural decay rate of contaminant, l is the average rate of intake of contaminant by S and I and V is the constant volume of the environment.

Theorem 1.1. Let $(S(t), I(t), C(t))$ be the solution of the model (1), with initial condition $(S_0, I_0, C_0)$ and the compact set

$$\Omega = \left\{ (S,I,C) \in \mathbb{R}^3_+, W_H \le \frac{Ak_1}{4m}, W_P \le \frac{4mg}{4mm_0 + Alk_1} \right\}$$

under the flow described by model system, $\Omega$ is a positively invariant set that attracts all solutions in $\mathbb{R}^3_+$.

Proof: Consider the following Lyapunov function candidate: $W(t) = (W_H, W_C) = (S+I, C)$.

The time derivative is given by

$$\frac{dW}{dt} = \left( \frac{dW_H}{dt}, \frac{dW_C}{dt} \right) = \left( \frac{dS}{dt} + \frac{dI}{dt}, \frac{dC}{dt} \right)$$

$$= \left( AS\left(1 - S/k_1\right) - mS - (m+v)I, \frac{1}{V}\left[g - m_0 C - l(S+I)C\right] \right)$$

This gives

$$\begin{cases} \dfrac{dW_H}{dt} = AS\left(1 - S/k_1\right) - mW_H - vI \le \dfrac{Ak_1}{4} - mW_H \le 0, for W_H \ge \dfrac{Ak_1}{4m} \\ \dfrac{dW_C}{dt} = \dfrac{1}{V}\left[g - m_0 W_C - lW_C W_H\right] \le \dfrac{1}{V}\left[ g - \left( m_0 + \dfrac{Alk_1}{4m} \right) \right] \le 0, for W_C \ge \dfrac{4mg}{4mm_0 + Alk_1} \end{cases} \quad (1.1)$$

From Eq. (2) we have $\dfrac{dW}{dt} \le 0$ which implies that $\Omega$ is a positively invariant set. We also note that by

solving (2) we have,

$$0 \le (W_H, W_C) \le \left( \frac{Ak_1}{4} + W_H(0)e^{-mt}, \frac{4mg}{4mm_0 + Alk_1} + W_C(0)e^{-\frac{t}{V}\left[m_0 + \frac{Alk_1}{4m}\right]} \right)$$

where $W_H(0)$ and $W_C(0)$ are respectively the initial condition of $W_H(t)$ and $W_C(t)$. Thus as $t \to \infty$ $0 \le (W_H, W_C) \le \left( \frac{Ak_1}{4}, \frac{4mg}{4mm_0 + Alk_1} \right)$ and hence $\Omega$ is an attractive set. The proof is complete.

### 1.2 Endemic equilibrium local and global stability

Since there is a constant rate of deposition of the contaminant there is no disease free equilibrium state for the model of contaminated site if g>0. However the endemic equilibrium could be determined as follows:

$$\varepsilon^* = (S^*, I^*, C^*), C^* = \frac{g}{m_0 + l(S^* + I^*)}, I^* = \frac{(A-m)S^* - \frac{AS^{*2}}{k_1}}{m+v}$$

And $S^*$ is the root of the equation $\zeta_1 S^4 - \zeta_2 S^3 - \zeta_3 S^2 - \zeta_4 S = 0$ where

$$\left.\begin{aligned} \zeta_1 &= \frac{NlA^2(ei-m-v-r)}{((m+v)k_1)^2}; \zeta_2 = \frac{A(2A+v-m)}{k_1}; \zeta_3 = \\ &(A+v)(A-m) + \frac{A(ei-m-v-r)(g+Nm_0)}{k_1(m+v)} \\ \zeta_4 &= eg - \frac{(A-m)(ei-m-v-r)(g+Nm_0)}{m+v} \end{aligned}\right] \quad (1.2)$$

The Jacobian matrix for the system is

$$\begin{pmatrix} A - \frac{2AS}{k_1} - \frac{eC}{C+N} - eiI - m & -eiS + r & -\frac{eNS}{(C+N)^2} \\ \frac{eC}{C+N} & eiS - (m+v+r) & \frac{eNS}{(C+N)^2} \\ -\frac{lC}{V} & -\frac{lC}{V} & -\frac{m_0 - l(S+I)}{V} \end{pmatrix} \quad (1.3)$$

Theorem2: Consider the following general system of ordinary differential equation with a parameter $\phi$ :

$$\frac{dx}{dt} = f(x,\phi), f: \mathbb{R}^n \to \mathbb{R}, and \quad f \in \mathbb{R}^2(\mathbb{R}^n \times \mathbb{R}) \quad (1.4)$$

Where 0 is an equilibrium of the system, that is $f(0,\phi) = 0$ for all $\phi$ and we assume

A1: $A = D_x f(0,0) = \left( \frac{\partial f_i}{\partial x_j}(0,0) \right)$ is the linearization of the system (1) around the equilibrium 0 with $\phi$ evaluated at 0. Zero is a simple eigenvalues of A have negative real parts.

A2: Matrix A has a right eigenvector u and a left eigenvector v corresponding to the zero eigenvalue. Let $f_k$ be the k[th] component of $f$ and

$$a = \sum_{k,i,j=1}^{n} v_k u_i u_j \frac{\partial^2 f_k}{\partial x_i \partial x_j}(0,0), b = \sum_{k,i,=1}^{n} v_k u_i \frac{\partial^2 f_k}{\partial x_i \partial \phi}(0,0)$$

The local dynamics of (1.4) around zero are totally governed by a and b.

(i) a>0, b>0, when $\phi < 0$ with $|\phi| << 1$, 0 is locally asymptotically stable, and there exists a positive unstable equilibrium; when $0 < \phi << 1$, 0 is unstable and there exists a negative and locally asymptotically stable equilibrium.

(ii) a<0, b<0, when $\phi < 0$ with $|\phi| << 1$, 0 is unstable; when $0 < \phi << 1$, 0 is asymptotically stable and there exists a positive unstable equilibrium.

(iii) a>0, b<0, when $\phi < 0$ with $|\phi| << 1$, 0 is unstable and there exists a locally asymptotically stable negative equilibrium; when $0 < \phi << 1$, 0 is stable, and a positive unstable equilibrium appears.

(iv) a<0, b>0, when $\phi$ changes from negative to positive, 0 changes it's stability from stable to unstable. Correspondingly a negative equilibrium becomes positive and locally asymptotically stable.

If e is taken as a bifurcation parameter at $e=e^*$ so that the linearized system has a simple zero eigenvalue. Then from central manifold theory it can be shown that the Jacobian (1.3) at $e=e^*$ $J(\varepsilon^*)$ has a right eigenvector associated with zero eigenvalue denoted by $u = (u_1, u_2, u_3)^T$ and a left eigenvector associated with zero eigenvalue given by $v = (v_1, v_2, v_3)^T$.

Computation of a and b: from model system (1) the associated non-zero partial derivatives of $f$ at endemic equilibrium are given by:

$$\frac{\partial^2 f_1}{\partial x_1^2} = -\frac{2A}{k_1}, \frac{\partial^2 f_1}{\partial x_1 \partial x_2} = -ei, \frac{\partial^2 f_1}{\partial x_1 \partial x_3} = -\frac{eN}{(x_3+N)^2}, \frac{\partial^2 f_2}{\partial x_1 \partial x_2} = ei, \frac{\partial^2 f_2}{\partial x_1 \partial x_3} = \frac{eN}{(x_3+N)^2}$$

$$\frac{\partial^2 f_3}{\partial x_1 \partial x_3} = -\frac{l}{V}, \frac{\partial^2 f_3}{\partial x_2 \partial x_3} = -\frac{l}{V}, \frac{\partial^2 f_1}{\partial x_1 \partial e^*} = -\frac{x_3}{x_3+N}, \frac{\partial^2 f_1}{\partial x_3 \partial e^*} = -\frac{Nx_1}{(x_3+N)^2}, \frac{\partial^2 f_2}{\partial x_1 \partial e^*} = \frac{x_3}{x_3+N}$$

$$\frac{\partial^2 f_2}{\partial x_3 \partial e^*} = \frac{Nx_1}{(x_3+N)^2},$$

$$\begin{pmatrix} x_1 \\ x_2 \\ x_3 \end{pmatrix} = \begin{pmatrix} S \\ I \\ C \end{pmatrix} and \begin{pmatrix} f_1 \\ f_2 \\ f_3 \end{pmatrix} = \begin{pmatrix} \frac{dI}{dt} \\ , \frac{dS}{dt} \\ \frac{dC}{dt} \end{pmatrix}.$$

Where Therefore $a = \sum_{k,i,j=1}^{n} \nu_k u_i u_j \frac{\partial^2 f_k}{\partial x_i \partial x_j}(0,0)$

$$= \begin{bmatrix} -\frac{2A}{K_1} u_1^2 - eiu_1u_2 - \frac{eN}{(C^*+N)^2} u_1u_3 \end{bmatrix} v_1 + \begin{bmatrix} eiu_1u_2 + \frac{eN}{(C^*+N)^2} u_1u_3 \end{bmatrix} v_2 - \frac{l}{V}[u_1u_3 + u_2u_3] v_3$$

$$\text{and}, b = \sum_{k,j,=1}^{n} \nu_k u_i \frac{\partial^2 f_k}{\partial x_i \partial \phi}(0,0) = -\begin{bmatrix} \frac{C^*}{C^*+N} u_1 + \frac{NS^*}{(C^*+N)^2} u_3 \end{bmatrix} v_1 + \begin{bmatrix} \frac{C^*}{C^*+N} u_1 + \frac{NS^*}{(C^*+N)^2} u_3 \end{bmatrix} v_2 \Bigg| \quad (1.5)$$

Now for sufficient condition for global stability of $\varepsilon^*$ consider the following positive definite function around $\varepsilon^*$:

$$\Gamma = \frac{q_1}{2}\left(S - S^*\right)^2 + \frac{q_2}{2}\left(I - I^*\right)^2 + \frac{q_3}{2}\left(C - C^*\right)^2$$

$$\frac{d\Gamma}{dt} = \left(S - S^*\right)\frac{dS}{dt} + \left(I - I^*\right)\frac{dI}{dt} + \left(C - C^*\right)\frac{dC}{dt}$$

$$= q_1\left[ AS(1 - \frac{S}{k_1}) - eS\frac{C}{N+C} - eiSI - mS + rI \right]\left(S - S^*\right) +$$

$$q_2\left[ eS\frac{C}{N+C} + eiSI - (m + r + v)I \right]\left(I - I^*\right)$$

$$+ q_3\left[ \frac{g - m_0 C - l(S+I)C}{V} \right]\left(C - C^*\right)$$

For sufficient condition for global stability $\frac{d\Gamma}{dt}$ will be negative definite, showing $\Gamma$ isa Lyapunov function with respect to $\varepsilon^*$ whose domain is contained in $\phi$.

## 2. Stochastic Extension of the Model

Early modelling contributions for infectious disease spread were often for specific diseases. For example Bernoulli aimed at evaluating the effectiveness a certain technique of variolation against smallpox, and Ross modelled the transmission of malaria. One of the first more general and rigorous studies was made by Kermack and McKendrick [13]. Later important contributions were for example by Bartlett [14] and Kendall [15], both also considering stochastic models. Early models were often deterministic and the type of questions that were addressed were for example: Is it possible that there is a big outbreak infecting a positive fraction of the community?, How many will get infected if the epidemic takes off?, What are the effects of vaccinating a given community fraction prior to the arrival of the disease?, What is the endemic level? As problems were resolved, the simple models were generalised in several ways towards making them more realistic. Some such extensions were for example to allow for a community where there are different types of individual, allowing for non-uniform mixing between individuals (i.e. infectious individuals don't infect all individuals equally likely), for example due to social or spatial aspects, and to allow seasonal variations. A stochastic model is of course preferable when studying a small community. But, even when considering a large community, which deterministic models primarily are aimed for, some additional questions can be raised when considering stochastic epidemic models. For example: What is the probability of a major outbreak? and for models describing an endemic situation: How long is the disease likely to persist (with or without intervention)? Later stochastic models have also shown to be advantageous when the contact structure in the community contains small complete graphs; households and other local social networks being common examples. Needless to say, both deterministic and stochastic epidemic models have their important roles to play.

Here we consider two compartments corresponding to susceptible and infective individuals. We will use the letters S and I respectively to refer to the compartments and also, without confusion we hope, to the number of individuals in each class. It is assumed that the total number of individuals is constant and equal to N, that is, S+I = N. An individual who belongs to the class S may be contacted by an individual in I, who can transfer the infection. If that is the case, the susceptible individual changes his classification and belongs now to the class I, where he will remain indefinitely. Assume that individuals in each compartment are interchangeable, that the classes are homogeneously mixed, and that contacts between susceptible and infective individuals, or equivalently the movement of individuals from the class S to the class I, occur at random times. If β is the average number of contacts made by an average infective per unit of time that leads to an infection, the probability of a susceptible individual moving from class S to class I in the time interval [t; t +Δt], that is,

$S \to S-1, and, I \to I+1$ is $\beta \frac{SI}{N}\Delta t + O(\Delta t)$.

This stochastic infection rate has come to be widely used, with various possible interpretations of the N in the denominator. One can think of each

susceptible contacting everyone in the population with a rate b and encountering a proportion I=N of infectives. Or one may think of each infective contacting everyone in the population with a rate β and encountering a proportion S=N of susceptibles. Or one may think of the N in the denominator as a reduction of the infection rate due to incomplete mixing in population. From this last point of view, the denominator might be a different power of N or some other function of N [16]. The process ($S_t$ ; $I_t$ ), will represent the number of susceptible and infective individuals at time t. The probability of an infection during the time interval

t ; t+ Δt] is :

$$P\left(\left(S_{t+\Delta t}, I_{t+\Delta t}\right)-\left(S_t; I_t\right)=(-1,1)\right)=\beta\frac{S_t I_t}{N}\Delta t+O(\Delta t)$$

with the complementary probability

$$P\left(\left(S_{t+\Delta t}, I_{t+\Delta t}\right)-\left(S_t; I_t\right)=(0,0)\right)=1-\beta\frac{S_t I_t}{N}\Delta t+O(\Delta t)$$

taking the limit $\Delta t \to 0$ and applying the extension on deterministic model (1) we get the continuous stochastic SIS model with probabilities of susceptible, infectious and concentration as:

$$\begin{cases}\dfrac{dS}{dt}=AS(1-\dfrac{S}{k_1})-eS\dfrac{C}{N+C}-eiSI-mS+rI+\eta_1\\ \dfrac{dI}{dt}=eS\dfrac{C}{N+C}+eiSI-(m+r+v)I+\eta_2\\ \dfrac{dC}{dt}=\dfrac{1}{V}\left[g-m_0C-l(S+I)C\right]+\eta_3\end{cases} \quad (2)$$

Here we apply Gaussian additive white noise to incorporate randomness of the infection spread. Where $\eta_i(t)$, i =1, 2, 3, are additive Gaussian white noise characterize by $\langle\eta_i(t)\rangle$ = 1, and $\langle\eta_i(t\ ),\eta_j(t_1)\rangle=2\xi\delta_{ij}(t-t_1)$ for ; i, j = 1, 2, 3. Where ξ is the intensity or strength of the random perturbation, $\delta_{ij}$ is the Dirac delta function with t and $t_1$ being the distinct times, and the bracket $\langle\ \rangle$ represents the ensemble average.

Further more realistic model with randomness is obtained by adding independent noise terms each proportional to square root of corresponding terms in the differential equation; that is each interaction term is assumed to fluctuate randomly and the fluctuation is proportional to the square root of the interaction, as follows:

$$\begin{cases}\dfrac{dS}{dt}=AS(1-\dfrac{S}{k_1})-eS\dfrac{C}{N+C}-eiSI-mS+rI-\sqrt{AS(1-\dfrac{S}{k_1})}\eta_1+\sqrt{eS\dfrac{C}{N+C}}\eta_2+\sqrt{eiSI}\,\eta_3+\sqrt{mS}\,\eta_4-\sqrt{rI}\,\eta_5\\ \dfrac{dI}{dt}=eS\dfrac{C}{N+C}+eiSI-(m+r+v)I-\sqrt{eS\dfrac{C}{N+C}}\eta_2-\sqrt{eiSI}\,\eta_3+\sqrt{rI}\,\eta_5+\sqrt{(m+v)I}\,\eta_6\\ \dfrac{dC}{dt}=\dfrac{1}{V}\left[g-m_0C-l(S+I)C\right]+\sqrt{\dfrac{l(S+I)C}{V}}\eta_7-\sqrt{C}\,\eta_8\end{cases} \quad (2.1)$$

Where $\eta_i(t)$, i =1, 2,....., 8 are statistically independent Gaussian random variables with zero mean and unit variance and the stochastic term is proportional to the square root of each term.

## 3. Spatiotemporal SIS Model with Advection-Diffusion Equation

Advection-dispersion equation with reaction is applicable various disciplines of engineering such as chemical engineering, petroleum engineering, civil engineering, etc to describe the behaviour of solute concentration. Warrick [17,18] shown the miscible displacement processes with time-varying velocity and dispersion coefficients and solutions are used in the analysis of experimental data. Van Genuchten [19] had obtained the solutions for Advection Dispersion equation with reaction analytically. Ataie-Ashtiani [20] examined an explicit finite difference scheme for the truncation errors on the solution of an advection – dispersion with a first order reaction term. Consider the one-dimensional flow of underground water through fixed soil or rock matrix. In this work, the fixed soil through which water is flowing is represented as saturated homogeneous porous medium. Porosity of the porous medium is 'ω', considering as a constant. Let C(x, t) be the concentration of a chemical, radiological or biological tracer dissolved in the water; S(x, t) and I(x, t) are the biomass of susceptible and infectious individuals respectively. The concentration is measured as mass of tracer present per unit volume of water or soil. The movement of tracer particles in soil by the bulk motion of water signifies [21,22]. The spreading of tracer in water due to the variability of macroscopic velocities through the pores of the soil is mentioning the Dispersion. Let D be the dispersion coefficient of the dispersion [21]. The tracer created or destroyed with rate k, measured in mass per unit volume of soil per unit time, referred as Reaction term

[21]. Using reaction term we can measure the decay rate, the rate of consumption in a chemical reaction and even growth or death rate can obtain if the tracer is biological. The specific discharge of water through the soil is denoted as U, which is the Darcy velocity. Assume U is a constant [21]. The velocity 'u 'of the tracer in water is expressed as $u = \frac{U}{\omega}$ known as average velocity. The basic physical law for the flow of fluid through a porous medium is derived from the mass balance of the tracer. By using the Mass Balance Law, we get the equation for one-dimensional advection –dispersion with reaction and expressed as follows:

$$\begin{cases} \frac{\partial S}{\partial t} = \frac{\partial^2 S}{\partial x^2} + AS(1-\frac{S}{k_1}) - eS\frac{C}{N+C} - eiSI - mS + rI \\ \frac{\partial I}{\partial t} = \frac{\partial^2 I}{\partial x^2} + eS\frac{C}{N+C} + eiSI - (m+r+v)I \\ \frac{\partial C}{\partial t} = D\frac{\partial^2 C}{\partial x^2} - u\frac{\partial C}{\partial x} - kC - l(S+I)C \end{cases}$$

With boundary condition S(0,t)=0, I(0,t)=0 and $C(0,0)=c_0$ and

$$\frac{\partial C(0,t)}{\partial t} = \frac{1}{V}[g - m_0 C] \text{ and } \frac{\partial S(L,t)}{\partial x} = \frac{\partial I(L,t)}{\partial x} = \frac{\partial C(L,t)}{\partial x} = 0$$

Where u is the water velocity, ($LT^{-1}$), D is the dispersion coefficient, ($L^2T^{-1}$), k is the first order reaction rate coefficient, ($T^{-1}$), x is the distance from the centre of contamination (L)

## 4. Spatiotemporal SIS Model with Fuzzy Parameters

Physical models often have some uncertainty in their parameters and estimates are usually based on statistical methods and experimental data. Since Zadeh [23] introduced the concept of fuzzy sets, there has been a great deal of research in this area, including studies of fuzzy partial differential equations (PDEs). The concept of fuzzy derivative was first introduced by S.L. Chang [24]. It was followed by D.Durbis [25]. Other methods have been discussed by O. Kaleva [26, 27] and by S.Seikkala [28]. The numerical methods for solving fuzzy differential equations were introduced using standard Euler method[29]. J. Buckley [30] proposed a procedure to examine solutions of fuzzy partial equation. They checked to see if the Buckley-Feuring solution exists. If the Buckley-Feuring solution fails to exist they check if the Seikkala solution exists. In this paper we consider the parameters for the fuzzy partial differential model system are considered as fuzzy numbers taking into account the lack of precise knowledge [31]. From a theoretical point of view, we show the continuity of the deterministic solution with respect to the parameters. This provides a method for building numerical simulations to obtain qualitative properties of the fuzzy solution. Some studies considered application of PDEs with fuzzy parameters obtained through fuzzy rule-based systems Jafelice [32]. Oberguggenberger [33] described weak and fuzzy solutions for PDEs and Chen et al. [34] presented a new inference method with applications to PDEs. More recently Cecconello et. al. [35] used Zadeh's extension principle to determine a fuzzy solution for a PDE with initial fuzzy conditions.

Definition 4.1: Let X be a nonempty set. A fuzzy set u in X is characterized by its membership function u: X→[0,1]. Then $(x)$ is interpreted as the degree of membership of a element x in the fuzzy set u for each $x \in X$. Let us denote by $\mathbb{R}_F$ the class of fuzzy subsets of the real axes i.e. u: $\mathbb{R}\to[0,1]$ satisfying the following properties:

(i) $\forall u \in \mathbb{R}_F$, u is normal, i.e. $\exists x_0 \in \mathbb{R}$ with $u(x_0) = 1$;

(ii) $\forall u \in \mathbb{R}_F$, $u$ is convex fuzzy set(i.e. $u(tx+(1-t)y) \geq \min\{u(x), u(y)\}, \forall\, t \in [0,1], x, y \in \mathbb{R}$;

(iii) $\forall u \in \mathbb{R}_F$, $u$ is upper semi-continuous on R;

(iv) $cl\{x \in R; u(x) > 0\}$ is compact, where $cl(A)$ denotes the closure of subset A.

Then $\mathbb{R}_F$ is called the space of fuzzy numbers. Obviously $\mathbb{R} \subset \mathbb{R}_F$. For $0 < \alpha \leq 1$ denote

$[u]^\alpha = \{x \in \mathbb{R}; u(x) \geq \alpha\}$ and $[u]^0 = cl\{x \in R; u(x) > 0\}$. Then it is well-known that for each $\alpha \in [0, 1]$, $[u]^\alpha$ is a bounded closed interval.

For $u, v \in \mathbb{R}_F$, $\lambda \in \mathbb{R}$, the sum $u + v$ and $\lambda.u$ are defined by $[u+v]^\alpha = [u]^\alpha + [v]^\alpha$, $[\lambda.u]^\alpha = \lambda[u]^\alpha$, $\forall\, \alpha \in [0, 1]$, where $[u]^\alpha + [v]^\alpha$ means the usual addition of two intervals of R and $\lambda[u]^\alpha$ means the usual product between a scalar and a subset of $\mathbb{R}$. The metric structure is given by the Hausdorff distance $D$: $\mathbb{R}_F \times \mathbb{R}_F \to \mathbb{R} + \cup\{0\}$

$$D(u,v) = \sup_{\alpha \in [0,1]} \max\left\{\left|\underline{u}_\alpha - \underline{v}_\alpha\right|, \left|\overline{u^\alpha} - \overline{v^\alpha}\right|\right\}$$

Where $[u]^\alpha = [\underline{u^\alpha}, \overline{u^\alpha}]$, $[v]^\alpha = [\underline{v}^\alpha, \overline{v^\alpha}]$, $(\mathbb{R}_F, D)$is a complete space and the following properties are well-known: $D(u+w, v+w) = D(u,v), \forall u, v, w \in \mathbb{R}_F$,

$D(k.u, k.v) = |k| D(u,v), \forall k \in \mathbb{R}, u, v \in \mathbb{R}_F$, , $(u+v, w+e) \leq (u,) + (v,)$ , $\forall u, v, w, e \in \mathbb{R}_F$.

Definition 4.2: Let $x \in \mathbb{R}_F$. If there exists $z \in \mathbb{R}_F$ such that $x = y+z$, then $z$ is called the H-difference of $x$ from y and it is denoted by $x \ominus y$.

- Note that $x \ominus y \neq x + (-1).\, y = x - y$.

Bede [36] introduced a more general definition of a derivative for a fuzzy-number-valued function. In this paper we consider the following definition [37].

The extension of a map between fuzzy sets, the so-called fuzzification of the map ,is defined by Zadeh's extension principle as follows:

Definition 4.3: The Zadeh extension of a function $f : X \to Z$ where X and Z are nonempty metric spaces, is a function $\hat{f}$ that, when applied to a fuzzy set $D \subset X$, returns a fuzzy set $\hat{f}(D)$ in Z, the membership function of which is

$$\mu_{\hat{f}(D)}(Z) = \begin{cases} \sup^{\mu_D(X)}_{\{X : f(X) = Z\}}, if \to \{X : f(X) = Z\} \neq \Phi \\ 0, otherwise \end{cases}$$

- Note that $\hat{f}(D) = f(D)$ if D is a classical set of X.

As a consequence of Zadeh's extension principle, we have that the image of a strong α-cut is a strong α-cut of the extension. It has been proved that this property holds for α-cuts that are not necessarily strong, provided that f is continuous [38,39]. We summarize this property in the following proposition.

Proposition: Let X and Z be nonempty metric spaces, let D be a fuzzy set of X and let $f : X \to Z$ be continuous. Then for every $0 \le \alpha \le 1, \left[\hat{f}(D)\right]^{\alpha} = f\left([D]^{\alpha}\right)$.

Definition 4.4: Let $f : I \to \mathbb{R}_F$ be given. Fix $t_0 \in I$. We say $f$ is 1-differentiable at $t_0$ and its derivative denoted by $D_1 f$, if there exists an element $f'(t_0) \in \mathbb{R}_F$ such that for all h>0 sufficiently small, there exist $f(t_0+h) \ominus f(t_0)$, $f(t_0) \ominus f(t_0-h)$ and the following limits (in metric Hausdorff): where we fix $I = (a,b)$, for $a,b \in \mathbb{R}$.

$$\lim_{h \to 0^+} \frac{f(t_0+h) \ominus f(t_0)}{h} = \lim_{h \to 0^+} \frac{f(t_0) \ominus f(t_0-h)}{h} = f'(t_0).$$

Similarly a function $f$ is 2-differentiable at $t_0$ and its derivative denoted by $D_2 f$, if there exists an element $f'(t_0) \in \mathbb{R}_F$ such that for all h>0 sufficiently small, there exist $f(t_0+h) \ominus f(t_0)$, $f(t_0) \ominus f(t_0-h)$ and the following limits:

$$\lim_{h \to 0^-} \frac{f(t_0+h) \ominus f(t_0)}{h} = \lim_{h \to 0^-} \frac{f(t_0) \ominus f(t_0-h)}{h} = f'(t_0).$$

Theorem 4.1: Let $F : I \to \mathbb{R}_F$ and put $[F(t)]^{\alpha} = [f_{\alpha}(t), g_{\alpha}(t)]$ for each $\alpha \in [0,1]$.

(i) If $F$ is 1-differentiable then $f_{\alpha}$ and $g_{\alpha}$ are differentiable functions and $[D_1 F(t)]^{\alpha} = [f_{\alpha}'(t), g_{\alpha}'(t)]$.

(ii) If $F$ is 2-differentiable then $f_{\alpha}$ and $g_{\alpha}$ are differentiable functions and $[D_2 F(t)]^{\alpha} = [g_{\alpha}'(t), f_{\alpha}'(t)]$.

Proof. See [37].

Definition 4.5. Generalized Characterization Theorem

Let us consider the FDE with initial value condition:

$$x'(t) = f(t,x),\ x(t_0) = x_0 \tag{4.1}$$

Where $f$: $[t_0,T] \times \mathbb{R}_F \to \mathbb{R}_F$ is a continuous fuzzy mapping and $x_0 \in \mathbb{R}_F$ and $T$ is positive number or infinity with $x_0$ fuzzy initial condition defined on the n-dimensional domain Y. We interpret this notation as a fuzzy extension of an ordinary differential equation. We consider a fuzzy differential equation as a deterministic differential equation where some coefficients or initial condition are uncertain and represented in a possibilistic form: its solution is then the time evolution of a fuzzy region of uncertainty which Corresponds to the possibility distribution in the phase space.

Theorem 4.2: Let $f$: $[t_0,] \times \mathbb{R}_F \to \mathbb{R}_F$ is a continuous fuzzy function. If there exists $k > 0$ such that $D(f(t,x), f(t,z)) \le kD(x,z)$ ,$\forall t \in I, x,y \in \mathbb{R}_F$. Then the problem (1) has two solutions on I. One is 1-differentiable solution and the other one is 2-differentiable solution.

Proof. See [37].

Definition 4.6: Let $y : I \to \mathbb{R}_F$ be a fuzzy function such that $D_1 y$ or $D_2 y$ exists. If $y$ and $D_1 y$ satisfy problem (1), we say $y$ is a 1-solution of problem (1). Similarly, if $y$ and $D_2 y$ satisfy problem (1), we say $y$ is a 2-solution of problem (1).

By using theorem 4.1 we can state useful approach for solving FBVP for partial differential system: Let us suppose α-cut of functions u(t,x), $f(t,x,u)$ , u(0, x), u(t, L), u(0,x) are the following form:

$$\left.\begin{array}{l} [u(t,x)]^{\alpha} = [\underline{u}_{\alpha}(t,x), \overline{u}_{\alpha}(t,x)], [u(0,x)]^{\alpha} = [\underline{u}_{\alpha}(0,x), \overline{u}_{\alpha}(0,x)] \\ [u(t,x)]^{\alpha} = [\underline{u}_{\alpha}(t,x_i), \overline{u}_{\alpha}(t,x_i)], [u(t,x_f)]^{\alpha} = [\underline{u}_{\alpha}(t,x_i), \overline{u}_{\alpha}(t,x_f)] \\ [f(t,x,u(t,x))]^{\alpha} = [\underline{f_{\alpha}}(t,x,\underline{u}_{\alpha}(t,x), \overline{u}_{\alpha}(t,x)), \overline{f_{\alpha}}(t,x,\underline{u}_{\alpha}(t,x), \overline{u}_{\alpha}(t,x))] \end{array}\right] \tag{4.2}$$

Then we have two following cases:

Case (I): if u(t, x) is 1-differentiable then solving FBVP (1) translates into the following algorithm:

Step (i) Solving the following system of PDEs:

**Table 1. Estimated model parameters and their interpretation:**

| Parameters | `Temporal Model (1), (2), (2.1) | Spatiotemporal Model (3) | Fuzzy Spatiotemporal Model (4.5) | Units |
|---|---|---|---|---|
| Intrinsic growth rate (A) | A=1.3; | A=1.3; | A=[0.91,1.3]; | $T^{-1}$ |
| Rate of infection spread by contaminant (e) | e=0.62; | e=0.62; | e=[0.053,0.62]; | $T^{-1}$ |
| Rate of infection spread by infectious (ei) | ei=0.045; | ei=0.045; | ei=[0.045,0.078]; | $T^{-1}$ |
| Natural mortality rate (m) | m=0.2; | m=0.2; | m=[0.2,0.4]; | $T^{-1}$ |
| Recovery rate of infectious (r) | r=0.28; | r=0.28; | r=[0.28,0.36]; | $T^{-1}$ |
| Infection induced death rate (v) | v=0.52; | v=0.52; | v=[0.24,0.52]; | $T^{-1}$ |
| Average rate of intake of contaminant by others (l) | l=0.02; | l=0.0002; | l=[0.0002,0.0005]; | $T^{-1}$ |
| Half saturation constant for infection by contaminant (N) | N=12.77; | N=12.77; | N=[12.77,18.66]; | $M\,L^{-1}$ |
| Decay rate of contaminant ($m_0$) | $m_0$=0.05; | m0=0.05; | m0=[0.05,0.07]; | $M\,T^{-1}$ |
| Initial concentration ($c_0$) | c0=0.0887; | c0=0.0887; | c0=[0.0887,0.11]; | $M\,L^{-1}$ |
| Volume of the environment (V) | V=50; | V=65; | V=[65,85]; | $L^3$ |
| Rate of deposition of contaminant (g) | g=0.4215; | g=0.42; | g=[0.33;0.42]; | $M\,T^{-1}$ |
| First order reaction rate coefficient (k) | k=0; | k=0.1; | k=[0.1,0.3]; | $T^{-1}$ |
| Dispersion coefficient (D) | D=0; | D=1; | D=[1,2.11]; | $L^2T^{-1}$ |
| Medium velocity (u) | u=0; | u=1.71; | u=[1.71,2.33]; | $LT^{-1}$ |
| Half saturation constant for logistic growth ($k_1$) | $k_1$=18.66 | $k_1$=18.66 | $k_1$=[14.46,20.66] | unit less |

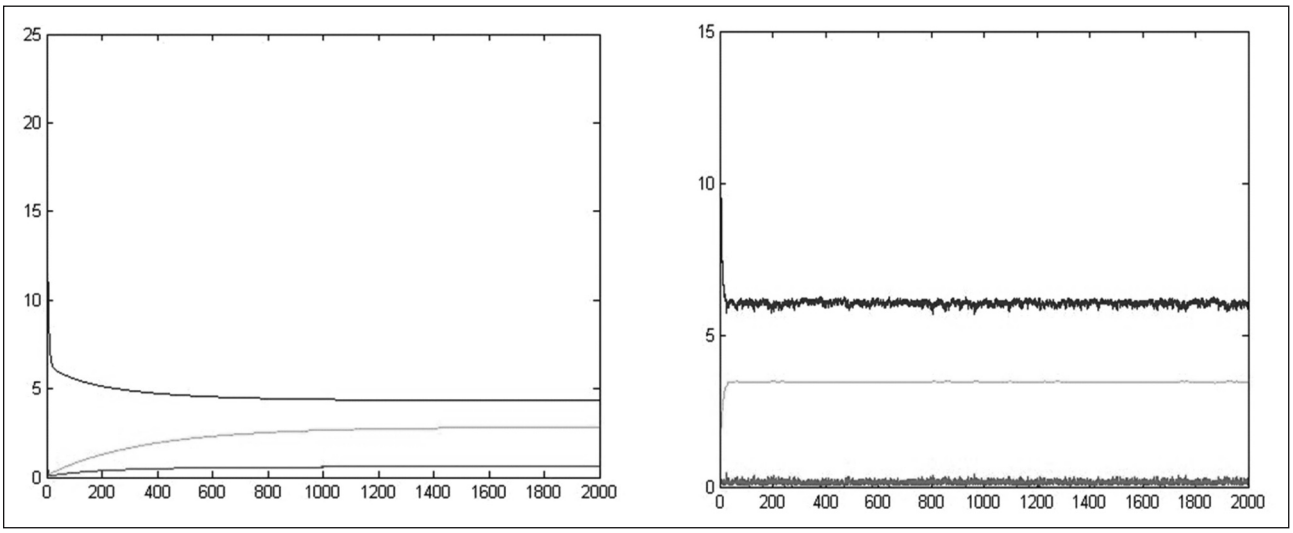


*Figure 1. Deterministic (left) and Stochastic (with additive noise) (right) time evaluation of the model system -- susceptible (S) in blue, Infectious (I) in red and Concentration (C) in green.*

$$\left.\begin{aligned}
&\underline{u}'_\alpha(t,x) = \underline{f}_\alpha(t,x,\underline{u}_\alpha(t,x),\overline{u}_\alpha(t,x)) = F(t,x,\underline{u}_\alpha(t,x),\overline{u}_\alpha(t,x)),\left[u(0,x)\right]^\alpha = \underline{u}_\alpha(0,x)\\
&\left[u(t,x_i)\right]^\alpha = \underline{u}_\alpha(t,x_i),\left[u(t,x_f)\right]^\alpha = \underline{u}_\alpha(t,x_i)\\
&\overline{u}'_\alpha(t,x) = \overline{f}_\alpha(t,x,\underline{u}_\alpha(t,x),\overline{u}_\alpha(t,x)) = G(t,x,\underline{u}_\alpha(t,x),\overline{u}_\alpha(t,x)),\left[u(0,x)\right]^\alpha = \overline{u}_\alpha(0,x)\\
&\left[u(t,x_i)\right]^\alpha = \overline{u}_\alpha(t,x_i),\left[u(t,x_f)\right]^\alpha = \overline{u}_\alpha(t,x_i)
\end{aligned}\right] \quad (4.3)$$

Step (ii) Ensure that the solution $\left[\underline{u}_\alpha(t,x),\overline{u}_\alpha(t,x)\right]$ and $\left[\underline{u}'_\alpha(t,x),\overline{u}'_\alpha(t,x)\right]$ are valid level sets.

Step (iii) by using the representation theorem again, we construct a 1-solution ($t$) such that $\left[u(t,x)\right]^\alpha = \left[\underline{u}_\alpha(t,x),\overline{u}_\alpha(t,x)\right]$, for all α∈[0,1].

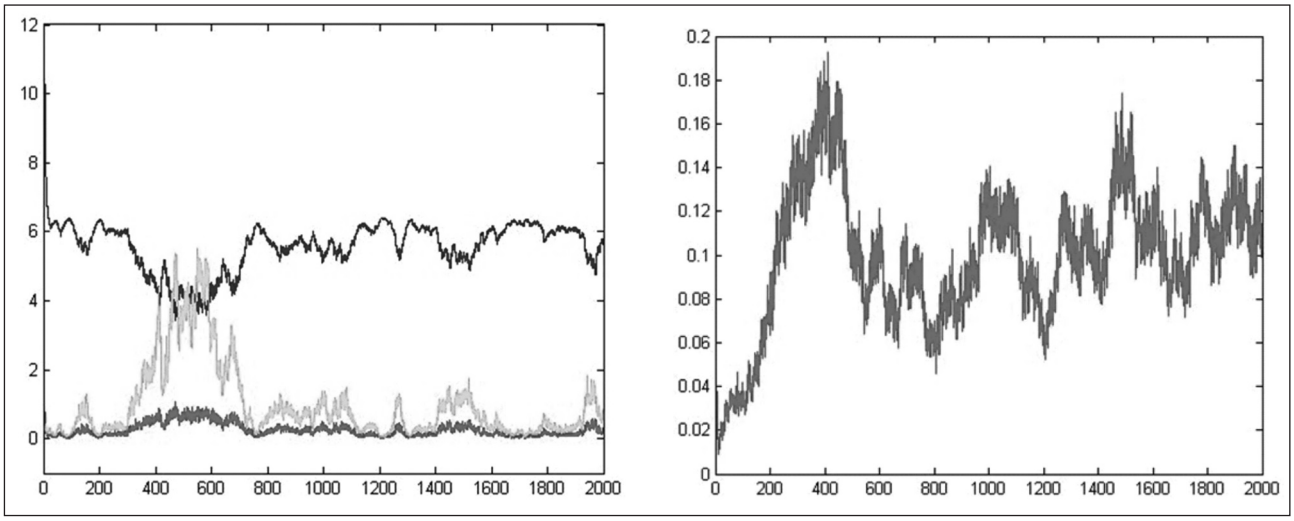


*Figure 2. Stochastic (with white noise proportional to the square root of each term) time evaluation (left) of the model system and probability of infection (right) -- susceptible (S) in blue, Infectious (I) in red and Concentration (C) in green.*

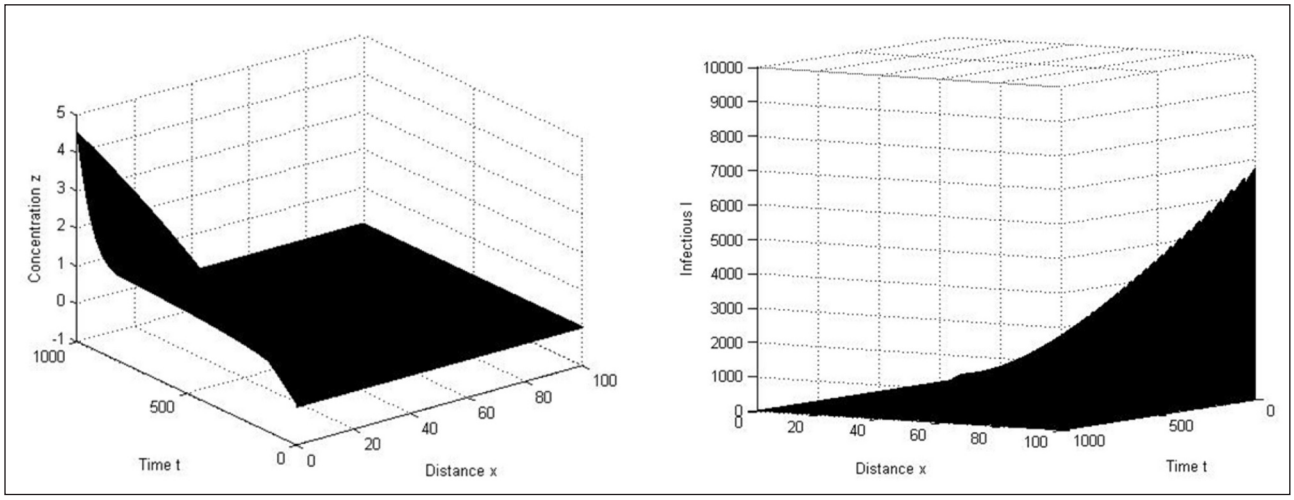


*Figure 3. Deterministic spatiotemporal evaluation of the model system concentration (left) Infectious (right).*

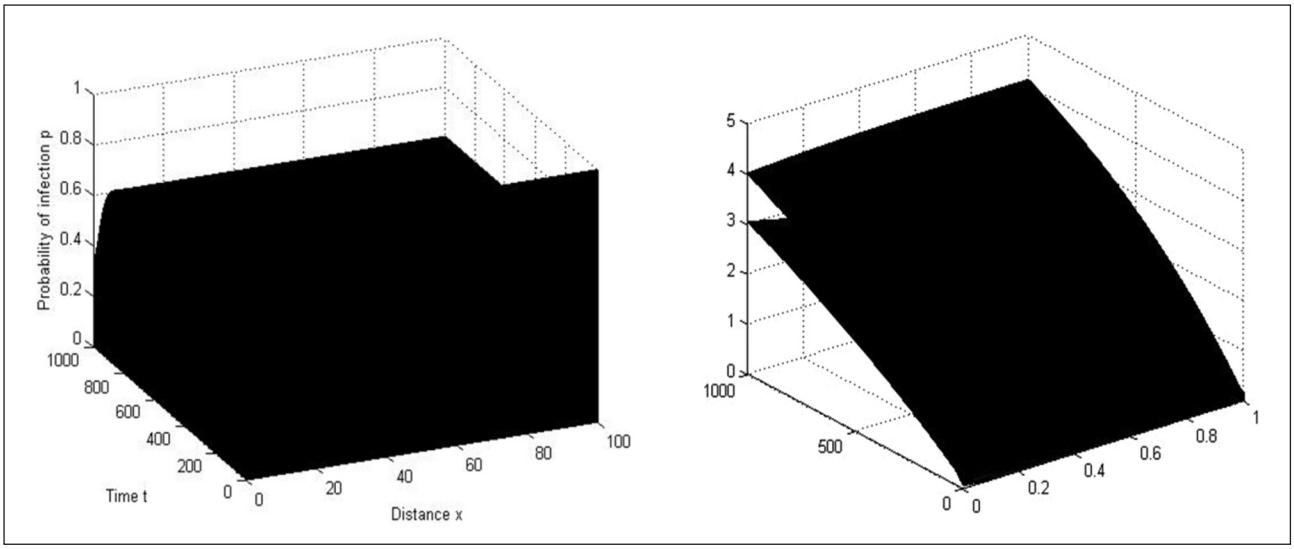


*Figure 4. Deterministic spatiotemporal evaluation of the model system for probability of being infected (left). Spatiotemporal evaluation of the model system with fuzzy parameters concentration (right)*

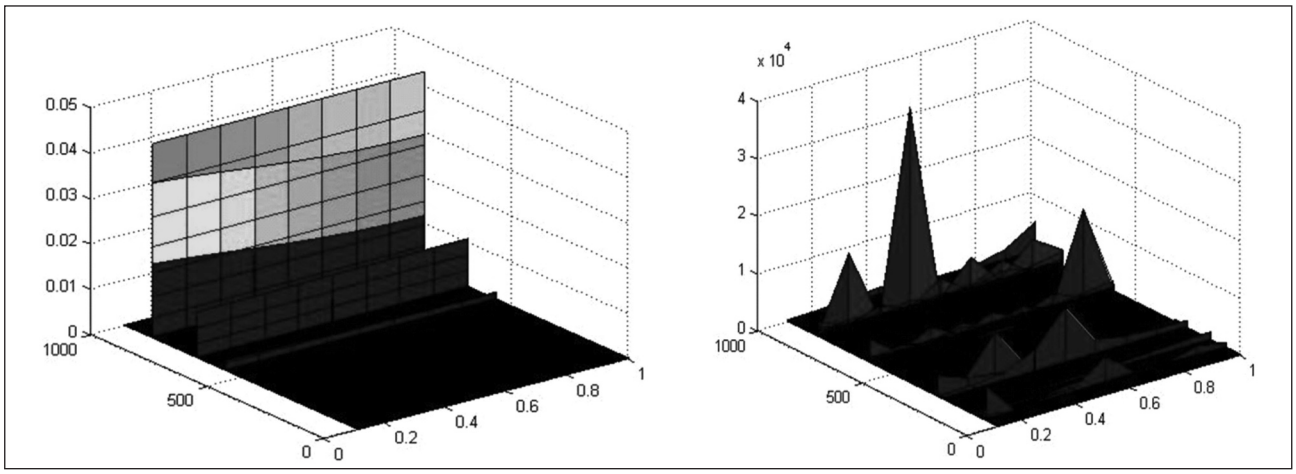


*Figure 5. Spatiotemporal evaluation of the model system with fuzzy parameters for possibility of being infected; maximum (left) and minimum (right) possibility of infection.*

Case (II): if u($t$, x) is 2-differentiable then solving FBVP (1) translates into the following algorithm:

Step (i) Solving the following system of ODEs:

$$\left.\begin{array}{l} \underline{u}'_\alpha(t,x)=\underline{f}_\alpha(t,x,\underline{u}_\alpha(t,x),\overline{u}_\alpha(t,x))=G(t,x,\underline{u}_\alpha(t,x),\overline{u}_\alpha(t,x)),\left[u(0,x)\right]^\alpha=\underline{u}_\alpha(0,x) \\ \left[u(t,x_i)\right]^\alpha=\underline{u}_\alpha(t,x_i),\left[u(t,x_f)\right]^\alpha=\underline{u}_\alpha(t,x_i) \\ \overline{u}'_\alpha(t,x)=\overline{f}_\alpha(t,x,\underline{u}_\alpha(t,x),\overline{u}_\alpha(t,x))=F(t,x,\underline{u}_\alpha(t,x),\overline{u}_\alpha(t,x)),\left[u(0,x)\right]^\alpha=\overline{u}_\alpha(0,x) \\ \left[u(t,x_i)\right]^\alpha=\overline{u}_\alpha(t,x_i),\left[u(t,x_f)\right]^\alpha=\overline{u}_\alpha(t,x_i) \end{array}\right\} \quad (4.4)$$

Step (ii) Ensure that the solution $\left[\underline{u}_\alpha(t,x),\overline{u}_\alpha(t,x)\right]$ and $\left[\underline{u}'_\alpha(t,x),\overline{u}'_\alpha(t,x)\right]$ are valid level sets.

Step (iii) by using the representation theorem again, we construct a 1-solution ($t$) such that

$\left[u(t,x)\right]^\alpha=\left[\underline{u}_\alpha(t,x),\overline{u}_\alpha(t,x)\right]$, for all α∈[0,1].

Thus we extend our previous model to FBVP by considering fuzzy parameters to capture natural fluctuation in real system. Here the model is same with (1) but all the parameters and the state variables are fuzzy and indicated by 'bar' at the top.

$$\begin{cases} \dfrac{\partial\overline{S}}{\partial t}=\dfrac{\partial^2\overline{S}}{\partial x^2}+\overline{A}\overline{S}(1-\dfrac{\overline{S}}{\overline{k}_1})-\overline{e}\overline{S}\dfrac{\overline{C}}{\overline{N}+\overline{C}}-\overline{f}\overline{S}\overline{I}-\overline{m}\overline{S}+\overline{r}\overline{I} \\ \dfrac{\partial\overline{I}}{\partial t}=\dfrac{\partial^2\overline{I}}{\partial x^2}+\overline{e}\overline{S}\dfrac{\overline{C}}{\overline{N}+\overline{C}}+\overline{f}\overline{S}\overline{I}-(\overline{m}+\overline{r}+\overline{v})\overline{I} \\ \dfrac{\partial\overline{C}}{\partial t}=\overline{D}\dfrac{\partial^2\overline{C}}{\partial x^2}-\overline{u}\dfrac{\partial\overline{C}}{\partial x}-\overline{k}\overline{C}-\overline{l}(\overline{S}+\overline{I})\overline{C} \end{cases} \quad (4.5)$$

With boundary condition $\overline{S}(0,t)=[0,0];\overline{I}(0,t)=[0,0],\overline{C}(0,t)=[\underline{c}_0,\overline{c}_0]$ and

$$\frac{\partial\overline{C}(0,t)}{\partial t}=\frac{1}{\overline{V}}\left[\overline{g}-\overline{m}_0\overline{C}\right] \text{ and}$$

$$\frac{\partial\overline{S}(L,t)}{\partial x}=\frac{\partial\overline{I}(L,t)}{\partial x}=\frac{\partial\overline{C}(L,t)}{\partial x}=0$$

Where $\overline{u}$ is the water velocity, ($LT^{-1}$), $\overline{D}$ is the dispersion coefficient, ($L^2T^{-1}$), $\overline{k}$ is the first order reaction rate coefficient, ($T^{-1}$),are fuzzy parameters and x is the distance from the centre of contamination (L).

## 5. Numerical simulation

Numerical simulations of model systems are carried out using a set of parameter values given in the table 1. A fourth ordered Runge-Kutta numerical scheme coded in C++ programming language, Mathematica 9.0 and Matlab R2012a is used in numerical simulation. The result of the simulation is presented in graphically in the next section.

## 6. Result and Discussion

In this section we present the solution of our model systems with an estimated set of deterministic and interval valued fuzzy parameters. The spatiotemporal distribution of concentration, infectious, susceptible and risk in term of probability and possibility of being infected by a contamination induced diseases or health hazards, are evaluated and shown graphically.

The deterministic simulation of model (1) shows the existence of endemic steady state; however the model doesn't have any disease free equilibrium. Hence if the rate of deposition of contaminant be positive, there is always a risk of human health hazard to spread.

However the stochastic models with Gaussian noise are found to fluctuate around the same average

value of the state variables. From this simulation stable nature of the steady state could be reviled. Also the probability of being infected is calculated at each time instance, which gives a probabilistic assessment of health hazard risk in temporal scale.

In model (3) the spatiotemporal description of the system allows to analyze the spatiotemporal behaviour of the health hazard spread. The simulation of the model shows how the state variables changes with time and the distance from the centre of deposition. In figure (3), (4), (5) the surfaces denotes the distribution of the state variables and the probability in two dimensional spatiotemporal framework.

Simulations of model (3) and (4.5) allow to assess the probability of occurring human health hazard in broader aspect. From the assessment of spatiotemporal distribution of that probability; the decision makers could sketch a danger zone; that is a region around the centre of deposition of the contaminant, were the probability of occurring human health hazard is above some desired threshold. Special strategy waste treatment and supervise the health condition of the habitat should be employed for this zone. However simulation of the model (4.5) with fuzzy parameters, here we consider interval valued fuzzy parameters; results a spatiotemporal distribution of the fuzzy valued state variables. The spatiotemporal distribution of the maximum and minimum value of the interval valued fuzzy state variables is found. In figure (4) the two surfaces, representing maximum and minimum values, of the spatiotemporal distribution of concentration of the contaminant.

Simulation of model (4.5) with fuzzy parameters allows to assess the possibility of occurring human health hazard under the imprecise parameter value. Thus in this framework we assess the maximum and minimum possibility of occurring human health hazard from contamination. Here the possibility of occurring human health hazard is a fuzzy number between 0 and 1. This minimum and maximum possibility could be assign as belief and plausibility function and carry out risk assessment through Evidence theory in case of lack of knowledge about the effect of some new type of contaminant. Thus maximum (plausibility) and minimum (belief) possibility of occurring human health hazard provides a base to assess risk in uncertain environment.

## 7. Conclusion

A mathematical model for assessing human health risk from biological, radiological, chemical etc. contamination incorporating spatial spread of the concentration of contaminant is presented as system of ordinary, stochastic, partial and fuzzy differential equations. The endemic equilibrium is obtained. The local stability of endemic is analyzed and shown to be locally asymptotically stable using central manifold theory and also supported by numerical results. The conditions for global stability are derived using a suitable Lyapunov function. By incorporating randomness (stochastic) fluctuation we have show the effect of natural perturbation to the model system and assess the probability of human health hazard risk caused by contaminant. This allows us to estimate the system average state and a deviation around it and provide a risk assessment framework under random perturbation. Also we consider the dynamics of spatiotemporal spread of concentration of contaminant as advection diffusion equation and analyzed numerically the spatiotemporal distribution of state variables and probability of human health hazard risk. This work could be a model for future to sketch different zone with same distribution of risk probability and employ same type of restoration strategy for them. In this paper the imprecise nature of the parameters in real system is incorporated by considering interval valued fuzzy parameters and thus provide a fuzzy possibility; that is an upper value and a lower value of possibility under the uncertainty of imprecision. This possibility could further be difuzzified by any standard method. Like any model development, our model is not without limitation. One limitation to the model simulation is with regard to the sensitivity analysis of parameters. This clearly compromises the conclusion of the simulation and the conclusion drawn. Also, the model that we proposed does not include many features of the complex spatiotemporal spread of contaminant and diseases causes by it and the complexity of heterogeneity of genotype. Nonetheless, the study highlights some important aspect of the dynamics of contaminant deposition and diseases caused by it. The model system is liable to apply and verify it's risk assessment at some real contaminated site by means of appropriate data collection, interpretation and parameter estimation. However, the model system shows that there is no disease free equilibrium state and alert about the necessity of employing suitable waste treatment and public health treatment plane. This model will be useful for public health planning and cost-effectiveness analysis.

## Reference


1. Ferson, S., (1996). "What Monte Carlo methods cannot do.", Human and Ecological Risk Assessment 2, 990e1007.
2. Roucher, R.S., Agras, J., Mills, D., Harrod, M., Chestnut, L., (2002), "Quantifying Public Health Risk Reduction Benefits", AWWA Research Foundation and AWWA, Denver, USA. ISBN 1-58321-192-6
3. Chen, S.J., Hwang, C.L., (1992). "Fuzzy Multiple Attribute Decision Making-Methods and Applications.", Springer-Verlag, Berlin, Germany. ISBN 3-540-54998-6.
4. Klir, Yuan, (1995), "Fuzzy Sets and Fuzzy Logic e Theory and Applications.", Prentice-Hall, Englewood Cliffs, NJ, USA.
5. Zimmermann, H.J., (2001)." Fuzzy Set Theory-and Its Applications", fourth ed. Kluwer Academic Publishers, Norwell, Massachusetts.
6. Chowdhury, S., (2004), " Decision Support System for Produced Water Discharges in Offshore Operations.", Master of Engineering Thesis, Memorial University of Newfoundland, Canada.
7. Dubois, D., Parade, H., (1988). "Possibility Theory: An Approach to Computerized to Uncertainty", first ed. Plenum, New York.
8. USEPA (U.S. Environmental Protection Agency), (1999b), "Cancer Risk Coefficients for Environmental Exposure to Ra dionuclides", Federal Guidance Report No. 13. EPA-402-R-99-001. Air and Radiation, Washington DC, USA.
9. Vegueria, S.F.J., Godoy, J.M., Miekeley, N., (2002). "Environmental impact in sediments and seawater due to discharges of Ba, 226Ra, 228Ra, V, Ni, and Pb by produced water from the Bacia de Campos Oil Field Offshore Platforms", Environmental Forensics 3, 115e123.
10. Hamilton, L.D., Meinhold, A.F., Nagy, J., (1992), "Health risk assessment for radium discharges in produced water", In: Ray, J.P., Engelhardt, F.R. (Eds.), Produced Water Technological/Environmental Issues and Solutions. Plenum Press, New York, pp. 303e314.
11. Stephenson, M.T., Supernaw, I.R., (1990)." Offshore Operators Committee 44 Platform Study Radionuclide Analysis Results", Offshore Operators Committee, New Orleans, Louisiana.
12. Anderson, R.M., May, R.M., (1992), "Infectious Diseases in Humans", Oxford University Press, Oxford, p. 4.
13. Kermack W.O, McKendrick A.G, (1927), "A contribution to the mathematical theory of epidemics", Proceedings of the Royal society of London. Series A, 115, no. 772, 700–721.
14. Bartlett M.S, (1949), "Some evolutionary stochastic processes", J. Roy. Statist. Soc. B, 11, 211–229.
15. Kendal D.G l, (1956), "Deterministic and stochastic epidemics in closed populations", Proc. Third Berkeley Symp. Math. Statist. Probab. 4, 149–165. University of California Press, Berkeley.
16. Stroud P.D, Sydoriak S.J, Riese J.M, Smith J.P, Mniszewski S.M, Romero P.R, (2006), "Semiempirical power-law scaling of new infection rate to model epidemic dynamics with inhomogeneous mixing", Mathematical Biosciences, 203, 301-318.
17. Warrick, A.W.; Lomen, D.O.; Yates, S.R. (1985), "A generalized solution to infiltration", Soil Science Society of America Journal 49: 34-38.
18. Warrick, A.W.; Mullen, G.J.; Nielsen, D.R. (1977), "Scaling of field measured hydraulic properties using a similar media concept", Water Resources Research 13: 355-362.
19. Van Genuchten, M. Th. and Alves, W. J.: (1982), "Analytical Solutions of the One-Dimension Convective-Dispersive Solute Transport Equation", US Depar tment of Agriculture, Techn Bulletin No. 1661, Washington, DC, USA, 151 pp.
20. Ataie-Ashtiani B, Lokhington DA, Volker RE., (1996), "Numerical correction for finite difference solution of the advection-dispersion equation with reaction", J. Contaminant Hydrology, Elsevier:, 23: 149-156.
21. Logan JD. (2001), "Transport modeling in Hydrogeochemical Systems", Springer, 15 (223): 50.
22. Cussier EL, (2007), "Diffusion- Mass Transfer in fluid systems", Cambridge University, 3: 1-57.
23. Zadeh L.A, (1965), "Fuzzy sets", Inf. Control 8, 338–353.
24. Chang S.L., Zadeh L.A., (1972), "On fuzzy mapping and control", IEEE Trans system Man Cybernet,2, 30-34.
25. Durbis D. , Prade H., (1982), "Towards fuzzy differential calculus", Part 3, Differential Fuzzy Sets and Systems 8, 225-233.
26. Kaleva O., (1990), "The Cauchy problem for fuzzy differential equations", Fuzzy Sets and Systems, 35, 389-396.
27. Kaleva O., (1987), "Fuzzy Differential Equation", Fuzzy Sets and Systems, 24, 301-317.
28. Seikkala S., (1987), "On the fuzzy initial value problem", Fuzzy Sets and Systems, 24, 319-330.
29. Ma M., Friedman M., Kandel A., (1999), "Numerical solution of fuzzy differential equations" , Fuzzy Sets and Systems, 105, 133-138.
30. Buckley J. and Feuring T., (1999), "Introduction to fuzzy partial differential equation", Fuzzy Sets and Systems, 241-248.
31. Dubois .D, Prade .H, (2012), "Gradualness, uncertainty and bipolarity: making sense of fuzzy sets", Fuzzy Sets Syst. 192 3–24.
32. Jafelice R.M, Almeida C.G, Meyer J.F, Vasconcelos H.L, (2011), "Fuzzy parameter in a partial differential equation model for population dispersal of leaf-cutting ants", Nonlinear Anal. Real World Appl. 12 3397–3412.
33. Oberguggenberger .M, (2004), "Fuzzy and weak solutions to differential equations", Proceedings of the 10th International IPMU Conference, pp. 517–524.
34. Chen Y.Y, Chang Y.T, Chen B.S, (2009), "Fuzzy solutions to partial differential equations: adaptive approach", IEEE Trans. Fuzzy Syst. 17) 116–127.
35. Cecconello M S., Leite J., Bassanezi R.C., and Silva J.M., (2013), "About Projections of Solutions for Fuzzy Differential Equations", Journal of Applied Mathematics Volume 2013 , Article ID 184950, http://dx.doi.org/10.1155/2013/184950.
36. Bede., S.G Gal S.G., (2005), "Generalizations of the differentiability of fuzzy-number-valued functions with applications to fuzzy differential equations", Fuzzy Sets and Systems 151, 581-599.
37. Chalco-Cano .Y, Roman-Flores .H, (2008), "On new solutions of fuzzy differential equations,Chaos", Solitons and Fractals 38, 112-119.
38. Barros . L.C, Bassanezi .R.C, Tonelli . P.A, (1997), "On the continuity of Zadeh's extension", Proceedings of the 7th IFSA World Congress, Prague, Vol. II, pp. 3–8.
39. Goo . H.Y, Park . J.S, (2007), "On the continuity of the Zadeh extensions", J. Chungcheong Math. Soc. 20 (4) 525–533.
40. Stephenson, M.T., Supernaw, I.R., (1990)." Offshore Operators Committee 44 Platform Study Radionuclide Analysis Results", Offshore Operators Committee, New Orleans, Louisiana.

*Life Cycle Reliability and Safety Engineering*
*Vol.2 Issue 4 (2013) 28-34*

# Reliability Evaluation of Weibull and Exponentiated Weibull Distribution Estimates for Wind Speed Data through Uncertainty Analysis

**[1]D. Datta and [2]Debanshee Datta**
*[1]Health Physics Division, Bhabha Atomic Research Centre, Mumbai*
*[2]Department of Instrumentation Engineering, A.C. Patil College of Engineering, Navi Mumbai*
*Email: ddatta@barc.gov.in*

Abstract

***Literature study reveals that the probability distribution of wind speed can be fitted by Weibull distribution and it has been accepted blindly without any statistical investigations. Uncertainty always presents in any curve fitting which should be taken into account prior to establish any distribution through any dataset. Similar to Weibull distribution, a better fitting of wind speed data is possible by Exponentiated Weibull distribution. Maximum likelihood method is adopted to estimate the parameters of the probable distribution prior its usage in any uncertainty analysis. Akaike information criterion has been applied to justify the best fit. Shannon entropy of Weibull and Exponentiated Weibull distribution has been computed to account the uncertainty associated with the random variable sampled from these two distributions. Mean and variance of wind speed data are computed by fitting through both Weibull and Exponentiated Weibull distributions. A comparison of the representative estimates through respective probability distributions is also presented in this study. The mail goal of this paper is to point out the better performance of the Exponentiated Weibull distribution compared to Weibull distribution in uncertainty and reliability analysis.***

***Keywords:*** *Weibull distribution, Exponentiated Weibull distribution, Maximum likelihood*

## 1. Introduction

There are two types of uncertainty, viz. (1) Aleatory uncertainty which is due to randomness of the parameters of any model, and (2) Epistemic uncertainty, which is due to fuzziness, vagueness of the model parameters. Measurement uncertainty falls into the category of epistemic type, which is alternately called as type-II uncertainty. Aleatory uncertainty cannot be reduced but epistemic uncertainty can be reduced by gaining sufficient knowledge of the parameters of interest. Therefore, uncertainty analysis of any system consisting of parameters which are random in nature and characterized by the probability distribution such as normal, lognormal, etc. can be quantified by propagation of their parametric uncertainty. Very often a model/system may not be possible to define in a closed form, especially in case of defining a system or any model through any data set. However, common practice is to fit a model through the defined data set. Therefore, it is very essential to evaluate the reliability of that fit assuming that the data is of good quality and highly reliable. At this point it can be easily stated that if the inherent uncertainty of the probability distribution selected for fitting the given data set is very large then the model defined by that data set through fitting is not reliable. That is to point out that uncertainty of the surrogate model should be as small as possible to declare it as highly reliable. So, evaluation of reliability of any surrogate model can be done through uncertainty analysis of the estimates of the relevant distribution parameter.

Environmental impact assessment (EIA) models depend on field or experimental data. As an example, EIA of any industry is always carried out with respect to the estimated concentration of the toxic pollutant at any instant of time and at any spatial location in the environment. Impact of the toxic effluent on the atmospheric environment if released into the atmosphere depends not only on the quantity released but also on the wind speed, wind direction, wind stability class, surface roughness, etc. Basic notion is here to notify that wind speed is one of the parameter required to know very accurately for assessing environmental impact. For example, according to Gaussian plume model, if wind speed increases then the concentration of the toxic effluent decreases at

any spatio-temporal location. Amount of radioactive or any other toxic materials released into the environment due to mal-operation of any industry can be obtained from the plant operation; however, due to the fluctuation of wind speed for a specified span of time, knowledge related to the crisp value of the wind speed is an uncertain quantity. Therefore, knowledge of the wind speed is very important component for safety analysis of the specified industry. Evidence based on a large number of literature study indicates that wind speed is always characterized by a variety of standard parametric probability density functions (PDF) [1]. Weibull distribution with two parameters is usually applied for probability distribution of wind speeds. It is generally accepted that measured wind data can be best characterized by Weibull distribution [1, 2]. But in most studies of fitting of data set to Weibull distribution was not examined. In order to obtain a fitting of the wind speed data through Weibull distribution it is essential to estimate the parameter Weibull distribution [3, 4]. However, from the point of improvement in wind data fitting, similar to the Weibull family, a new family of distributions, namely Exponentiated Weibull distribution [5] is being proposed; in this context it is customary to say that a typical two parameter Weibull distribution does not accurately represent the entire wind regime in nature [6]. The Exponentiated Weibull distribution has been compared with the two parameter Weibull distribution. Parameters of the Exponentiated Weibull distribution and classical Weibull distribution are estimated using maximum likelihood method algorithm [8]. Shannon entropy of each distribution have been computed to provide the amount of uncertainty associated with the corresponding random variable sampled from the respective distributions. Akaike information criterion (AIC) and the logarithm of the maximized likelihood for each fit have been calculated.

In this paper, we have fitted both Weibull distribution and Exponentiated Weibull distribution through a set of yearly maximum wind speed data. Uncertainty analysis of the fitting parameters examines the better suitability of the Weibull and Exponentiated Weibull distribution for this kind of fitting. We described the Exponentiated Weibull distribution with its many properties. Maximum likelihood based estimation of the parameters of this new distribution and that of Weibull distribution has been presented in detail. Akaike information criterion has been evaluated to assess the best fit. Shannon entropy of the fitted distributions is computed to evaluate the uncertainty of the fitted model. Quantile-Quantile plots are made to compare the fitting.

## 2. Mathematics of Weibull and Exponentiated Weibull Distribution

### 2.1 Weibull Distribution

The Weibull probability density function (PDF) and its cumulative distribution function (CDF) for a random variable V having the value of v possessing the wind speed is defined by

$$f_W(v;\gamma,\beta)=\frac{\gamma}{\beta}\left(\frac{v}{\beta}\right)^{\gamma-1}\exp\left[-\left(\frac{v}{\beta}\right)^{\gamma}\right],\quad v>0 \tag{1}$$

and

$$F_W(v;\gamma,\beta)=1-\exp\left[-\left(\frac{v}{\beta}\right)^{\gamma}\right] \tag{2}$$

respectively, where $\gamma > 0$ is a shape parameter and $\beta > 0$ is a scale parameter. The parameter $\beta$ depends on $\gamma$ and is related to the mean value of the wind speed. The two Weibull parameters and the mean wind speed are related by

$$\bar{v}=\beta\,\Gamma\left(1+\frac{1}{\gamma}\right) \tag{3}$$

where $\Gamma\left(1+\frac{1}{\gamma}\right)$ is the gamma function.

It is easily proved that the $n^{th}$ moment of the wind speed by the Weibull PDF is given by

$$\left\langle v^n\right\rangle=\beta^n\Gamma\left(1+\frac{n}{\gamma}\right) \tag{4}$$

where the angular bracket $\left\langle v^n\right\rangle$ denotes the expectation value of the wind speed and represents the gamma function. $\Gamma\left(1+\frac{1}{\gamma}\right)$

Based on Eq.(1) and Eq.(4), the variance of the wind speed is given by

$$\sigma_v^2=\frac{\Gamma(1+2\gamma)}{\Gamma(1+1/\beta)^2}-1\approx\gamma^{-1\ /6} \tag{5}$$

For the derivation of the scale parameter, $\beta$, without loss of generality, it is assumed that the $\left\langle v\right\rangle=1$ and setting n = 1 in Eq. (4), yields

$$\beta=\frac{1}{\Gamma(1+1/\gamma)} \tag{6}$$

### 2.2 Exponentiated Weibull Distribution

Exponentiated Weibull distribution (EW) has a scale parameter and two shape parameters. The PDF

and CDF of a random variable v described by the EW distribution in [7] is given by

$$f_{EW}(v;\gamma,\beta,\alpha) = A \times B \tag{7}$$

where,

$$A = \frac{\alpha\gamma}{\beta}\left(\frac{v}{\beta}\right)^{\gamma-1} \exp\left[-\left(\frac{v}{\beta}\right)^{\gamma}\right],$$

$$B = \left\{1 - \exp\left[-\left(\frac{v}{\beta}\right)^{\gamma}\right]\right\}^{\alpha-1}$$

and

$$F_{EW}(v;\gamma,\beta,\alpha) = \left\{1 - \exp\left[-\left(\frac{v}{\beta}\right)^{\gamma}\right]\right\}^{\alpha} \tag{8}$$

respectively; where $\gamma > 0$ is a shape parameter related to the wind speed, and $\beta > 0$ is a scale parameter, that depends on $\gamma$ and is related to the mean wind speed as in the precedent case. The additional parameter, compared with Eq. (2), $\alpha > 0$ is an extra shape parameter that gives more versatility to the EW distribution in the shape of the tails. Figure 1 shows that the density function of EW is unimodal and for fixed value of $\beta$ and $\gamma$ it becomes more and more symmetric as $\alpha$ increases. It can be easily noted that for $\alpha = 1$ Eq.(7) reduces to the Weibull distribution (e.g. Eq.(2)). If we calculate the nth moment of the EW PDF, it can be easily mention that the analytical derivation of the EW parameters is rather a complete task. Therefore, a heuristic approach, based on simulation data was used to obtain first approximation to the EW parameters.

The shape parameter $\gamma$ can be related with the random variable v as

$$\gamma \cong (\alpha\sigma_v^2)^{-6/11} \tag{9}$$

where $\sigma_v^2$ denotes the variance of the random variable v. The scale parameter $\beta$ can be written as

$$\beta = \frac{1}{\alpha\ \Gamma(1+1/\gamma)\,\Phi} \tag{10}$$

where,

$$\Phi = \sum_{p=0}^{\infty} \frac{(-1)^p (p+1)^{-(1+\gamma)/\gamma}\,\Gamma(\alpha)}{p!\ \ (\alpha - p)}$$, p represents an index.

It can be easily verified that for fixed values of the shape parameter $\gamma$ and the scale parameter, $\beta$, the shape parameter $\alpha$ controls the steepness of the lower-tail of the distribution if data is visualized in a logarithmic scale. This is an attractive property of the EW distribution. Some of the fundamental statistical properties of the Exponentiated Weibull distribution are quoted from the reference [7]. As per the reference [7] we define the moments of the EW distribution.

The $k^{th}$ moment of the exponentiated Weibull variable, v, with distribution function given in Eq. (8) is written as

$$E(v^k) = \alpha\ \beta^k\ \Gamma\left(\frac{k}{\gamma}+1\right)\xi \qquad \text{where,}$$

$$\xi = \sum_{i=0}^{\alpha-1} \binom{\alpha-1}{i} (-1)^i\ (i+1)^{-\frac{k}{\gamma}-1}, \quad \text{if } \alpha \in N \tag{11b}$$

where, ${}_aP_i = a(a-1)(a-2)\ldots\ldots(a-i+1)$ and N is the set of natural numbers. Since Eqs. (11a and 11b) are a convergent series for all $k \geq 0$, all moments exist.

The expectation value of the EW random variable v can be written as by using Eqs. (11a) and (11b) as

$$E(v) = \left\{\alpha\ \beta\ \Gamma\left(\frac{1}{\gamma}+1\right)\zeta \tag{12a}$$

where, $\zeta = \sum_{i=0}^{\alpha-1} \binom{\alpha-1}{i} (-1)^i (i+1)^{-\frac{1}{\gamma}-1}$,

if $\alpha \in N$

$$E(v) = \alpha\,\beta\,\Gamma\left(\frac{1}{\gamma}+1\right)\varsigma \tag{12b}$$

where,

$$\varsigma = \sum_{i=0}^{\alpha-1} \frac{{}_{\alpha-1}P_i}{i!} (-1)^i\ (i+1)^{-\frac{1}{\gamma}-1}, \quad \text{if } \alpha \in N$$

In a similar way, the variance of the EW random variable v can be written as

$$\sigma_v^2 = E(v^2) - [E(v)]^2 \tag{13}$$

where,

$$E(v^2) = \left\{\alpha\ \beta^2\ \Gamma\left(\frac{2}{\gamma}+1\right)\Delta \tag{14a}$$

where,

$$\Delta = \sum_{i=0}^{\alpha-1} \binom{\alpha-1}{i} (-1)^i (i+1)^{-\frac{2}{\gamma}-1}, \quad \text{if } \alpha \in N$$

$$E(v^2) = \alpha\,\beta^2\,\Gamma\left(\frac{2}{\gamma}+1\right)\ \Xi \tag{14b}$$

where,

$$\Xi = \sum_{i=0}^{\alpha-1} \frac{\alpha-1 P_i}{i!} (-1)^i (i+1)^{-\frac{2}{\gamma}-1}, \quad \text{if } \alpha \notin N$$

## 3.0 Maximum Likelihood Estimation

### 3.1 Weibull Distribution Parameters

Maximum likelihood is a method of estimation of parameters of a distribution. Maximum likelihood technique [9-11] with many required features is the most widely used technique among parameter estimation techniques. The abbreviation MLE may refer to maximum likelihood estimation (the method), to the estimate, or to the estimator. The method finds a value of the parameter that maximizes the likelihood function. The MLE method has many large sample properties that make it attractive for use. It is asymptotically consistent, which means that as the sample size gets larger, the estimates converge to the true values. It is asymptotically efficient, which means that for large samples, it produces the most precise estimates. It is asymptotically unbiased, which means that for large samples, one expects to get the true value on average. The estimate themselves are normally distributed if the sample is large enough. These are all excellent large sample properties.

Let $x1, x2, ....,xn$ be a random sample of size drawn from a probability density function $f_x(x; \theta)$ where $\theta$is an unknown parameter. The likelihood function of this random sample is the joint density of the random variables and is a function of the unknown parameter. Thus,

$$L = \prod_{i=1}^{n} f_{x_i}(x;\theta) \tag{15}$$

is the likelihood function. The maximum likelihood estimator (MLE) of $\theta$, say $\hat{\theta}$ is the value of $\theta$ that maximizes $L$ or, equivalently, the logarithm of $L$. Often, but not always, the MLE of $\theta$ is a solution of

$$\frac{\mathrm{d}\log L}{\mathrm{d}\theta} = 0 \tag{16}$$

where solutions those are not functions of the sample values are not admissible, nor are solutions which are not in the parameter space. Now, we are going to apply MLE to estimate the Weibull parameters, namely the shape and the scale parameters. Consider the Weibull PDF given in (1), then the likelihood function will be

$$L(x_1, \dots, x_n; \gamma, \beta) = \prod_{i=1}^{n} \left(\frac{\gamma}{\beta}\right) \left(\frac{x_i}{\beta}\right)^{\gamma-1} e^{-\left(\frac{x_i}{\beta}\right)^{\gamma}} \tag{17}$$

On taking the logarithms of Eq. (17), differentiating with respect to and in turn and equating to zero, we obtain the estimating equations

$$\frac{\partial \ln L}{\partial \gamma} = 0 = \frac{n}{\gamma} + \sum_{i=1}^{n} ln\, x_i - \frac{1}{\beta} \sum_{i=1}^{n} x_i^{\gamma} ln\, x_i \tag{18}$$

$$\frac{\partial \ln L}{\partial \beta} = -\frac{n}{\beta} + \frac{1}{\beta^2} \sum_{i=1}^{n} x_i^{\gamma} = 0 \tag{19}$$

On eliminating $\beta$ between these two equations and simplifying, we have

$$\frac{\sum_{i=1}^{n} x_i^{\gamma} \ln x_i}{\sum_{i=1}^{n} x_i^{\gamma}} - \frac{1}{\gamma} - \frac{1}{\beta} \sum_{i=1}^{n} ln\, x_i = 0 \tag{20}$$

which may be solved to get the estimates of $\widehat{\mu_k} = \gamma$. This can be accomplished by the use of standard iterative procedures (i.e. Newton-Raphson method). Once is determined, can be estimated using Eq. (21) as

$$\beta = \frac{\sum_{i=1}^{n} x_i^{\gamma}}{n} = 0 \tag{21}$$

### 3.2 Estimates of EW Parameters

Computation related to the estimation of the parameters of EW distribution by using generalized least square method is complicated due to nonlinearity involved in the first order derivative. Therefore, in order to estimate the parameters of the EW distribution, we have adopted the maximum likelihood method.

Let $v_1, v_2, \dots v_n$ be a random sample of size n from the EW distribution given by Eq.(8). Now the log likelihood function can be written as

$$L(\alpha, 1/\beta, \gamma) = n \ln \alpha + n \ln \gamma +$$

$$n\gamma \ln(1/\beta) + (\gamma - 1) \sum_{j=1}^{n} \ln v_j + (\alpha - 1) \times \Omega \tag{22}$$

where,

$$\Omega = \sum_{j=1}^{n} \ln[1 - \exp\{-(v_j/\beta)^{\gamma}\}] - \sum_{j=1}^{n} (v_j/\beta)^{\gamma}$$

Now, by taking the derivative of L, MLE estimates of $\alpha$, $1/\beta$, $\gamma$ that maximizes Eq. (22), normal equations can be written as

$$\frac{d}{d\alpha} L(\alpha, 1/\beta, \gamma) = \frac{n}{\alpha} + \sum_{j=1}^{n} \ln[1 - \exp(-(v_j/\beta)^{\gamma})] = 0 \tag{23}$$

$$\frac{d}{d(1/\beta)} L(\alpha, 1/\beta, \gamma) =$$

$$n\gamma\beta + (\alpha-1)\gamma(1/\beta)^{\gamma-1} \sum_{j=1}^{n} \frac{e^{-(v_j/\beta)^{\gamma}}}{1-e^{-(v_j/\beta)^{\gamma}}} v_j^{\gamma} - \quad (24)$$

$$\gamma(1/\beta)^{\gamma-1} \sum_{j=1}^{n} v_j^{\gamma} = 0$$

$$\frac{d}{d\gamma} L(\alpha, 1/\beta, \gamma) = \frac{n}{\gamma} + \quad (25)$$

$$n \ln(1/\beta) + \sum_{j=1}^{n} \ln v_j$$

$$+ (\alpha-1)(1/\beta)^{\gamma} \Theta = 0$$

where,

$$\Theta = \sum_{j=1}^{n} \frac{\exp\{-(v_j/\beta)^{\gamma}\}}{1-\exp\{-(v_j/\beta)^{\gamma}\}} v_j^{\gamma} \ln(v_j/\beta) - \quad (25)$$

$$(1/\beta)^{\gamma} \sum_{j=1}^{n} v_j^{\gamma} \ln(v_j/\beta)$$

From Eq. (23) we obtain the MLE of α as a function of $(1/\beta, \gamma)$, say $\hat{\alpha}(1/\beta, \gamma)$ given by

$$\hat{\alpha} = \hat{\alpha}(1/\beta, \gamma) = -\frac{n}{\sum_{j=1}^{n} \ln[1-\exp(-(v_j/\beta)^{\gamma})]} \quad (26)$$

Multiplying Eq. (24) by $(1/\beta, \gamma)$ we get

$$n + (1/\beta)^{\gamma} \times$$

$$[(\alpha-1) \sum_{j=1}^{n} \frac{\exp\{-(v_j/\beta)^{\gamma}\}}{1-\exp\{-(v_j/\beta)^{\gamma}\}} v_j^{\gamma} \quad (27)$$

$$- \sum_{j=1}^{n} v_j^{\gamma}] = 0$$

Subtracting $\ln(1/\beta)$ times Eq. (27) from Eq. (25) we have

$$\frac{n}{\gamma} + \sum_{j=1}^{n} \ln v_j + (1/\beta)^{\gamma}[(\alpha-1) \times$$

$$\sum_{j=1}^{n} \frac{\exp\{-(v_j/\beta)^{\gamma}\}}{1-\exp\{-(v_j/\beta)^{\gamma}\}} v_j^{\gamma} \ln v_j - \quad (28)$$

$$\sum_{j=1}^{n} v_j^{\gamma} \ln v_j] = 0$$

Using Eq.(26) in Eqs.(27) and (28) we get two equations, which are satisfied by the MLEs $(1/\hat{\beta})$ and $\hat{\gamma}$ of $(1/\beta)$ and $\gamma$, respectively.

## 4. Shannon Entropy

Entropy refers to the amount of uncertainty associated with a random variable. It is an important concept in many fields of science, especially for probability based applications. Shannon [12] entropy is the most popular measure of entropy. For a continuous distribution G(x) with density g(x), the Shannon entropy is defined as

$$H[g(x)] = \langle -\log(g(x)) \rangle = -\sum_{j} \log(g(x_j))\, g(x_j) \quad (29)$$

For the Weibull and EW distribution, the Shannon entropies are given by

$$H_W = \left\langle \frac{\gamma}{\beta}\left(\frac{v}{\beta}\right)^{\gamma-1} \exp\left[-\left(\frac{v}{\beta}\right)^{\gamma}\right] \right\rangle \quad (30)$$

$$H_{EW} = \left\langle \frac{\alpha\gamma}{\beta}\left(\frac{v}{\beta}\right)^{\gamma-1} \times \exp\left[-\left(\frac{v}{\beta}\right)^{\gamma}\right] \times \left\{1-\exp\left[-\left(\frac{v}{\beta}\right)^{\gamma}\right]\right\}^{\alpha-1} \right\rangle \quad (31)$$

## 5. Akaike Information Criterion

The Akaike information criterion (AIC) is ameasure of the relative quality of a statistical model for a given set of data. As such, AIC provides a means for model selection. AIC is founded on information entropy. It offers a relative estimate of the information lost when a given model is used to represent the process that actually generates the data. AIC is defined as

$$AIC = 2p - 2\ln(L) \quad (32)$$

Where p is the number of parameters in the statistical model and L is the maximized value of the likelihood function of the estimated model.

## 6. Results and Discussion

In this study we estimated the mean and variance of the wind speed data. The yearly maximum wind speed data, in miles/hour, used in this study has been quoted from Castillo (1988) [13] and is presented in Table 1. Before the estimation, Weibull and Exponentiated Weibull distributions have been fitted independently. Fitted probability distributions are shown in Figures 2 and 3. Since fitting a probability

**Table 1. Yearly Maximum Wind Speed Data**

| Serial No | Wind Speed (miles per hour) | | | | |
|---|---|---|---|---|---|
| **1** | 22.64 | 22.80 | 23.75 | 24.01 | 24.04 |
| **2** | 24.24 | 24.74 | 25.45 | 25.55 | 25.66 |
| **3** | 25.99 | 26.63 | 26.69 | 26.88 | 26.89 |
| **4** | 27.12 | 27.43 | 27.69 | 27.71 | 28.12 |
| **5** | 28.58 | 28.88 | 29.12 | 29.45 | 29.48 |
| **6** | 30.18 | 31.31 | 31.55 | 31.57 | 32.54 |
| **7** | 32.98 | 33.83 | 33.86 | 34.64 | 35.21 |
| **8** | 36.82 | 37.23 | 38.09 | 38.26 | 38.82 |
| **9** | 38.96 | 38.90 | 42.99 | 43.66 | 44.61 |
| **10** | 45.24 | 47.91 | 54.75 | 69.40 | 98.16 |

**Table 2. Parameters of the Fitted Distributions with Uncertainty**

| Distribution | Parameters | |
|---|---|---|
| | Shape (uncertainty) | Scale (uncertainty) |
| Weibull ($\beta$, $\alpha$) | $\beta$=2.57 (0.23) | $\alpha$=38.09 (2.2) |
| Exponentiated Weibull ($\alpha$,$\beta$, $\gamma$) | $\alpha$= 91.27 (71.69), $\gamma$ = 0.90 (0.15) | $\beta$= 5.50 (2.46) |

**Table 3. AIC and Entropy**

| Distribution | AIC and Entropy | |
|---|---|---|
| | AIC | Entropy |
| Weibull ($\beta$, $\alpha$) | 398.7 | High |
| Exponentiated Weibull ($\alpha$,$\beta$, $\gamma$) | 363.4 | Low |

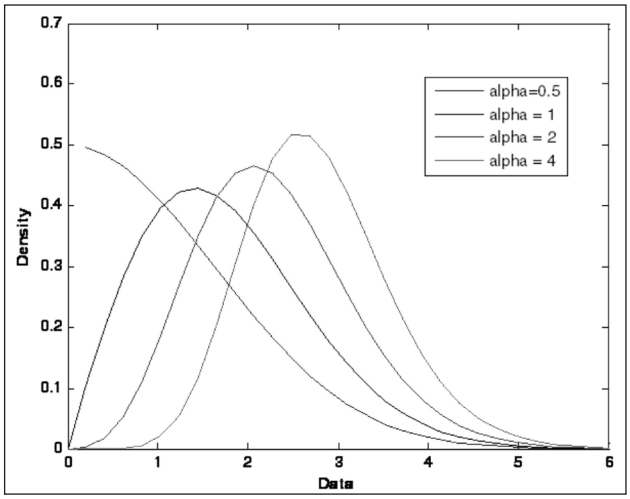


*Figure 1. PDF of Exponentiated Weibull distribution with $\beta$=2, $\gamma$=2 when a =0.5, 1, 2, 4 The shape parameter $\gamma$ can be related with the random variable v as*

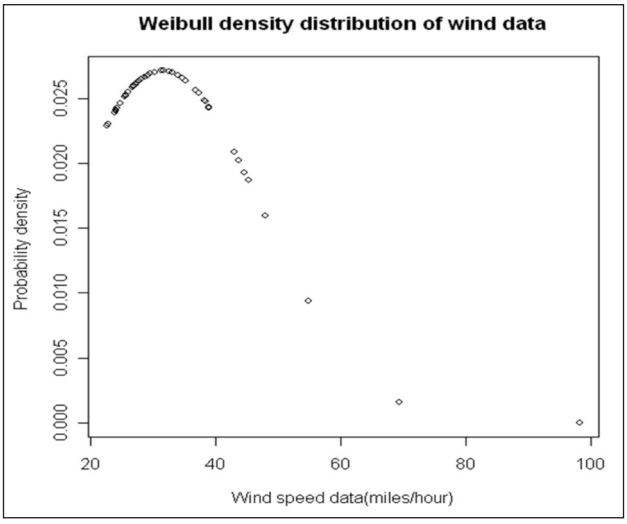


*Figure 2. Fitted Weibull density Distribution of wind speed data*

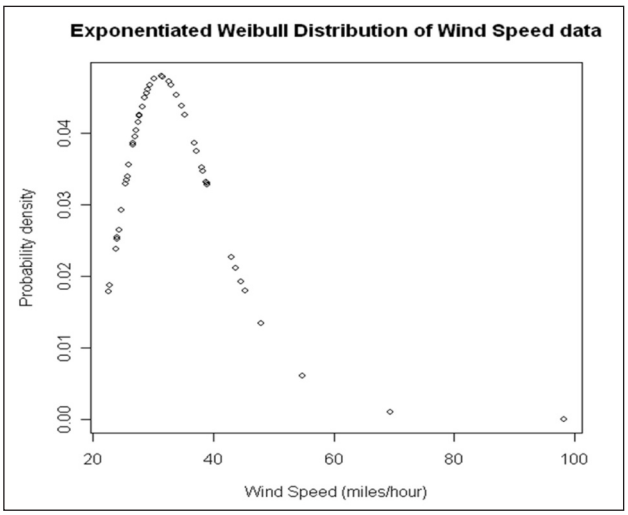


*Figure 3. Fitted Exponentiated Weibull density distribution of wind speed data*

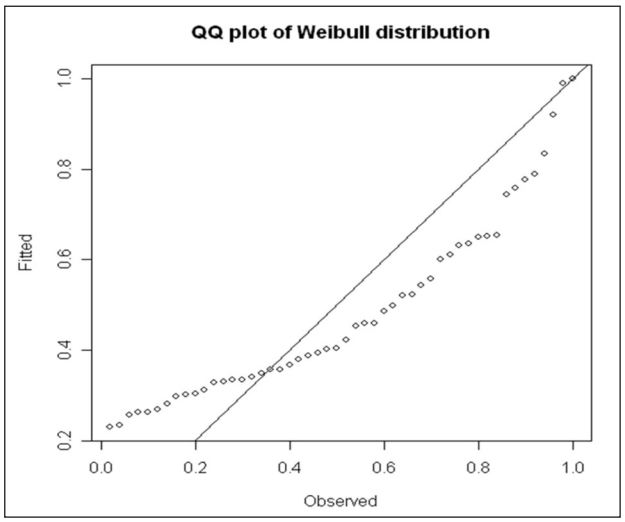


*Figure 4. QQ plot of Weibull Distribution of wind speed data*

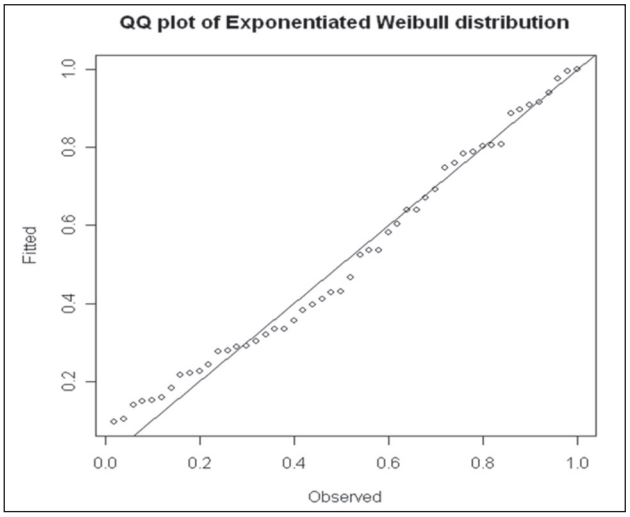


*Figure 5. QQ plot of Exponentiated Weibull Distribution of wind speed data*

distribution through a set of relevant data is nothing but the estimation of the parameters of the respective probability distributions, maximum likelihood based estimated value of the parameters of the corresponding probability distributions with their standard error are presented in Table 2. Mean value of the wind speed and the corresponding variance of the wind speed on the basis of Weibull distribution are estimated as 33.82 and 198.64 respectively. Further, the mean and variance of the wind speed based on the exponentiated Weibull distribution are estimated as 31.16 and 32.92 respectively. Table 3 presents the results of AIC and Shannon entropy. Lower value of the AIC decides that fitting the distribution through the given data set is the best fit. Thus it shows very clearly that Exponentiated Weibull distribution for the wind speed data is the better model compared to Weibull model. Moreover, entropy provides the knowledge of the uncertainty and since Shannon entropy of EW distribution is low compared to the Weibull, the EW distribution has less uncertainty and more reliable compared to Weibull distribution for fitting wind speed data.

It also follows by the standard likelihood ratio test that the exponentiated Weibull distribution is a much better fitted distribution than the classical Weibull distribution for fitting of the wind speed data. This observation has been confirmed further by the probability plots corresponding to the two fits as shown in Figure 4 and Figure 5.

## References

1. J.A. Carta, P. Ramlrez, S. Velquez, A Review of wind speed probability distributions used in wind energy analysis case studies in the Canary Islands. *Energy Conversion and Management* 13: 933-955, 2009.
2. Atsu S.S. Dorvlo, Estimating wind speed distribution, *Energy Conversion and management,* 43:2311-2318, 2007.
3. J.A. Carta, P. Ramrez, Analysis of two-component mixture Weibull statistics for estimation of wind speed distributions, *Renewable energy,* 32:518-531, 2007.
4. J.A. Carta, P. Ramrez, Use of finite mixture distribution models in the analysis of wind energy in the canarian Archipelago, *Energy Conversion & Management*, 48:281-291, 2007.
5. Gupta, R.D., Kundu, D., "Exponentiated exponential family: an alternative to gamma and Weibull", Biometrical Journal, vol. 43(1), pp. 117-130, 2001.
6. Qingzhen Meng, Mozhi Tang, On asymptotic distributions of yearly maximum values of surface temperature and wind speed over Chengdu and the estimation of their parameters, *Journal of Chengdu Institute of Meteorology,* 12:284-291, 2007.
7. Mudholkar, G.S., Srivastava, D.K., "Exponentiated Weibull family for analyzing bathtub failure rate data", IEEE Transactions on Reliability, vol. 42, pp. 299-302, 1993.
8. Dempster, A. Laird, N. and Rubin, D., Maximum likelihood from incomplete data via the EM algorithm, *Jornal of the Royal Statistical Society Series B,* 39(1):1-38, 1977.
9. Harter, H. L. and A. H. Moore, "Point and interval estimators based on order statistics, for the scale parameter of a Weibull population with known shape parameter", Technometrics, Vol. 7, No. 3, August 1965a.
10. Harter, H. L. and A. H. Moore, "Maximum likelihood estimation of the parameters of Gamma and Weibull populations from complete and from censored samples", Technometrics, Vol. 7, No. 4, November 1965b.
11. Cohen, A. C., "Maximum likelihood estimation in the Weibull distribution based on complete and on censored samples", Technometrics, Vol. 7, No. 4, November, 1965.
12. Shannon, C.E. A mathematical theory of communication, Bell Syst. Tech. J. , vol. 27, pp.379-432, 1948.
13. Castillo, E., "Extreme Value Theory in Engineering", Academic Press, INC.(London), Harcourt Brace Jovanovich Publishers, ISBN 0-12-163475-2, pp. 334, 1988.

*Life Cycle Reliability and Safety Engineering*
*Vol.2 Issue 4 (2013) 35-68*

# Review on Prognostics and Health Management of Digital Systems and its Application to Nuclear Plants

**S.V. Shrikhande, P.V. Varde and D. Datta**
*Bhabha Atomic Research Centre, Mumbai, India 400 085*
*Email: svs@barc.gov.in*

## Abstract

***Prognostics gives early warning of failure. It is gaining importance and the application areas of prognostics for health monitoring include civil and mechanical structures, machine-tools, vehicles, space applications, consumer electronics, computers, and even human health. Prognostics involves predicting a future state based on current health and usage conditions. The extent of degradation of a system is monitored to predict remaining useful life (RUL). It aids forecasting for reducing maintenance cycles and life extensions. Condition monitoring existing in current protection and process control systems for nuclear plants is mentioned. The paper presents current state-of-research in the area of prognostics and health management for electronics and its implementation challenges. The paper introduces use of fuses and canary devices. It reviews modelling of accumulated damage based on measured life-cycle loads. It proposes applications of prognosis in nuclear plants. This paper mentions various applications where prognostics is successfully deployed. It covers different approaches and methodologies for prognostics and RUL estimation. It describes data reduction and simplification techniques, various techniques for intelligent algorithms including Machine Learning and also sensors for Prognostics and Health Management (PHM) of Complementary Metal Oxide Semiconductor (CMOS) Integrated Circuits (ICs). The thrust of this paper is on review of prognostics of electronic component, its related issues and mathematical techniques useful for prognostic algorithms.***

**Keywords-** ***Prognostics, On-line diagnostics, Prognostics and Health Management, PHM, CMOS failure mechanisms, Physics of Failure, PoF, RUL, Fault Progression, Support Vector Machines, SVM.***

## 1. Introduction

Electronics components have increasingly critical role in avionics systems and nuclear power plant. Prognostics of these components is becoming a very important field of research for providing system level health information. For electronic components, predicting RUL is the most challenging task of Prognostic and Health Management systems.

Digital systems are employed in nuclear plants for protection, control and monitoring purposes. Computer Based Systems (CBS) used for protection function like Reactor Trip Logic System, Emergency Core Cooling System and Programmable Digital Comparator System have been deployed in nuclear reactors. CBS for regulation function include important primary and secondary side process control systems and reactor regulating systems which have been deployed in various Nuclear Power Plants (NPPs). Safety critical systems are designed with triplicate channels. Each channel is configured using microcomputer boards which are the basic building blocks. It has CPU card, Ethernet communication card, VME (Versa Module Eurocard) bus to proprietary I/O bus interface card, intelligent I/O cards, signal conditioning cards and bus extender cards.

Reliability prediction of these safety critical and safety related systems is a mandatory requirement of the regulatory authorities. Failure rate estimation of these boards is carried out using 'Part Stress' methodology of RIAC-HDBK-217Plus. Channel failure rate is predicated based on these boards failure rates, using Fault Tree Analysis technique. For system level reliability metrics like Probability of failure on Demand (PFD), Spurious Failure Probability (SFP), availability, etc. Markov modelling technique is used. Shortcomings of handbook-based reliability analysis method is discussed in one of the sections below and compared with Physics of Failure (PoF) method.

Safety systems of nuclear plants are built on the principles of simplicity, redundancy, diversity and single failure criterion. These aspects do reduce probability of failure of a system. However, the latest design of computer based systems largely employ programmable devices like Field Programmable Gate Array (FPGA)/ Complex Programmable Logic Devices (CPLD), and failure of these can impair functionality of the systems. Therefore on-line monitoring of the critical components is required for health monitoring of these systems..

Diagnostics identify sources of malfunctions, post-failure within the system. Diagnostics reports a fault without telling the cause, and causes the system to reconfigure. An extension of fault diagnosis is prognosis which anticipates impending failure by identification of degrading components prior to a catastrophic failure [1].

Offline and online diagnostics also termed as Built-In-Test (BIT) have been implemented in current digital systems in Indian and also outside systems e.g. Motorola systems [2]. Current BIT techniques are capable of detecting a hard fault and do not provide any prognosis of impending hardware failure. Failures are treated as unpredictable events or random failures and planning is done based on estimated MTBF. The approach to maintenance is to replace on failure, i.e. unscheduled maintenance.

BIT is defined as an on-board hardware-software diagnostic means to identify and locate faults, and includes error detection circuits. Diagnostic tests are provided to check integrity of software using Cyclic Redundancy Check (CRC) checks. Checks are provided on digital channels using Finite-Impulse-Testing (FIT). Analog to Digital Converter (ADC) check is carried out by having a constant reference voltage connected to one channel of multiplexer. Relay output is checked by reading back the status of the energizing coil of relay. Analog outputs of 4-20mA are checked by reading back as an input. The above checks are carried out periodically during operation as background tasks. However during system start-up i.e. after powering, some checks are performed. These are called Power-On Self-Test (POST). In POST additional tests are carried out like Watch-Dog Timer (WDT) tests which cannot be performed once system starts its operation. The system is started only after it undergoes POST checks successfully, else it halts. There is extra circuitry and additional software for BIT. Some off-line tests are also carried out to identify system faults for debugging, troubleshooting, and performing preventive maintenance.

Board-level diagnostics are performed to identify board failure. The replaceable unit during system maintenance is board. A board after testing in an offline test unit is used for replacement of a faulty board in a system. The board failure, especially I/O board failure is diagnosed by on-line diagnostic programs. WDT is provided to take care of some failures of the processor board and improper execution of the software. Long cycle WDT trip takes care of the software getting into an improper execution and thereby not able to reset the WDT before the timeout period. Short cycle WDT trip is provided to cater to the software getting into the loop where it resets the WDT.

Literature survey of diagnostics in Motorola systems was carried out [2]. A board-level BIT implemented by Motorola (MBIT), consists of hardware diagnostics and an API to control operation of the test driver suite. Examples of tested devices are the processor, L2 cache, VME bus ASIC, ECC RAM, serial EPROM, Flash, NVRAM and real-time clock. Internal operation tests include checking register stuck-at conditions, register manipulations, and device setup instructions. The system-level MBIT, connects to all board-level versions to enable system-wide testing.

Various levels of BIT include: 1) circuit-level BIT for fault logging and diagnostics of individual circuits 2) module level BIT that supports one or more circuit card assemblies, 3) system-level BIT that performs diagnostics and operational testing of entire electronic system.

The AI-ESTATE standard provides a foundation for diagnostic assessment and includes four alternatives for diagnosis—static fault trees (or decision trees), D-matrix-based systems (e.g., dependency models), logic-based models (e.g., rule-based expert systems) and Bayesian networks. All four alternatives have been demonstrated to provide effective and accurate diagnostics.

## 2. Prognostics

Prognostics is prediction of future state of health based on current and historic health condition. Prognostics helps in predicting onset of system degradation and time to system failure giving improved health information of the product [3]. It uses parameters which are correlated to progression of

faults which are caused due to accumulated damage, for prediction RUL. Prognostics capability to give RUL has become a requirement for a system sold to U.S. Department of Defense [4]. NASA is interested in predicting failures even a few seconds in advance for certain safety critical electronic systems [5].

Reliability is defined as the probability of a product to perform the intended function (without failure and within specified performance limits) for a specified time, in its (life cycle) application environment. The accuracy of any reliability prediction depends upon both the prediction methodology used, accurate knowledge of the product, system architecture, material properties, fabrication process and product life cycle conditions [6]. The life cycle conditions consist of the assembly, storage, handling, and use of the product. The life cycle loads include environmental conditions (e.g. temperature, humidity, vibration, shock, etc.) and operational parameters (e.g. voltage, current, power dissipation, etc.) [7]. The severity and duration of such loads are influenced by product usage profile (e.g., utilization duration and frequency, transportation and storage) [8].There may be difference between expected and actual conditions, and this provides a strong motivation for monitoring actual product application environments. Temperature, in terms of either spatial or temporal gradients, or absolute temperature, is a parameter that influences the reliability of electronic products [6]. Though semiconductor die circuit electrical performance can be operating temperature dependent, many integrated circuit (IC) packaging failure mechanisms, have been found to have multiple life cycle temperature dependencies.

Prognostics can be implemented using various techniques by sensing and interpreting the parameters in following ways:

1) Performance degradation, such as deviation of operating parameters from their expected values;
2) Physical or electrical degradation, such as material cracking, corrosion, interfacial delamination, increase in electrical resistance or threshold voltage;
3) Changes in a life cycle environment, such as usage duration and frequency, ambient temperature and humidity, vibration, and shock.

The problem in the domain of prognosis is to identify appropriate 'monitoring index' characterizing the system condition, both in type and in level of faults. The proposed monitoring indices include time domain features, frequency spectrum, wavelet amplitude pattern of residual signal and signal energy, etc. Various statistically derived metrics can also be useful e.g. for monitoring gear pitting [9], the index used was normalized kurtosis of overall residual signal for the faulty gear with an hourly time step.

Diagnostic system model, a simple low order formulation that requires less computation power of a single device, in an distributed architecture, to track the measured variable indicative of component health and then trigger the prognostic routine when certain predetermined thresholds are crossed [10]. The prognostic model is more complex in order to handle the increased uncertainty of health prediction.

The use of PHM promises to enable significant economics to be made in the support infrastructure by relieving the need for rapid reaction to failures. The benefits come at the cost of additional hardware and software carried within the electronics. But the cost benefit is also achieved by saving upon the loss of useful life arising from replacement before failure. Employing prognosis for complex systems will definitely give cost benefit.

### 2.1 Possible Applications of Prognosis in NPPs

Prognostics has begun from medical applications but has also been applied for digital Instrumentation and Control (I&C) systems. In control room operations, the idea is to characterize the behaviour for the set of critical performance characteristics and promote the ability to take either human initiated or system initiated action at earlier time t1 instead of time t2. Prognosis can be employed for analysis of controls systems and its failure modes. Hybrid prognostics techniques can be employed for overcoming, to some extent the human limitations during stress. It is useful in detecting material failure. Using traditional experimental methods, such critical scenarios can be constructed by either 1) taking validated scenarios from the literature or 2) designing new scenarios and then conduct pilot studies to validate it.

Development of a system model that can detect, assess, and classify operator's cognitive and affective states; and developing a system model that can choose the best course of actions given the states of the operator. For this Artificial intelligence systems based on Bayesian Network can be used.

Periodic surveillance (and inspections which typically occur during refuelling outages) cannot be adequate to help ensure fitness for service for critical safety systems and components. Developing methodology and designing systems for on-line continuous monitoring becomes a critical component in providing operators better plant situation awareness and reliable predictions of remaining life of critical systems and components. The monitoring technology needs to be expanded to include prognostics in addition to the presently employed on-line monitoring and diagnostics for condition-based maintenance. Digital I&C with advanced diagnostics and prognostics are being developed in the wider high-technology industry communities and are now being considered for NPP deployment.

The advantage of adopting condition-based maintenance (CBM) and on-line diagnostics in power plants is already accepted and seen from the current practices followed. There is a need to move beyond current approaches into the realm of prognostics. Operators need enhanced situational awareness if unwanted outages need to be avoided [11].

The use of digital I&C can support addition of increased functionality and also addition of prognostics for key system elements. The adoption of advanced diagnostic and prognostic technologies for future generation nuclear power plants can significantly impact plant economics [12]. However, before the deployment of such systems is possible it is necessary to demonstrate methodologies, understand stressors, sensors, communication, analysis and quantify uncertainty in RUL prediction as well as to demonstrate long term monitoring of system reliability.

### 2.2 Deployed Applications of PHM

PHM has been implemented by various companies- Sun Microsystems, Schlumberger, General motors, Dell, etc. PHM is used in various fields like aerospace [76], automotive, electronic systems etc. as given below.

#### 2.2.1 Aerospace

PHM for RUL estimation was done for the end effect for electronics unit (EEEU) inside the robotic arm of the space shuttle remote manipulator system [13]. A life-cycle loading profile for thermal and vibration loads was developed for the EEEU boards. A damage assessment was conducted using failure mechanical and thermo-mechanical damage models.

RUL assessment of circuit cards inside a space shuttle solid rocket booster (SRB) was done [14]. Vibration time history recorded on the SRB from the pre-launch stage to splashdown was used in conjunction with physics-based models to assess the damage caused by vibration and shock loads. Using the entire life cycle loading profile of the SRBs, the remaining life of the components and structures on the circuit cards was predicted.

#### 2.2.2 Automotive

The test vehicle -'Underhood Electronics', was a circuit board assembly placed under the hood of an automobile and subjected to normal driving conditions [7], [8] and [15]. The test board incorporated eight surface-mount leadless components soldered onto a FR-4 substrate using eutectic tin-lead solder. Solder joint fatigue was identified as the dominant failure mechanism. Damage accumulated through solder joint fatigue was updated periodically using in-situ collected data on temperature and vibration. It was found that the predicted life of the solder joint based on PHM algorithm was within 8% of the actual experimental life.

#### 2.2.3 Electronic Systems

##### 2.2.3.1 Computer Server

Systems are based on current, voltage, and temperature, which are continuously monitored at various locations inside the system. Sun Microsystems [16] refers to this approach as continuous system telemetry harness. Along with sensor information, soft performance parameters such as loads, throughputs, queue lengths, and bit error rates were tracked. Multivariate state estimation technique using this data was used to predict the signal of a particular variable based on learned correlations among all variables. Based on the expected variability in the value of a particular variable during application, a sequential probability ratio test (SPRT) is constructed. During actual monitoring SPRT is used to detect the deviations of the actual signal from the expected signal based on distributions (and not on single threshold value).

##### 2.2.3.2 GPS system

A commercial global positioning system (GPS) used a data precursor to failure approach [17]. The failure modes for the GPS system included precision failure due to an increase in position error and solution failure due to increased outage probability. These failure progressions were monitored in situ by

recording system-level features reported using the National Marine Electronics Association Protocol 0183. The GPS system was characterized to collect the principal feature values for a range of operating conditions. The approach was validated by conducting accelerated thermal cycling of the GPS system with the offset of the principal feature value measured in-situ. Based on experimental results, parametric models were developed to correlate the offset in the principal feature value with solution failure. During the experiment the built-in-test (BIT) provided no indication of an impending solution failure.

#### 2.2.3.3 Power Supply

The power supply was subdivided into component elements based on material characteristics [18]. Degradation in any individual or combination of component elements was extrapolated into an overall reliability prediction for the entire power supply system. Their PHM technique consisted of four steps: (1) acquiring the temperature profile using sensors; (2) conducting finite element analysis to perform stress analysis; (3) conducting fatigue prediction for each solder joint; (4) predicting the probability of failure of the power supply system. A PoF-based prognostics assessment of failure of a gull-wing lead power supply chip was performed [21].

#### 2.2.3.4 Home Appliances

The European Union funded a project from September 2001 through February 2005 called Environmental Life Cycle Information Management and Acquisition (ELIMA) for consumer products to improve life cycles management of products [19]. The ELIMA technology included sensors and memory built into a product to record dynamic data such as operation time, temperature, and power consumption. This was added to static data about materials and manufacturing. As a case study, the member companies monitored the application conditions of a game console and a household refrigerator. These included not only the operational and maintenance environments, but also the pre-operational environment, where stresses imposed on the parts during manufacturing, assembly, inspection, testing, shipping, and installation might have a significant impact on the eventual reliability of the equipment.

#### 2.2.3.5 Circuit Board Components

Life cycle vibration loads was used for RUL estimation of PCB [20]. A PCB with electronic components was mounted on a vibration shaker, which generated random vibration loading. The responses of the PCB to vibration loading in terms of bending curvature were monitored using strain gauges in situ. The interconnect strain values were then calculated from the measured PCB response and used in a vibration failure fatigue model for damage assessment. Damage estimates were accumulated using Miner's rule and then used to predict the life consumed and RUL. Uncertainty analysis was also performed, which included measurement uncertainty, parameter uncertainty, model uncertainty, failure criteria uncertainty, and future usage uncertainty. Sensitivity analysis was used to identify the dominant input variables that influenced prediction results. Then uncertainty propagation was conducted to perform reliability assessment with confidence levels.

### 2.2.4 Electronic Components

#### 2.2.4.1 Battery

Prototype battery health monitoring algorithms based on support vector machine, dynamic neural network, confidence prediction neural network, and usage pattern analysis are considered [22]. The batteries are important in back-up environments such as telecommunications and uninterruptible power supply (UPS). Various algorithms were tested on the battery data (voltage, current, temperature, etc.) collected from several lithium ion battery cells. The battery data was collected under different operating conditions (storage and charge /discharge cycling at room temperature and 50 $^{o}$C). This was used to give the probability of battery failure with time.

#### 2.2.4.2 Insulated Gate Bipolar Transistor (IGBT)

RUL estimation was done for IGBT by identifying failure precursor parameters and monitoring them [23]. In this study, IGBTs aged by thermal /electrical stresses were evaluated in comparison with new components to determine the electrical parameters that change with stressing. Three potential precursor parameters viz. threshold voltage, trans-conductance, and collector-emitter (ON) voltage, were evaluated by comparing aged and new IGBTs under temperatures ranging from 25 to 200 $^{o}$C. The trends in the three electrical parameters with temperature were correlated to device degradation. Then these precursors were monitored in-situ and precursor trending data were input into PoF models to allow for anomaly detection and prediction of RUL of these devices.

Prognostics application was deployed for electronics components within avionics systems, and in

particular its application to IGBT [24]. This application utilizes particle filter framework for RUL prediction, based on data from accelerated aging tests on IGBTs. The tests induced thermal-electrical over stresses by applying thermal cycling to the IGBT devices. In-situ state monitoring, including measurements of steady-state voltages and currents, electrical transients, and thermal transients are recorded and used as potential precursors of failure. For prognostic purposes the externally observable metrics of the device, such as collector current / voltage measurements during duty cycle on /off states of the IGBT showing degradation trends towards thermal runaway or latch-up, are correlated to PoF mechanisms like hot carrier injection, electromigration, etc., and used in a particle filtering (PF) framework to carry out RUL prediction

#### 2.2.4.3 Capacitor

Performance degradation of multilayer ceramic capacitors (MLCCs) under temperature-humidity-bias conditions and then prediction RUL is done [25]. In the tests, three performance parameters (capacitance, dissipation factor, and insulation resistance) were monitored in situ. A prognostics approach was developed to detect and predict failures using a multi-parameter regression, residual, detection, and prediction analysis on four types of MLCCs. For eight failed capacitors out of the 96 capacitors, all failures were detected with no missed alarms. Five out of the eight failed capacitors also gave advance warning of failure.

### 2.3 Challenges in Prognostics

Earlier only periodic inspection was carried out; which was later supplemented by on-line diagnostics or BITS for condition-based maintenance. This has to be eventually enhanced by prognostics; requiring advanced sensors; better understanding of what and how to measure parameters within the plant; enhanced data interrogation, communication and integration; predictive models for damage / aging; system integration for real world deployments; quantification of uncertainties of inherently random varying problems; and integration of enhanced condition-based maintenance / prognostics philosophies into new plant designs.

Algorithm needs to have adaptive capability and needs to be robust. For Uncertainty handling, reference [27] present techniques of Dampster-Shafer theory and Bayesian framework which are given in later part of this paper.

## 3. Prognostics and Health Management (PHM)

### 3.1 Background

Systems health management started in manufacturing, power generation and military systems. Rotating machinery were the first where it got implemented, because downtime or breakdown incurred significant costs. However PHM into the world of electrical and electronic devices is more recent and most of the work today has diagnostics i.e. fault detection, identification and isolation. The field of prognostics is still very much new, although Condition-based Maintenance (CBM) emphasizes on failure prediction and prevention. Initial efforts in machinery diagnostics were mostly data-driven techniques applied to vibration data. Integrated diagnostics and prognostics approaches have emerged in recent years. Health monitoring techniques are used to provide advance warning of failure, prevent catastrophic failure, assess reliability and reduce unscheduled maintenance [10].

### 3.2 Objectives of PHM

There are many related objectives, all of which converge to life cycle cost minimization. To provide continuous and real-time indication of the state of health of an electronic item as it is exposed to various life cycle loads during its normal operation. The state of health can also be given as the fraction of life consumed. PHM has the potential to mitigate the risks associated with new technology of Commercially Off The Shelf (COTS) components and assemblies with possibly short life, by providing a physics-based methodology to measure the degradation with time of electronic components and assemblies, and to forecast with some level of confidence the expected occurrence time of a failure.

### 3.3. Methods for PHM

#### 3.3.1 Physics Model-Based Methods

The most effective method is physics-of-failure (PoF) models to degradation and health monitoring systems. PoF methods focus on issues such as material deformation, fracture, fatigue, and material loss. Recent attempts at applying PoF methods to electronic prognosis have focused on the material degradation of interconnects and substrates. While highly accurate, PoF approaches tend to be computationally prohibitive for applying at the system level, alternative approaches are being

developed and applied, sometimes in combination with PoF methods.

### 3.3.2 Reliability-Based Methods

The simplest approach to failure prediction is based on statistical reliability models of component failure. Usually, reliability predictions are used to estimate future failure, based on current test results by applying a probability distribution such as the exponential distribution i.e. $R(t) = \exp(-\lambda t)$. One of the main shortcomings of exponential distribution is that it imposes a "Markov" assumption, i.e. the future prediction of a failure is independent of the history of the unit given the current measurement. Alternative reliability methods are applying the Weibull distribution for the predictions as it relaxes the assumption of constant failure rates and the Markov assumption [1].

### 3.3.3 Probability-Based Methods

The dynamic Bayesian network (DBN) architectures, hidden Markov models (HMM) and Kalman filters have been suggested as methods for using historical, sequential data to predict future failure. The concern with these models relates to the so-called "diffusion of context" phenomenon where, because of conditional independence, the effect of past experience diffuses the ability to predict. This is similar to the Markov assumption, also inherent in the reliability models discussed above. The use of "input-output HMM" has been suggested to overcome this problem.

### 3.3.4 Data-Driven Methods

PoF and reliability based methods form extremes of techniques for prognostics. PoF methods depend on high-resolution models but do not scale well. Reliability methods rely on statistical characteristics of populations of systems and do not handle specifics of a chosen system. In recent years, several diagnostic and prognostic models based on statistical, artificial intelligence (AI) and soft computing (SC) techniques have been proposed [11]. The AI and SC techniques include Artificial Neural Network (ANN), Fuzzy Logic, Non-Fuzzy statistical learning theory and support vector machines (SVMs). SVM is gaining applications in the areas of machine learning, computer vision and pattern recognition because of its high accuracy and good generalization capability. Each offers an advantage of being able to learn models based on empirical data but also suffer from the inability to learn portions of the model where no such data exists. The main drawbacks of the ANN-based predictors (against SVM) are a slow training speed and lack of transparency of the solution process, terming the ANNs as 'blackboxes'.

**Table 1: Potential Failure Precursors For Electronics [2]**

| Electronic Subsystem | Failure Precursor Parameter |
|---|---|
| Switching power supply | - DC output (voltage and current levels)<br>- Ripple<br>- Pulse width duty cycle<br>- Efficiency<br>- Feedback (voltage and current levels)<br>- Leakage current<br>- RF noise |
| Cables and connectors | - Impedance changes<br>- Physical damage<br>- High-energy dielectric breakdown |
| CMOS IC | - Supply leakage current<br>- Supply current variation<br>- Operating signature<br>- Current noise<br>- Logic level variations |
| Voltage controlled oscillators | - Output frequency<br>- Power loss<br>- Efficiency<br>- Phase distortion<br>- Noise |
| FET | - Gate leakage current/ resistance<br>- Drain-source leakage current/ Resistance |
| Electrolytic & Ceramic chip capacitors | - Leakage current/Resistance<br>- Dissipation factor<br>- RF noise |
| General purpose diodes | - Reverse leakage current<br>- Forward voltage drop<br>- Thermal resistance<br>- Power dissipation<br>- RF noise |
| RF power amplifier | - Voltage standing wave ratio (VSWR)<br>- Power dissipation |

### 3.4 Models of PHM

For electronic systems, system-level and major component failures are caused by a mixture of failure mechanisms [28]. These failure mechanisms result from defects, wearout, overstress conditions and random system interactions. These types of failures are a mixture of predictable and partially predictable events. Test results from accelerated testing of a CMOS device are presented as a basis to indicate the ability to capture fault indicators indicating impending failure and track the degradation of performance measurements [29].

PHM are typically modelled in one of the following three broad categories [3]:

(1) Modelling of damage accumulation and deterioration in electronic parts and assemblies utilizing exposure conditions (temperature / vibration) to compute the accumulated damage to the electronic circuits and structures.

(2) Monitoring or trending of parameters that are precursors to failure.

(3) Use of expendable devices such as "canaries" and fuses. Physics of failure (PoF) models, data trending for precursors, and fusion approaches which combine both the data-trending and PoF methodologies can be used to predict reliability.

#### 3.4.1 Damage Accumulation

The basic philosophy is that damage is a function of the loads experienced by the system in its life cycle environment. Exposure to life cycle loads listed in Table 1, leads to an accumulation of damage and eventually leads to failure. This approach is most useful in assessing wearout type failure mechanisms such as fatigue, corrosion, electro-migration, etc. The monitored data is used along with PoF models for damage estimation and RUL prediction. This PHM methodology gives more accuracy in RUL prediction, than traditionally used electronics reliability prediction methods. A case study is done of electronic prognostics for Switched-Mode Power Supplies - SMPS based on damage accumulation and also for Global Positioning System-GPS receiver [17] [30].

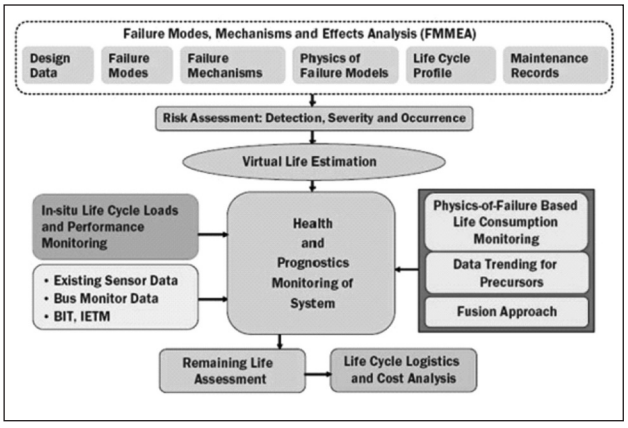


*Figure 1: PoF based PHM methodology [4]*

A major challenge in PHM is environmental and usage load profiles, which need to be efficiently and accurately captured in the application environment, and utilized in real time or near real time health assessment and prognostics. Some generic strategies for load monitoring and conversion of the sensor data into a format that can be used in PoF models, for both damage estimation and RUL prediction (due to specific failure mechanisms) are given in [28].

For PHM, the following needs to be provided as a minimum [1]:

- Means for representing graded health information and not discrete outcomes as diagnostics.
- Given the ability to represent graded health information, a means to take up failure progression information to higher levels of system hierarchy.
- Relaxation approach as compared to diagnosis to support state estimation based on real-valued test results.
- The ability to support periodic measurements and correlation between time series.
- Incorporation of usage, operational, and environmental data in performing state assessment and diagnostics.
- A framework for fusing information from multiple models and model types (e.g., physics-of-failure based, reliability-based, and data driven) to exploit the specific advantages of each type.

Major features of PoF based PHM methodology is shown in Figure 1. The first step involves failure modes, mechanisms, and effects analysis (FMMEA), which includes design data, failure modes, failure mechanisms, failure models, life cycle profile, and possible maintenance records. FMMEA is based on an understanding of the relationships between product requirements and the physical characteristics of the products (and their variation in the production process); the interactions of product materials with loads (stresses at application conditions); and their influence on product failure susceptibility with respect

to use conditions [2]. The next step involves risk assessment to rank the risk priority, which includes the estimation for detection, severity, and occurrence of failure. Then the results for the virtual (reliability) life assessment can be given. Based on this information, the monitoring parameters relevant to key failure mechanisms are selected, and existing sensor data, bus monitor data, and built-in test results can be used to identify health status (e.g., abnormal conditions) and parameters. Physics-based approaches (also known as model-based approaches) assume that accurate mathematical or physical models are available. It is a technically comprehensive approach dealing with failure mode progression, e.g. the crack propagation model. The drawback of this approach is inflexibility, which means it can only be applied to specific types of components.

PoF is an approach that utilizes knowledge of a product's life cycle loading and failure mechanisms to perform reliability modelling and assessment [4]. The life–cycle loads (thermal, mechanical, chemical, electrical, and so on), in combinations leads to performance or physical degradation of the product and reduce its service life. The PoF approach is based on the identification of potential failure modes, failure mechanisms and failure sites for the product at a particular life cycle loading condition. The stress at each failure site is obtained as a function of both the loading conditions and the product geometry and material properties. Damage models are then used to determine fault generation and propagation. The use of PoF modelling approaches for electronic components and devices, like those used for mechanical systems, is also a powerful tool in support of electronic prognostic capabilities. PoF based PHM is being looked upon as a cost-effective solution to predict the reliability of electronic products and systems [31]. Current research is focused on building physics-based damage models for electronics, obtaining the life cycle data of product, and assessing uncertainty in RUL prediction in order to make the PHM more realistic.

If the system reliability is predictable and very reliable, it would not make sense to implement a PHM solution. Return of investment from PHM implementation should consider advanced sensor technologies, communication technologies and decision making methods [32].

### 3.4.2 Trending of Precursors to Failure

This approach to PHM is focused on monitoring failure precursor indications for health monitoring. The system failures are non-deterministic in nature, but requires that the failure precursor have a deterministic link to the actual system failure. There is considerable existing work on failure precursors for mechanical systems, but only a few attempts have been made to apply health monitoring to electronics [5] [24]. The electronic PHM problem is characterized by imperfect and partial monitoring; and a significant random / overstress failure component must be considered in the decision process [28]. Wear and damage in electronics is comparatively more difficult to detect and inspect due to geometric scales and complex architecture [3].

Among the three main approaches to prognosis viz. statistical approaches, artificial intelligent approaches and model-based approaches, artificial intelligent approaches are most popular [33] [34].

Statistical approaches are usually applied to predict the chance that a machine operates without failure up to a future time given the current machine condition and past operational profile. These approaches requires plenty of previous data and information on historical data.

Artificial intelligence approaches, also known as data-driven approaches, are derived directly from routine condition monitoring (CM) data of the monitored system (e.g. temperature, vibration, oil debris, current, etc.) [35]. These methods predict the selected features that correlate with the failure progression based on the learning or training process. The more prior data is used for the training process, the more accurate the model obtained. The example features of a vibration signal that indicates the failure progression are root mean square (RMS), kurtosis, crest factor, shape factor, etc. Several data-driven prognosis methods have been developed and published.

### 3.4.3 Fuses and Canaries

Consumable devices such as fuses and canaries are a traditional method of protection. The word canary has come from the canary bird in coal mine

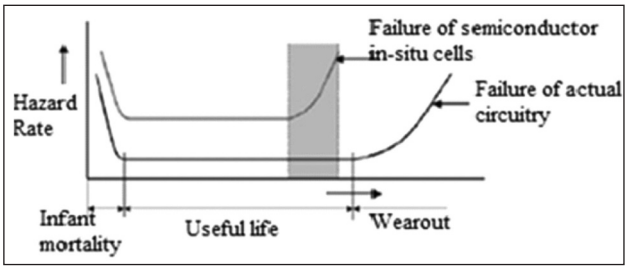


*Figure 2: Prognostic Cells [38]*

which gave warning of hazardous gas. Since the canary bird is more sensitive to hazardous gases than humans, the death or sickening of the canary was an indication to the miners to get out of the mine. Canary devices mounted on the actual product are used to provide advance warning of failure due to early occurrences of the specific wearout failure mechanisms on the canary devices [2]. Study of the applicability of semiconductor-level health monitors by using pre-calibrated cells (circuits) located on the chip along with the actual circuitry is given in [8]. The canary thus provides an effective early warning of catastrophic failure. The prognostics cell approach has been commercialized by Ridgetop Group (known as Sentinel Semiconductor technology) to provide an early-warning sentinel for upcoming device failures [36]. Prognostic cells made by the Ridgetop Group are able to provide precursor type information and are being embedded within custom ICs; but if implemented as a stand-alone component gives lower accuracy [6]. The prognostic cells are available for 0.35, 0.25, and 0.18 micron complementary metal oxide semiconductor (CMOS). The cell size is typically 800 micron at the 0.25 micron process size. Currently, prognostic cells are available for semiconductor failure mechanisms such as electrostatic discharge (ESD), hot carrier, metal migration, dielectric breakdown, and radiation effects. The time to failure of these prognostic cells can be pre-calibrated with respect to the time to failure of the actual product. Also a prognostic cell was used to monitor the time-dependent dielectric breakdown (TDDB) of the Metal Oxide Semiconductor Field Effect Transistor (MOSFET) on ICs [26].

Because of their co-existence, these cells experience substantially similar dependencies as does the actual product. The stresses that contribute to degradation of the circuit include voltage, current, temperature, humidity, and radiation. Since the operational stresses are the same, the damage rate is expected to be the same for both the circuits. However, the prognostic cell is designed to fail earlier through increased stress on the cell structure by virtue of scaling.

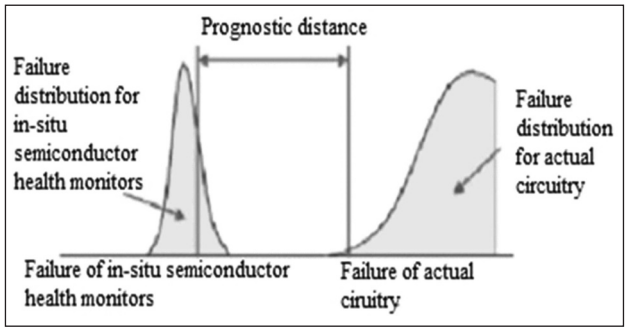


*Figure 3: Prognostic Cell Warning Period [38]*

Figure 2 illustrates the principle of operation of prognostic cells. The design of the cell is tuned to the particular application to give failure warning prior to failure of the host part. The warning provided by the prognostic cell has an inherent degree of uncertainty associated with it which is illustrated in Figure 3. Thus probabilistic techniques and reasoning are used to translate this warning period into a forecast of system failure.

A similar approach based on the use of consumable devices (canaries) having circuits that include the same physical features as the main system is followed in [3]. Degradation of these canaries due to environmental condition is assessed using accelerated testing, and the degradation levels are calibrated and correlated to actual failure levels of the main system. Scaling can be achieved by say increasing the current density inside the cells. Further increase in current density can be done by increasing the voltage level applied to the cells. Both of these techniques together can also be used. Higher current density leads to increased internal (joule) heating, leading to greater stress on the cells; and consequently they are expected to fail earlier than the actual circuit.

Figure 3 shows failure density functions of the actual product and the canary health monitors. Canaries can be calibrated to give sufficient advance warning of failure called prognostic distance; which enables appropriate maintenance and replacement activities. This point can be adjusted to some other early indication level. Multiple cells evenly spaced over the bathtub curve can be used to give multiple trigger points. The extension of this approach can be applied for board-level failures as proposed in [2], wherein are created canary components located on the same PCB that include the same mechanisms leading to failure in actual components.

### 3.5 Life-Cycle Loads

The life-cycle environment of a product is during its manufacturing, storage, handling, operating and non-operating conditions. The life-cycle loads (given in Table 2), either individually or in various combinations, may lead to performance or physical degradation of the product and reduce its service life [2]. The extent and rate of product degradation depends upon the magnitude and duration of exposure (usage rate, frequency, and severity) to

such loads. If one can measure these loads in-situ, the load profiles can be used in conjunction with damage models to assess the degradation due to cumulative load exposures. The surface temperatures can be dynamically monitored using thin film RTD sensors. All data can be recorded at a rate of one sample per minute. These data were applied in conjunction with PoF models for damage and RUL prediction. The health monitoring methodology was shown to effectively predict remaining life. Figure 9 shows measured absolute temperature profiles of CPU heat sink, hard disk drive, and external ambient air.

### 3.5.1 Radiation Risk

Data from CERN-LHC database showing radiation risk is given in [37]. Radiation induces Single event upsets (SEU) impact on system and the solution is mitigation by redundancy. SEU on ADC is acceptable, upset on data is acceptable, however upsets in Static Random Access Memory (SRAM) memory and FPGA used to store crucial information is an issue in control system. Latch-up (SEL) is usually the most threatening risk but can be mitigated with latch-up protection circuits against SEU. Upset rate depends on neutron energy. Neutron-induces upsets on SRAM-FPGA; wherein SEUs are susceptible to total dose. The measured cross section is 1 to 4 $*10^{-15}$ $cm^2$ / bit as against standard SRAM: 10 to 12 $*10^{-14}$ $cm^2$ / bit.

**Table 2: Examples of Life-Cycle Loads [2]**

| Load | Load Conditions |
|---|---|
| Thermal | Steady-state temperature, temperature ranges, temperature cycles, temperature gradients, ramp rates, heat dissipation |
| Mechanical | Pressure magnitude, pressure gradient, vibration, shock load, acoustic level, strain, stress |
| Chemical | Aggressive versus inert environment, humidity level, contamination, ozone, pollution, fuel spills |
| Physical | Radiation, electromagnetic interference, altitude |
| Electrical | Current, voltage, power |

XC4010E, XC4010XL Xilinx SRAM-FPGAs were tested with neutron of 11, 14, 100 MeV energy and the results are surprisingly good, better than SRAM. Since FPGA-SRAM have low pull up resistance of 5 kohms and showed no latch-up. For neutrons of energy less than 14 MeV there were no upset upto fluence of $10^{11}$ n/$cm^2$. But for neutrons of energy less than 100 MeV, 1 to 5 upsets for a fluence of 3 x $10^8$ n/$cm^2$ was found. XQR4013-36-62 XL, advanced FPGA in 0.35 μm CMOS, 30K-130K gates has much higher susceptibility, having threshold of equal or less than 10 MeV$cm^2$/mg, measured cross section $10^{-7}$$cm^2$/bit with ions which was very expensive.

For standard digital ICs (in majority CMOS), total dose qualification is not required for levels < 5krad for parts fabricated in modern technology but latch-up risk should be clarified. FPGA has robustness for total dose 3 krad to 300 krad but showed susceptibility to upset, even for "rad hard" version in peripheral circuits.

For SRAM for total dose of 5 to 50 krad, large variability between suppliers and lots, and upset is the main risk, to be checked.

## 4. Comparison of PoF and Statistical Handbook-Based Techniques

Traditional handbook-based reliability prediction methods for electronic products include MIL-Hdbk-217, Telcordia SR-332 (formerly Bellcore), PRISM, FIDES, CNET/RDF (European), Chinese GJB-299 and lately RAIC-HDBK-217 Plus [39]. These methods rely on analysis of failure data collected from the field and assume that the components of a system have constant failure rates that are derived from the collected data. These methods assume that the constant failure rates can be adjusted by independent "modifiers" to account for various quality, operating, and environmental conditions; despite the fact that most of the failure mechanisms are wear-out and not constant failure rate type. Therefore for COTS systems or components model-based techniques have more relevance. Furthermore, none of these handbook prediction methods consider failure modes or mechanisms, nor do they involve any uncertainty analysis. Thus they offer limited insight into practical reliability issues.

The bad thing of statistical-based preventative replacement is that limited failures continue to occur in the field and, more often, components are removed with significant useful life remaining due to extremely high reliability requirements. Premature component removal leads to lost component usage and increased cost. Maintenance planning is thus provisioning the fielded system with spares, supporting test equipment, personnel and facilities so that the probability of the system completing the next operating period successfully can be maintained at some pre-assigned level.

Prognostics and health management (PHM) is a practical and advanced way of looking at product reliability and life cycles conditions [40]. In PHM systems, the prediction is characterized as estimating RUL of a component or system. The benefits of PHM include: (1) providing advance warning of failures; (2) minimizing unscheduled maintenance, extending maintenance cycles, and maintaining effectiveness through timely repair actions; (3) reducing the life cycle cost of equipment by decreasing inspection costs, downtime, and inventory; and (4) improving logistical support of fielded systems.

There has been transition from military specific to commercial electronics technologies [6]. Avionics suppliers are necessarily turning to COTS electronic components and sub-systems partly because of the increasing lack of military qualified components and partly to take advantage of the high-performance components available in the COTS market with the advent of new technologies such as low-k dielectrics, copper interconnect and low voltage. The dominant market segment for commercial components is the high-volume commercial electronics sector (e.g. computer, telecom) and that military has almost no weight in this market. The needs of commercial electronics do not include long-term supportability or long product life. There is no incentive for electronic part manufacturers to design for a part whose life is in excess of about 3-7 years; particularly when part cost savings can be made by not doing so. Therefore low-volume/long support life industries such as military and aerospace are at risk from limited life electronic components.

## 5. Role of PoF and Data Driven Techniques for PHM

As mentioned earlier, electronic component reliability prediction is better with PoF approach compared with average statistics life-estimation approach based on MTBF. Data Driven (DD) techniques can be utilized for system-level monitoring, and PoF approach is adapted for parameter selection (that correlate with failure progression) and for detailed component behaviour, failure modes and life estimation. PoF involves in-depth understanding of the prevalent failure mechanisms and associated physics of failure affecting semiconductor devices. Specific fault to failure and system dependency inference models can be developed, and tuned based on accelerated failure testing and fault injection simulation efforts to provide increased confidence in the developed technology and prognostic output.

This involves two processes - 1. Offline learning and 2. Online tracking and prediction. One needs to explicitly derive PoF based aging models, identify their parameters from externally observable device characteristics and then use those models in a state prediction framework (e.g. PF) to carry out prognostics. In such a case, aging behavior will be linked to the changes in the internal model parameters which can then be linked to failure mechanisms like hot carrier injection, electromigration, etc. This involves devising aging experiments for the above objectives.

The measured variables are first transformed into uncorrelated variables with unit variances by PCA, map the input vectors into one feature space (possible with a higher dimension), either linearly or non-linearly, which is relevant with the selection of the kernel function. PCA aims at finding principal components that are uncorrelated and are combinations of observed variables. Then, within the feature space seek an optimized linear division, that is, construct a hyperplane which separates two classes (this can be extended to multi-class). SVM training always seeks a global optimized solution and avoids over-fitting, and it has the ability to deal with a large number of features. Suppose we are given a set of samples, that is, a series of input vectors $X \varepsilon R^d$ (i = 1 ,..., N) with corresponding class labels $y_i \varepsilon \{+1,-1\}$ (i = 1,. ..,N). Here, -l and +l are used to represent the two classes. The goal here is to construct one binary classifier or derive one decision function from the available data samples, which has small probability of misclassifying a future sample.

RUL has multiple sources of errors due to modelling inconsistencies, system noise and degraded sensor which leads to unsatisfactory performance from classical techniques- EKF (Extended Kalman Filter), ARIMA (Autoregressive Integrated Moving Average); RVM – Bayesian treatment to SVM is used for model development [41]. For non-linear systems with non-Gaussian noise in measurement, PF is the best technique. The model is incorporated in PF framework, where statistical estimates of noise and anticipated operational conditions are used to provide RUL as pdf. However, for linear system with Gaussian noise this method reduces to KF.

Using degradation data offers some important advantages for making reliability inferences and

predictions, especially when test time is severely limited and few or no failures are expected at lower levels of acceleration variables in an accelerated test. Library of data mining algorithms is required for such prognosis calculations.

Implementing an effective PHM strategy for an entire system will involve integrating different health monitoring approaches. An extensive analysis may be required to determine the weak link in the system to enable a more focused monitoring process [2]. Once the potential failure modes, mechanisms, and effects have been identified, a combination of BIT, canaries, precursor reasoning, and life-cycle damage modelling may be necessary, depending on the failure attributes. In fact, different approaches can be implemented based on the same sensor data. For example, operational loads, such as temperature, voltage, supply current, and acceleration, can be collected by BIT. The current and temperature data can be used with damage models to calculate the susceptibility to electromigration between metallizations. Also, the supply-current data can be used with precursor reasoning algorithms for identifying signs of transistor degradation.

## 6. Target Device Selection

This is to select an appropriate digital component or device, to focus for the development of PHM technology. The digital component categories considered for evaluation were:

- Digital Signal Processor
- Microprocessor
- Microcontroller
- FPGA
- Application Specific Integrated Circuit
- Static/Dynamic Random Access Memory (SRAM/DRAM)

While each of these digital component categories typically serves different functional purposes, they are structurally very similar, with the transistor as the common factor [29]. The component's function may have a greater influence on its susceptibility to faults than the actual architecture. For example, memory devices are used with built-in error checking for fault tolerance; FPGA's often run massively parallel, independent operations where a fault to a single element may have a negligible impact on the operation of the entire component.

FPGA are a category of digital components that are being extensively used in making intelligent I/O boards. The intelligent I/O boards - Digital Input board, Digital Output board and Analog Input and Output board are based on FPGA. They have a significant risk associated with an undiagnosed fault and a greater need for effective PHM. In consideration of this information, FPGA was selected as the focus of PHM development.

CMOS failure mechanisms such as HCI, EM, TDDB, NBTI occur in FPGA. The DD technique can be employed to determine the class of the device whether healthy or fail class. It can be formulated as a bi-class problem. The state prediction technique will be based on the model applicable. Experiments of accelerated testing gives the variation of the externally measurable metrics. These metrics can be correlated with the failure mechanisms for making prediction of device reliability or RUL. PHM implementing canaries and fuse devices can also be considered.

## 7. Failure Mechanisms in MOSFET

The area of digital devices is vast, from FPGAs and DSPs to general purpose processors and volatile and non-volatile memories. Inspite of functional and topological dissimilarities, all digital devices depend on semiconductor devices- transistors. Moreover, MOSFETs are everywhere in digital electronics and account for 99% of the FET market [4]. Thus, understanding PoF at the MOSFET level is important while seeing failure modes and mechanisms in digital systems.

Devices age due to electrical, mechanical and environmental stresses throughout lifetime. If knowledge of the time-dependent effects of these aging processes can be determined, development of physics based diagnostics and prognostics at the device or system level is possible. Documented semiconductor PoF models are available as a basis for deriving system level models describing the responses of the system over time to the environmental conditions [42].

Some major intrinsic faults of transistor physics include time dependent dielectric breakdown, hot carrier injection, negative bias temp instability and electromigration [43]. Some major extrinsic faults relevant to transistor packaging, include contact migration, wire lift, die solder degradation and package delamination. These PoF mechanisms serve as the basis for the accelerated aging processes of the devices.

The majority of semiconductor devices are based on silicon fabrication; however the following failure mechanisms can be extended to other materials such as silicon-germanium, gallium arsenide, and silicon carbide thereby providing foundation for analyzing almost all digital devices.

### 7.1 Thermal Cycling

Thermal cycling is one of the main environmental acceleration factors that cause MOSFET aging wherein deterioration occurs of the thermal circuit which allows the device to release generated heat.

Multiple materials in IC have different thermal expansion coefficients and when exposed to thermal cycling, a fracture or void space is produced as seen in Figure 4. These fractures deteriorate the functionality of the device, though not directly interfere with the software operation of the device. The semiconductor's ability to transfer heat reduces and accelerates the aging process for other failure mechanisms. Every time a device experiences a power-up and a power-down cycle, damage caused by thermal cycling accumulates. Thermal cycling eventually weakens metallic contacts, triggering the occurrence of gate-oxide breakdown or contact migration. The Coffin-Manson model, shown below [29], can be used to estimate the number of thermal cycles before failure for a specific device.

$$N_f = C_0 \times (\Delta T - \Delta T_0)^{-q} \quad (1)$$

Nf = Number of cycles to failure

To = Cycle in the Plastic region

Co = Material- Dependant Constant

$\Delta T$ = Entire Temperature Cycle

$\Delta T_o$ = Cycle in the Plastic region

q = Material–Dependant Const. [29]

### 7.2. Electromigration

Electromigration is the mass transport of the metal because of momentum transfer between the conducting electrons and the diffusing metal atoms. This phenomenon happens in metals and highly doped semiconductors (with negative thermo-impedance). The 50th percentile time to failure due to electromigration is calculated using the equation given below [29].

$$t_{50} = A_0 \times j^{-2} \times e^{\frac{E_a}{kT}} \quad (2)$$

where

$A_o$ = Constant

T = Temperature in K

j = Current density

k = Boltzmann's constant

$E_a$ = -0.1 to 0.2eV

In electromigration due to the action of the flowing current, die metallization is removed from one part of the trace and accumulated at a nearby place. This eventually leads to an open circuit trace or a short circuit or high resistance paths between adjacent traces. Electromigration is due to high current densities in silicon interconnects. Electromigration has an intrinsic incubation time and depends on material, geometry and current density, and the probability of failure is zero until the accumulated damage exceeds a threshold. Studies have shown that the rate of electromigration in the newer copper metallurgies are at a slower rate than the more common aluminum metallurgy [24].

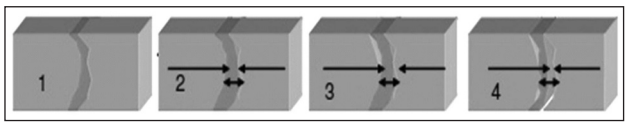


*Figure 4: Void Area Creation Process Due to Thermal Cycling [29]*

### 7.3 Hot Carrier Effects

Hot Carrier Effects lead to two distinct wearout mechanisms. These are Hot Carrier Degradation (HCD) and Negative Bias Temperature Instability (NBTI). Hot carriers effects are because of high-energy carriers, either holes or electrons, which enter the gate oxide of a transistor leading to degradation of the oxide's properties. Hot carriers are produced as current flows from the source to the drain through the channel and a small number of these hot carriers gain enough energy and get injected into the gate oxide causing charge trapping and the generation of interface states. With time, this leads to a drift in the performance characteristics of the device and is referred to as HCD. Device lifetime can be determined by defining failure in terms of percentage shift in threshold voltage, change in trans-conductance, or a variation in drive or saturation current. NBTI happens due to hole trapping and interface state generation and

results in threshold voltage drifts and delays within a CMOS device. As MOSFETs ages, the dielectric material of the device degrades. The silicon dioxide ($SiO_2$) bonds of the dielectric material break due to interaction between high energy electrons, known as hot carriers. This phenomenon is important in MOSFET technology wherein presence of high electric fields aids creation of hot carriers, as shown in Figure 5.The four common hot carrier injection mechanisms are

- Drain avalanche hot carrier injection (DAHC)
- Channel hot electron injection
- Substrate hot electron injection
- Secondary generated hot electron injection

**Drain Avalanche Hot Carrier (DAHC):** This phenomenon produces maximum accelerated device degradation under normal operating temperatures. This happens when the voltage applied at the drain under non-saturated conditions is higher than the voltage applied to the gate ($V_D > V_G$). High electric fields near the drain accelerates the carriers into the drain's depletion region.

**Acceleration of the channel carriers**: This phenomenon, also termed as impact ionization, happens when accelerated carriers collide with Si lattice atoms, creating electron-hole pairs. The created electron-hole could gain enough energy to overcome the electric potential barrier between the silicon substrate and the gate oxide, causing gate isolation deterioration. This leads to increase in gate current and reduction in the sub-threshold voltage ($V_{th}$).

**Substrate hot electron injection:** Due to the influence of the drain-to-gate field, hot carriers are generated also in the substrate. These hot carriers gets injected and becomes trapped in the gate oxide layer, causing the same degradation as DAHC.

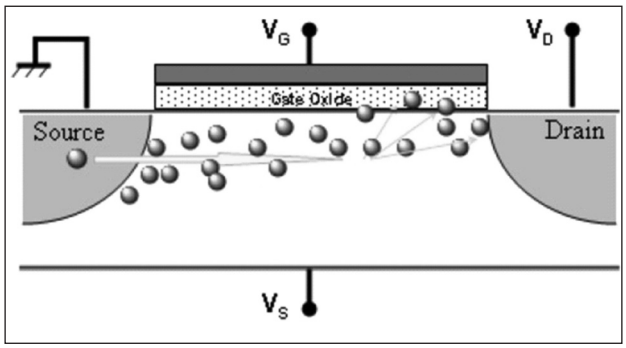


*Figure 5: MOSFET Cross-sectional Visualization of Hot Carrier Effect [29]*

**Secondary generated hot electron injection**: The number of electrons that become trapped in the interface between doped regions grows over time modifying the threshold voltage ($V_{th}$) and its transconductance ($g_m$).

Irrespective of their origin, hot carriers produce two types of degradations in FET technologies. The first is acceleration in time-dependant dielectric breakdown (TDDB) of the oxide barrier ($SiO_2$), and the second is migration and degradation of the semiconductor.

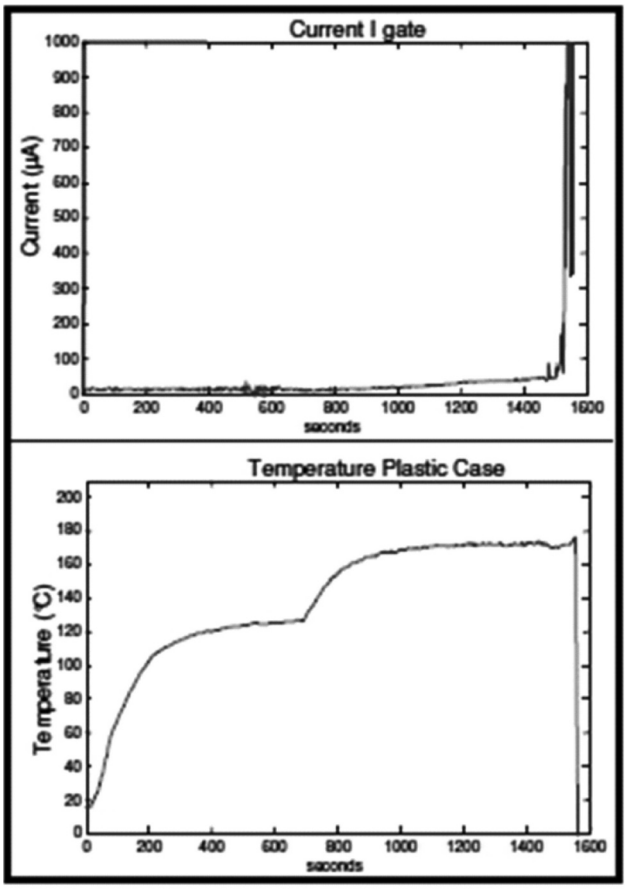


*Figure 6: Gate Current Increase in an Accelerated MOSFET Aging Test [29]*

A median time-to-failure approximation for hot carrier injection is given below [29]:

$$t_{50} = B_0 \times I^n \times e^{\frac{E_a}{kT}} \quad (3)$$

$B_o$ = Constant
k = Boltzmann's constant
n = 2-4
T = temperature in Kelvin (K)
$E_a$ = -0.1 to 0.2eV
I = N-channel - peak substrate current,

An example of a $SiO_2$ progressive breakdown in MOSFET is shown in Figure 6.

### 7.4 Time-dependent Dielectric Breakdown

Dielectric breakdown happens when strong electric field induces a current channel through a previously insulated medium. Acute dielectric breakdown is typically due to electrostatic discharge (ESD) and junction over-voltage. TDDB is the breakdown of gate oxide caused by defect accumulation in $SiO_2$ insulator. TDDB effect increases with increase in electric field strength. A strong electric field may induce energy into an electron or a hole thereby creating a "hot carrier". Due to high kinetic energy stored, sufficient energy is obtained for tunneling and becoming trapped in gate oxide, and is the primary cause of TDDB and contributing to device failures under normal operating conditions. In general, it relates to the $SiO_2$ oxidation barrier degradation under normal operating conditions. The reduction in life can be computed as [29]:

$$t_{50} = B_0 \times \left(\frac{1}{V}\right)^{(a-bT)} \times e^{\frac{X+\frac{Y}{T}+ZT}{kT}} \quad (4)$$

where

$B_o$ = Constant

Z = 8.37E- 4 eV/K

a = 78

k = Boltzmann's constant

b = -0.081

T = temperature in Kelvin (K)

X = 0.759eV

Breakdown occurs in $SiO_2$ films when local electric field is sufficiently high to cause avalanche multiplication in the dielectric. $SiO_2$ is a dielectric having property analogous to a 'band gap' of the order of ~9 eV. When the applied electronic field is sufficient, normally around 10 to 15 mV/cm; electrons that tunnel in from cathode cause impact ionization within the dielectric and the consequential current destroys the material by Joule heating. In $SiO_2$ this is a run-away phenomenon, because the holes, either tunneled in from the anode or produced by the impact ionization, are trapped creating a positive charge cloud that further increases the electric field. The electrons (mobility ~30$cm^2$/Vsec) hence are multiplied and cause destruction. This phenomenon is triggered when the electric field reaches the critical value required to cause carrier multiplication. Due to the minute imperfections in the film, the electric field is normally not perfectly uniformly distributed, so that this phenomenon takes place in local region, and the current flow and the consequential destruction occur in a filament in the film, i.e. a localized explosion occurs. This causes a total denaturing of the region and typically causes a short between the gate electrode and source/drain or substrate electrodes. If the film is nearly perfectly uniform, the degradation phenomenon takes place, but the local current densities are not excessive, and the film is not physically destroyed. However, this non-destructive breakdown typically results in films that are filled with trapped charge, and consequently device threshold voltages gets shifted. In either case, the device ceases to function.

### 7.5 Contact Migration

Contact migration forms metal voids between external contact metals and silicon. As metal voids grow, aluminum or other metals can diffuse into silicon. This can cause metal spikes to form deep in the silicon region resulting in shorting of p-n junctions

### 7.6 Tin Whiskers

The commercial drive to eliminate lead (Pb) from electronics has caused an interest in using tin (Sn) as an economical lead-free (Pb-free) plating option. Many electronic part manufactures have started providing pure tin (Sn) finishes and others are in the process of transition. This tin-plating has renewed concern over the threat of failure due to tin whiskers, first reported in the 1940s [38]. CALCE Consortium has posted an alert, warning manufacturers of electronic hardware that tin whiskers represent a current failure risk that must be addressed for the reliability of electronics that perform mission critical services and have long operation periods. Tin whiskers have been identified and are highly suspected in the failure of many electronic systems. Although new plating processes have been developed which reduces the risk of tin whisker growth, there is currently no industry-accepted test for determining the tendency of tin whiskers growth on a finished surface.

### 7.7 Package Related Fault

#### 7.7.1 Wire lift

When the bond between the package wires connecting to the silicon die fail, wire lift occurs. Wire lift is a dominant failure mode in high power devices -IGBT.

### 7.7.2 Die Solder Degradation

Die solder degradation is also a prominent package related fault.

### 7.8 Printed Wiring Assemblies

The three dominant wearout failure mechanisms in Printed Wiring Assemblies (PWA) are: Conductive filament formation (CFF), PTH / VIA fatigue, and solder joint fatigue [44]. These failure mechanisms usually manifest themselves as intermittent failures which results in the assembly being classified as retest-OK.

### 7.8.1 Conductive Filament Formation (CFF)

CFF is a electrochemical wearout process involving transport of metal through a non-metallic medium, under applied electric field. Occurrence of CFF leads to formation of electrical shorts.

### 7.8.2 Printed Through Hole (PTH) Fatigue

Failure of PTH / VIA contributes to an electrical discontinuity and occurs due to difference in the coefficients of thermal expansion (CTEs) of the PTH plating material and the PWA material in the thickness direction. The dominant failure mechanism in a well manufactured PTH is barrel cracking caused by thermo-mechanical fatigue. The plating thickness and the aspect ratio (height of PTH/diameter of PTH) are critical geometrical parameters.

### 7.8.3 Solder Joint Fatigue

Solder joint develop cracks as temperature cycles, caused by relative motion between the package and printed circuit board. These cracks starts developing from small discontinuities or inclusions in the material and eventually propagate right through the solder fillet causing failure. The mechanism can exhibit cyclic intermittent failure when the crack is physically forced closed again by the relative motion of chip and board under temperature variation, vibration and shock. There are models for solder joint failure for all the major attach technologies viz. through-hole, surface mount, ball grid array etc. Solder fatigue life is often correlated with amplitude of the shear strain which depends on the stress amplitude, mean value and dwell times.

## 8. Failure Mechanism Driven Reliability Monitoring

The first step in PHM is to select the life-cycle parameters to be monitored. Parameters are identified based on factors that cause catastrophic failures or that lead to long downtimes. Selection can be based on knowledge of the critical parameters established by past experience and field failure data on similar products and on qualification testing. Systematic methods, such as failure mode mechanisms and effects analysis (FMMEA) [2], can be used to determine parameters that need to be monitored. Testing needs to be conducted to demonstrate the potential of selected parameters to be useful for detecting incipient failures in electronic systems.

Based on virtual life assessment, critical failure modes and failure mechanisms can be prioritized [31]. The existing sensor data, maintenance and inspection record can also be used to identify the abnormal conditions and parameters. Based on such information, the monitoring parameters and sensor locations for PHM can be determined. Damage is calculated from PoF models to obtain RUL.

List of common failure mechanisms and failure sites in electronics with the relevant loads and associated failure models can be obtained from standards including JESD659-A: Failure-mechanism-driven reliability monitoring, JEP 122C: Failure mechanisms and models for silicon semiconductor devices, JEP143A: Solid-state reliability assessment and qualification methodologies, JESD91A: Method for developing acceleration models for electronic component failure mechanisms, SEMATECH #00053955A -XFR: Semiconductor device reliability failure models, and SEMATECH #99083810A-XFR: Use condition based reliability evaluation of new semiconductor technologies [45].

The current and temperature data can be used with damage models for calculating susceptibility to electromigration between metallizations [2]. Also, the supply-current data can be used with precursor reasoning algorithms for identifying signs of transistor degradation. Supply current monitoring is routinely performed for testing of CMOS integrated circuits (ICs). This method is based upon the notion that defective circuits produce significantly higher amount of current than the current produced by fault-free circuits. The power supply current has two elements: the quiescent current and the transient or dynamic current. Quiescent current ($I_{ddq}$) is the leakage current drawn by the CMOS circuit when it is in a stable (quiescent) state. Transient or dynamic current is the supply current produced by circuits under test (CUT) during a transition period after the input has been applied. $I_{ddq}$ has been reported to have the potential for detecting defects such as bridging,

**Table 3: Examples of Failure Models [38]**

| Failure Mechanism | Failure Sites | Relevant Stresses | Sample Model |
|---|---|---|---|
| Fatigue | Die attach, Wire bond/Tab, Solder leads, Bond Pads, Traces, Vias/ PTHs, Interfaces | Cyclic Deformations (ΔT, ΔH,ΔV ) | Nonlinear Power Law (Coffin-Mason) $N_f = C_0 \times (\Delta T - \Delta T_0)^{-q}$ [29] |
| Corrosion | Metallization | M, ΔV, T, chemical | Eyring (Howard) $t_f = \frac{wlhndF}{M_c V_b} \frac{\rho}{t}$ [52] |
| Electromigration | Metallization | T,J | Eyring (Black) $t_{50} = A_0 \times j^{-2} \times e^{\frac{E_a}{kT}}$ [29] |
| Conductive Filament Formation | Between Metallization | M, ΔV | Power Law (Rudra) $t_f = \frac{af(1000kL)^n}{V_{cf}{}^m (M_{cf} - M_t)}$ [52] |
| Time Dependent Dielectric Breakdown | Dielectric Layers | V, T | Arrhenius (Fowler-Nordieum) $t_f \propto E^{-1} \exp\left[ -\frac{q}{kT} \left( \frac{q}{\pi \varepsilon_0 k} \right)^{0.5} \sqrt{E} \right]$ [53] |
| ΔT: Temperature range T : Temperature ΔH: Humidity range ΔV: Voltage range<br>V: Voltage M: Moisture J: Current density $t_f$: Time to failure<br>w,l,h,n,d,$M_c$: width, length, thickness, valency, density, atomic weight of conductor respectively<br>$V_b$: Voltage bias ρ,t: density and thickness of electrolyte F: Faraday's constant | | | |

opens, and parasitic transistor defects. Operational and environmental stresses such as temperature, voltage, and radiation can quickly degrade and have undetected faults and increase the leakage current [2] [43] [46]. $I_{ddq}$ testing is in literature [47] and monitoring $I_{ddq}$ is more popular than $I_{dds}$ monitoring. Smith and Campbell developed a quiescent current monitor (QCM) that can detect elevated $I_{ddq}$ current in real time during operation. Some more information about current monitors is given in the 'Sensors for PHM of CMOS ICs' section below. A circuit for off-chip Iddq measurement is given in [48]. Evolution of circuits for Iddq measurement is stated in [49].

It is proposed by GMA Industries [4], to embed molecular test equipment (MTE) within ICs (in the chip substrate) to enable them to continuously test themselves during normal operation and to provide a visual indication of their failure. The molecular-sized sensor "sea of needles" could be used to measure voltage, current, and other electrical parameters, as well as sense changes in the chemical structure of integrated circuits that are indicative of impending or actual circuit failure. Development exists of specialized doping techniques for carbon nanotubes to form basic structure comprising the sensors.

An algorithm for health monitoring of pulse-width modulation (PWM) voltage source inverters (VSIs) is mentioned in [2]. The algorithm was designed to detect and identify transistor open circuit faults and intermittent misfiring faults occurring in electronic drives. The mathematical foundations of the algorithm were based on discrete transform (DWT) and fuzzy logic (FL). Current waveforms were monitored and continuously analyzed using DWT to identify faults that may occur due to constant stress, voltage swings, rapid speed variations, frequent stop/start-ups, and constant overloads. After fault detection, "if–then" fuzzy rules were used for very large scale integration (VLSI) fault diagnosis to pinpoint the fault device. The algorithm was demonstrated to detect

certain intermittent faults in laboratory experimental conditions.

Development of a damage precursor based RUL computation approach for various package elements to prognosticate electronic systems prior to the appearance of any macro-indicators of damage is mentioned in [2]. The precursor variables have been identified for various package elements and failure mechanisms. Model-algorithms have been developed to correlate precursors with impending failure for computation of residual life. Package elements investigated include, first-level interconnects, dielectrics, chip interconnects, underfills, and semiconductors. Examples of damage include phase growth rate of solder interconnects, intermetallics, normal stress at chip interface, and interfacial shear stress. The precursor based damage computation approach eliminates the need for knowledge of prior or posterior operational stresses and enables system reliability management of deployed non-pristine materials under unknown loading conditions. The approach can be used on redeployed parts, subsystems, and systems, since it does not depend on availability of prior stress histories.

## 9. Failure Modes

Analysis of failures throughout the lifespan identifies various failure mode possibilities triggered by various failure mechanisms. A failure mechanism is defined as the physical or chemical phenomenon causing the onset of failure; common examples in mechanical systems are vibration, corrosion, high friction, etc. The underlying failure mechanism becomes evident to the user through failure modes which are noticeable observations of how the system or device failed; for example overheating, unexpected shutdown, and reduced performance are observable failure modes. Commonly, single failure modes can be attributed to multiple failure mechanisms.

The characteristic changes as the device transits from useful life to end of life are of most interest when attempting to identify, classify, and track incipient signs of impending failure. Thermal stress and electrical stress are the most common aging methodologies. Thermal cycling and chronic temperature overstress are prevalent thermal stress methods.

Electromagnetic pulses or ESD is a leading cause of gate oxide failure and hard switching of inductive loads, causing voltage spikes which can cause significant damage to drain-source junctions. Steady-state methods include chronic over-voltage and over-current. Applying high gate voltages, setting gate voltage (Vg) to maximize drain current, and applying current overstress across the drain induces hot carrier and TBBD. Various failure mechanisms, their occurrence site, relevant stresses along with model type are given in Table 3.

### 9.1 Competing Failure Modes

As shown in the Fig.7, the functional failure threshold region is shown within feature space. Its advantage is that multiple and competitive failure modes can be mapped within the same N-dimensional feature space. As a result, the current health and time-to-failure can be assessed for each failure mode concurrently. Figure 7 represents the fault-to-failure progression of a number of competing failure modes (FM) using a statistical trending algorithm. The figure shows how the severity (or damage index) output of the feature space classifier (z-axis) changes for each failure mode (y-axis) over time (x-axis). The statistical trend of each FM (indicated by the dashed line) is obtained from the double exponential smoothing projection for each feature. The Figure also captures the concept of competing failure modes, wherein it can be seen that although Failure Mode 4 is classified as the most advanced failure mode by the classification routine (damage index of 0.78), the prognostic routine is able to determine that FM1 has a quicker fault-to-failure progression and would correctly identify that this failure mode is more likely to lead to the shortest RUL. Assuming both routines have properly captured the true health state of the system, the information presented in the figure is important from a number of perspectives [40] as given below.

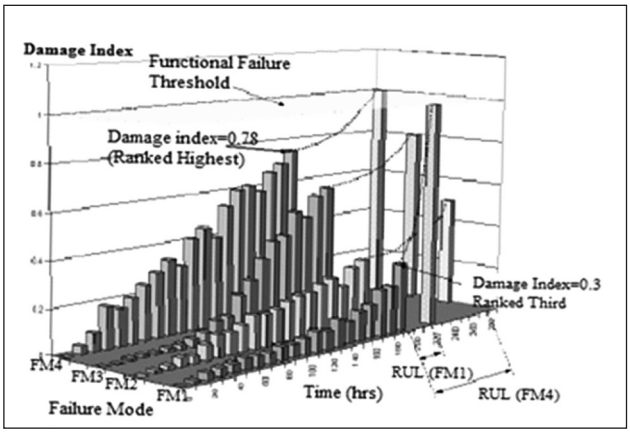


*Figure 7: Statistical Fault Progression Using Evolutionary Prognostics [50]*

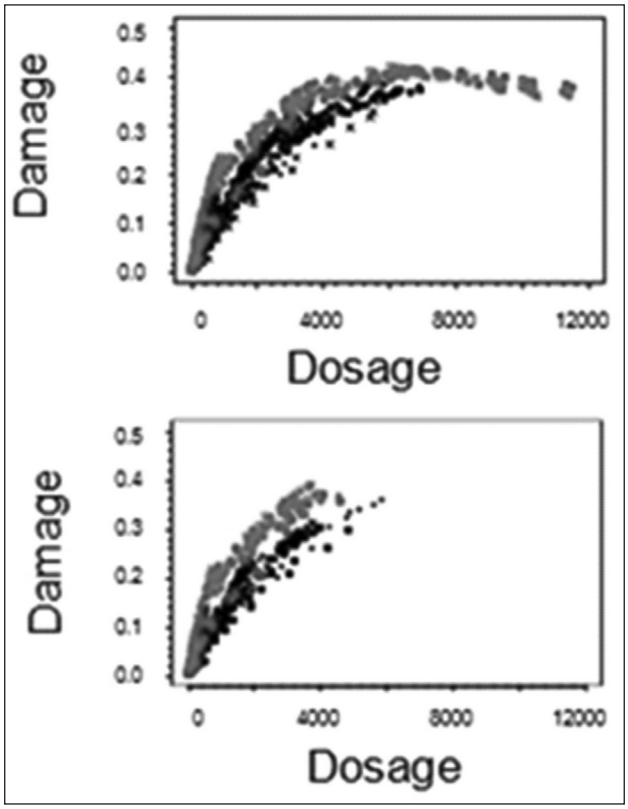


*Figure 8: Illustration of data cleaning for the peak [77]*

**Maintenance Perspective:** Parts can be ordered to correct FM1 and FM4, since both reach functional failure within the time frame of interest. In addition, maintenance actions can be planned for FM1 knowing that it will likely fail first. Given that FM1 and FM4 are both close to failure, it may be most efficient to correct both problems at the same time. Without prognostics, however, the FM1 problem would not be realized and only FM4 maintenance would be planned. This most likely would result in unnecessary downtime for the system while FM1 parts are being ordered, while FM1 maintenance is being performed, and possibly again to correct for FM4. The result is lost availability. Different fault progressions may also be generated based on altered mission plan to assess the risk associated with these new plans. Once again, without prognostics, the rapid fault progression and prediction horizon of FM1 may be overlooked.

This capability therefore results in increased mission readiness and safety. Under the current approach, both diagnostics and prognostics are assessed within the evolutionary prognostics routine. In different implementations any diagnostic process, such as fuzzy logic or neural networks, can be fused with any prognostic routine, such as Kalman filtering, to effectively achieve a similar result [50].

### 9.2 Change of Direction of the Monitoring Parameter

Traditional applications in reliability and service life prediction based on accelerated testing, involve chemical degradation that is accelerated by increasing variables like temperature, humidity, and current density or voltage stress (using statistical models based on knowledge from physical chemistry). Fig. 8 gives illustration of data cleaning for the peak a) shows original data paths. b) shows data paths after deleting outliers and increasing tails. Figure 8a shows that the parameter increases, peaks after which the degradation paths begin to decrease. This behaviour is caused by physical and chemical changes in the specimens. The turning point happens to be far beyond the definition of failure, modelling beyond the turning point is not needed. Thus increasing/decreasing tails are cut after the turning point for those cases where degradation paths changes direction.

## 10. Sensors for PHM of CMOS ICs

Power supply quiescent current $I_{ddq}$ is a good indicator of the failures occurring in CMOS ICs. As mentioned above, the quiescent current monitor (QCM) has been developed to detect elevated current in real time during operation [2]. The QCM performed leakage current measurements on every transition of the system clock to get maximum coverage of the IC in real time. A low-power built-in current monitor for CMOS devices is also proposed in the same reference. The current monitor developed by Pecuh et al. [2] was tested on a series of inverters for simulating open and short faults. Both fault types were successfully detected and operational speeds of up to 100 MHz were achieved with almost no effect on the performance of the circuit under test. The current sensor developed by Xue and Walker enabled monitoring at a resolution level of 10 pA. The system translated the current level into a digital signal with scan chain readout. This concept was verified by fabrication on a test chip. The mathematical foundations of the algorithm were based on discrete wavelet transform (DWT) and fuzzy logic (FL) [50].

## 11. Binning and Density Estimation of Load Parameters

Sensors give large volumes of data which can be well managed by data reduction processing on the raw data [6]. For e.g. damage accumulation models are not sensitive to infrequent and large excursions away from the mean. This property enables data

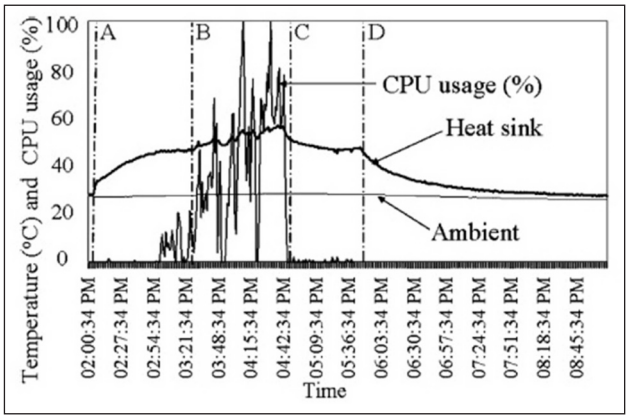


*Figure 9: Measured absolute temperature profiles of CPU heat sink, hard disk drive, and external ambient air [6]*

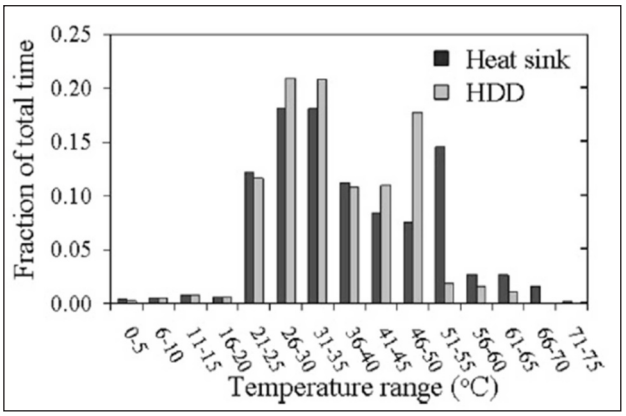


*Figure 10: Distributions of measured absolute temperature for the CPU heat sink and hard disk drive [6]*

reduction algorithms like Ordered Overall Range or Cycle Counting algorithms to reduce the data volume by an order of magnitude without losing significant amount of information.

This section shows how the captured data though appearing random, has information which can be extracted and used in the appropriate models. Examples from two references are given below.

Fig 9 shows measured absolute temperature profiles of CPU heat sink, hard disk drive, and external ambient air [6]. This collected data is analyzed statistically using data simplification and cycle counting algorithms, and converted into a format that can be used in PoF models, for both damage estimation and RUL prediction; due to specific failure mechanisms. Data simplification leads to gains in computing speed and testing time, condense load histories without losing important damage characteristics and preserve the interaction of load parameters. Figure10 shows CPU heat sink absolute temperature variation for different CPU utilization. Data is recorded for three events as indicated - Event A shows when notebook is powered on, events B to C shows when numerical simulation is executed and event D shows when Notebook is powered off. Based on this data, histograms were drawn as shown in Figure which shows the fraction of total time during which the product experienced a given range of absolute temperature. Similar histograms are drawn for the number of occurrences of a range of temperature cycle magnitudes. Histograms are also drawn for the fraction of total time during which the product experienced a given range of temperature ramp rate [6]. Temperature cycles of small amplitude may not significantly impact on the reliability of electronic packaging interconnections. The potential damage induced also depends on variables such as the mean cyclic temperature. Thus the above mentioned three types of histograms information about cyclic range (Δs), cyclic mean load (Smean), and rate of change of load(ds/dt) is applied in a life consumption monitoring methodology [7], [8], [78] to provide both damage estimation and RUL prediction due to specific failure mechanisms influenced by temperature. 51] on Histograms and kernel estimators are detailed in [51].

A similar data simplification techniques and a variety of tools such as filters, Fourier transforms, wavelets, Hayes method, ordered overall range, etc. are mentioned in [6]. It is extracts the relevant load parameters including cyclic mean, amplitudes, ramp rates, hold periods, power spectral densities, etc. Commonly used load parameter extraction methods include: cycle counting algorithms or extracting cycles from time-load signal, Fast Fourier transforms (FFT) for extracting the frequency content of signals, etc. Depending on the application and type of signal, load extraction methods may differ.

## 12. Machine Learning Techniques for PHM Algorithm

This section discusses various techniques that can be used for different purposes. ML techniques are based on datasets [79], translation of raw data to meaningful information is done by classification / clustering, regression and ranking, since the raw data do not provide any meaningful information. In PHM applications i.e. for detecting or predicting system health, ML techniques are closely related to problem of classification or clustering of input data. Classification algorithms are used and patterns of

collected data are analyzed for identification of healthy condition of system.

For Prognostics, Data Driven (DD) Approach and PoF Approach can be employed. In DD approach, future behaviour is predicted based on learning from the data available of past.. DD technique is an economical way to automatically monitor health of large multivariate systems. DD technique incorporates statistical and probability theory, data preprocessing, dimensionality reduction (by compression and transformations), feature extraction and denoising. PoF approach uses underlying engineering and failure principles to model and predict RUL. Hybrid Approach is best suited, utilizing information from PoF and DD approaches; since it gives advantages of both approaches while eliminating some of their drawbacks. Merits and limitations of various approaches (for machinery health prediction) are stated in [81].

### 12.1 Advantages of ML techniques

ML utilizes computational solutions to otherwise expensive or intractable theoretical alternatives. ML gives better accuracy for the statistical and probabilistic estimates. ML acts on relevant data to explain trends and characteristics of system health. ML is more useful for solving prognostics problems than diagnostics. ML is useful when user interaction is required for supervised learning, having information for relationship between data trends and physics, modes and mechanisms of failure.

### 12.2 Feature Selection for ML

Features or attributes having high interclass difference and intraclass similarity will have high weights. Features producing a larger deviation in output are considered important. Monitoring indices is quantifying feature characteristics. The desirable monitoring indices should be highly sensitive to the fault with low sensitivity to noise. The selection of monitoring indices involves different steps of signal processing and feature extraction.

Feature Processing techniques also include the following [11]:

i) Principal Component Analysis (PCA) reduces size of data sets. If input data are highly correlated, number of eigenvector will be small. This can be used to reduce huge quantity of information in given different data sets. It offers trade-off between computation time and prediction accuracy.

ii) Independent Component Analysis (ICA) separates mixed signal set into individual signal sets which are statistically independent. This is used in a neural network model to extract independent components from nonlinearly mixed signals.

### 12.3 Classification and Clustering

ML Classification techniques for Healthy versus unhealthy system behaviour can be achieved by engineering an appropriate kernel function for the given problem. ML techniques like Support vector Machines (SVM) are useful.

ML classification techniques categorized based on Supervised and unsupervised learning along with their Discriminative and Generative Approach are briefly introduced below:

#### 12.3.1 Supervised Learning

Supervised learning means training data is already labelled and health conditions of acquired input data are available. Some of the Supervised learning techniques are given below along with their applications.

i) (LDA) Linear Discriminant Analysis was used for multivariate variables to detect and classify faults in process of IC designs.

ii) (NN) Neural Networks based auto associator was built and used to detect imminent motor failures. It was trained with four motor current measurement data acquired from healthy motors [80].

iii) (SVM) Support Vector Machines. This technique is described in a section below.

iv) (DT) Decision Tree classifier algorithm based on tree structured model of feature attributes used to predict the class based on given data.

v) Random forests algorithm (RF) is a general term for ensemble methods using tree-type classifiers. A comparative study of classification algorithms for high dimensional data; for classifiers -Random Forests, K-Nearest Neighbours and Support Vector Machines is done [82].

#### 12.3.2 Unsupervised Learning

Unsupervised learning means the given data does not have its class-identification. Some of the Unsupervised learning techniques both Discriminative and Generative approaches are given below along with their applications.

#### 12.3.2.1 Discriminative approach in Unsupervised Learning

i) Hidden Markov Model (HMM) based approach- In HMM Hidden state sequence is inferred from observation sequence [54].

ii) SVM- based approach -Combination of PF and relevance vector machine (RVM) is used to predict Li ion battery RUL [55].

iii) (PF) Particle filtering also known as sequential Monte Carlo method- Alternative to extended Kalman Filter for nonlinear systems and non-Guassian noise, was used to predict RUL of IGBT.

#### 12.3.2.2 Generative Approach in Unsupervised Learning

Generative Approach include models of prior probability density P(X/y) for each class cj and then chooses the class that best fits observed data X based on optimization algorithm.

$$P\left(c_j \middle/ X\right) = \frac{P\left(X \middle/ c_j\right) \cdot P\left(c_j\right)}{\sum P\left(X \middle/ c_j\right) \cdot P\left(c_j\right)} \tag{5}$$

i) Naïve Bayes (NB) including Tree-augmented naïve Bayes (TAN), (FAN) Forest-augmented naïve Bayes- Naive Bayesian classifier [7] is based on the assumption that the features are independent given the class. The best class is found from the following calculation

$$\begin{aligned} \vec{z}_k &= \vec{z}_{k-1} \cdot \exp\left\{-\vec{\Delta}_k\left(t_k - t_{k-1}\right)\right\} + \vec{\omega}_k \\ \vec{\Delta}_k &= \vec{\Delta}_{k-1} + \vec{v}_k \\ \vec{x}_k &= \left[\vec{z}_k ; \vec{\Delta}_k\right] \\ \vec{y}_k &= \vec{z}_k + \vec{v}_k \end{aligned} \tag{6}$$

ii) Hierarchical classifier- e.g. Euclidian distance is used to find clusters; the distance between data points are defined.

iii) (kNN) k-nearest neighbour classifier (Divides data points into k-clusters that represent degrees of health of system. Varying degrees of health of a system are described by centroid and density. The relative position of centroid shows variation of health state from one condition to another and density of cluster gives change of health state within one condition. Some examples of objective functions are minimize distance between a point and its centroid, maximum distance to its centroid for any point, sum of variances over all clusters, etc.

iv) Fuzzy C mean classifier - a data point can belong to one or more clusters rather than belonging completely just to one cluster. Each data point belongs to each cluster with a degree of membership. Hence fuzzy C means clustering with a probabilistic approach to cluster boundaries.

### 12.4 Statistical Techniques used in ML

The two major statistical categories are Parametric methods and Non-Parametric methods. The various techniques under these methods are stated below.

Parametric methods are given below:

Maximum likelihood estimation (MLE) [79].

Neyman-Pearson Criterion- Classifier was used in minimizing probability of missed alarms and false alarm less than user specified level.

Expectation Maximization- This technique has been used in many applications.

Minimum Mean Square Error estimation -is a point estimator.

Maximize Posteriori (MAP) Estimation Classifier- MAP was used to estimate time varying fault parameters and applied to unmanned aerial vehicle.

Rao-Blackwellization Estimation- In this sensed parameter is transformed into another variable with sufficient statistics. It was used in electrical machines and path tracking applications.

Cramer-Rao Lower Bound- To check performance of an estimator as it sets lower limit for variance of any estimator which is achieved by unbiased estimator.

Non-Parametric methods along with their usage are given below -

k Nearest Neighbour Classification- kNN, Normalized distance from cluster centers is mostly considered to arrive at nearest neighbour. Distance in this context need not be Euclidean distance, it may be other distance metric eg. cosine distance. Weights can be added to vote of each neighbour, depending on distance from test point. Combination of PCA (dimensionality reduction technique and kNN was applied for fault detection in semiconductor manufacturing processes).

Kernel density/Parzen window estimation- In Kernel Density Estimation, the extent of contribution

to estimate of point $x_i$ depends on the shape of Kernel function and Band chosen. Gaussian is commonly used Kernel function. This was used in identification of damage initiation and growth on a box girder of a bridge using high frequency acoustic emission.

Wilcoxon rank-sum test is to check if two random variables arise from same pdf. This was used alongwith neural networks on a simulated statistical distribution for detection of abnormal conditions of aircraft engine.

Kolmogorov-Smirnov test- to compare observed and expected Conditional Density Functions (CDFs). Vertical difference between two CDFs under test is considered. This was used alongwith clustering algorithm for diagnostic testing on bearing of rotating machinery using acoustic emissions.

Chi square test- This is used as Goodness of fit check to determine if the distribution in question differs from that of known population.

All the above techniques of Statistical/ Machine learning are increasingly being used in modern applications. One such techniques viz. SVM which is a recent technique is being employed in various upcoming applications [56]. The following sections deals with SVM.

## 13. Support Vector Machines (SVM)

SVMs were introduced by Vapnik in the late 1960s on the foundation of the statistical learning theory [56] [69]. Since the middle of the 1990s, the algorithms used for SVMs started emerging with greater availability of computing power, paving the way for numerous practical applications. SVM for classification, is a modern machine learning method [57]. SVMs have become one of the most popular approaches to learning from data and have many potential applications in science and engineering. It is possible to incorporate techniques that can make decisions on the health of the machine automatically and reliably from the collected data by learning from known problems. Each data point is a N-dimensional vector and belongs to either of the two classes divided by N-1 dimensional hyperplanes. The goal is to maximize separation margins between two classes. Maximum margin hyperplane is set. SVM is essentially a two-class classifier. A direct multi-class extension of SVM usually leads to a very complex optimization problem and tedious computations. Therefore multi-class problems are often solved by training several binary SVM classifiers and fusing the outputs of the classifiers to find the global classification decision [58].

One-class SVM with RBF kernel was successfully applied for fault detecting in reactive ion etching system [59], to discriminate normal condition and abnormal condition. SVM based classification methodology can be used for fault detection in induction motors [80]. Motor had 7 classes- one healthy and 6 faulty conditions. Dynamic SVMs can be used for non-stationary time series forecasting.

Support Vectors are those data points which lie on the hyperplanes H1and H2 whose removal would change solution found. Margin between two hyperplanes is maximized [60]. SVMs have fast asymptotic rate of convergence. Useful properties of SVMs are that the optimization problem for constructing an SVM has a unique solution. The learning process for constructing an SVM is rather fast. The performance of the extracted rules is then evaluated in terms of accuracy, comprehensibility and area under the receiver operating characteristic curve (ROC). In all cases, sensitivity to the prior is substantial for small samples and decreases with increasing N [61]. Sparse kernel methods [62], like SVM have been applied with great success to classification and (standard) regression techniques however are not suitable for partly censored survival data, which are typically analyzed using Cox's proportional. The real data sets can be split into a random training set consisting, for e.g. 75% of the observations, and a validation set consisting of the remaining 25% of the observations [62].

Due to usage of Kernel function, number of faults is not limited; this is one of the powerful benefits of SVM approach over NN. SVMs are based on statistical theory and found to work well in comparison to NN in several applications. SVMs require few user-defined parameters and perform better. SVM perform better specially in handling large dimensions. For less training data SVMs outperform ANN. Multi-class SVMs perform well as compared to NN and Decision tree classifier. SVMs train and run one order of magnitude faster. SVMs scale better. SVMs give higher classification accuracy. SVM gives global solution unlike local minima in NN. SVM is good when dimensionality of input space and order of approximation create a dimensionality of feature space which is untractable with other methods. How and why algorithm has made a certain decision is supported by SVM. NN in general, cannot easily

explain their decisions. SVM offers flexibility in choosing a similarity function, sparseness of solution when dealing with large data sets, ability to handle large feature spaces and ability to handle outliers. As the number of inputs increases the performance of SVM also increases. SVM attributes are number of classes, kernels used, input feature selection and ranking methods.

The SVM-based blade damage detection system is more reliable and robust and shows no sudden fall in the damage class prediction performance with increase in noise level [56]. This system holds significant promise in the online damage detection system due to its ability to give optimal performance with a limited training data. The current damage detection system requires no data reduction technique and is based on the measurements obtained at non-rotating system.

SVM maps input vectors to a higher dimensional space where a maximal separating hyperplane is constructed. SVM maps the input patterns into a higher dimensional feature space through some non-linear mapping chosen a priori [63]. A linear decision surface is then constructed in this high dimension [64]. There are different kernel functions used in SVMs, such as linear, polynomial, Laplacian RBF, chi-square and Gaussian RBE, which avoid the computational burden of explicitly representing the feature vectors. Too many features can cause cures of dimensionality and peaking phenomenon [65] [66] that greatly degrade classification accuracy since some features are essential, some are less important, some of them may not be mutually independent and some may be useless. Usually 5 to 12 parameters are sufficient to perform the calculation and provide sufficient accuracy. The objective should be to identify the features that show high variability between different classes and thus help in distinguishing between them.

Typically, in the training process, the networks were trained until the mean square error is below 0.01 or the maximum epochs (=10000) were reached. The overall success of class classification ranges from 98 % to 100% for training and 88% to 98% for testing. Among these classifiers, Gaussian RBF is usually the best with high training and testing accuracy. Support vector machine, linear discriminant analysis, k-nearest neighbours, and random forests algorithm are employed as classifiers for fault diagnosis.

By applying a nonlinear kernel function that transforms data points into high-dimensional feature space, SVM can also treat nonlinear classification problem. Some common nonlinear kernels are polynomial, radial basis function (RBF), linear, and sigmoid.

Support vector regression (SVR) based on SVM for time-series prediction in a process-related application along with other models based on autoregressive moving average (ARMA) and recurrent NN (RNN) was presented [41]. The performance of SVR was found to be better than ARMA and RNN. The performance of SVR was also found to be better than that of adaptive neuro-fuzzy inference system (ANFIS). fuzzy inference models for failure definition are established using the domain experts with strong experiential knowledge [67]. SVM is used along with Bayesian framework for improving the classification accuracy [68]. However, the training time of SVR was much higher than for ANFIS; but training is off-line, done initially. Study of combination of a probability approach and a support vector machine [33], to predict the failure degradation and the trained SVM is used to predict the final failure time of individual bearing data. Systems for early fault detection and failure prediction have been developed for high end servers using continuous sensing of variables such as current, voltage, and temperature combined with analysis using pattern recognition algorithms. Support Vector Regression (SVR) is based on the principle of SVM and suitable for time-series prediction [70].

## 14. Prediction Algorithms

To implement a precursor reasoning-based PHM system, having identified the precursor variables for monitoring, development of a reasoning algorithm to correlate the change in the precursor variable with the impending failure is required and this characterization is typically performed by measuring the precursor variable under an expected or accelerated usage profile [50]. Based on the characterization, a model is developed, typically a parametric curve-fit, neural-network, Bayesian network, or a time-series trending of a precursor signal. This approach assumes that there is one or more expected usage profiles that are predictable and can be simulated in a laboratory setup. In some products the usage profiles are predictable, but this is not always true. For a fielded product with highly varying usage profiles, an unexpected change in the usage profile could result in a different (non-characterized) change in the precursor signal. If the precursor reasoning model is not characterized to factor in the uncertainty in life-cycle usage and environmental profiles, it may provide false alarms.

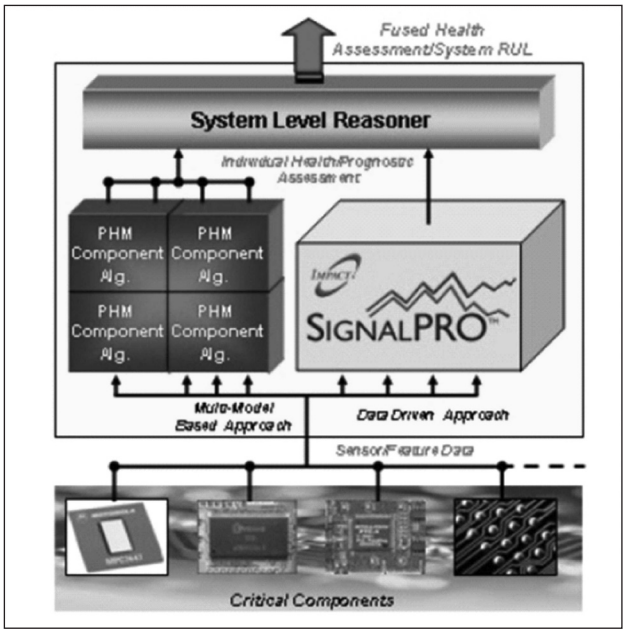


*Figure 11: System Health Assessment and RUL Analysis [29]*

For supporting temporal logic, dynamic Bayesian networks would be useful for prognostic algorithms. The classical approaches like autoregressive (AR) model or dynamic system approach are easy to understand but limited to simple applications. On the other hand, completely data-driven approach can quite easily be applied to complex systems but require data with a high level of confidence. The fusion of failure dynamics with diagnostic data offers some compromise between the two approaches.

Impact Technologies has developed Impact diagnostic/validation technology termed SignalPro which is capable of learning the relationships between an arbitrary set of inputs (be they features or raw sensor values) to evaluate a digital boards and its components at a system level [29]. SignalPro has a data driven condition monitoring approach for diagnostics and prognostics. It's engine has a system monitoring approach which evaluates electronics system performance by employing a combination of signal processing, statistics, and data-driven modelling techniques. A complete SignalPro system model is created by evaluating "healthy" data during training process. The generated model captures the interrelationships among sensor readings or extracted features. During training period, signal preprocessing is carried out and signal relationships and acceptable deviations are quantified.

Real-time data is used for monitoring along with a prediction model to assess whether the system is operating within acceptable limits. The model computes an estimate of the expected sensor values based on relationships between the new measurements and historical data. These data sets are compared with the actual data streaming and a residual signal is computed. This residual signal is further analyzed to arrive at unexpected (and potentially faulty) conditions. In addition, PHM algorithms are being present for critical components within the system, providing a system level model, and also having usage based monitoring. The health assessments provided by each of these independent paths are then be fused at a system level reasoner to provide a higher confidence analysis of the RUL of the electronic system, shown in Figure 11.

### 14.1 Particle Filter- A Prognostic Technique

Particle filter (PF) technique has been investigated from a distributed implementation context [10]. Three different distributed implementations for particle filtering are possible. A parallel particle filter implementation is done with a shared-memory multiprocessor cluster. In recent times, distributed particle filters for sensor networks and tracking applications have been explored.

PF is essentially Bayesian learning schemes that model the state equations as a first order Markov process with the outputs being conditionally independent. PF has the advantage of making the next state prediction dependent only on the current state and the current measurement, which requires lower memory and communication requirements than a Monte Carlo approach. PF methods are capable of identifying model parameters simultaneously by state

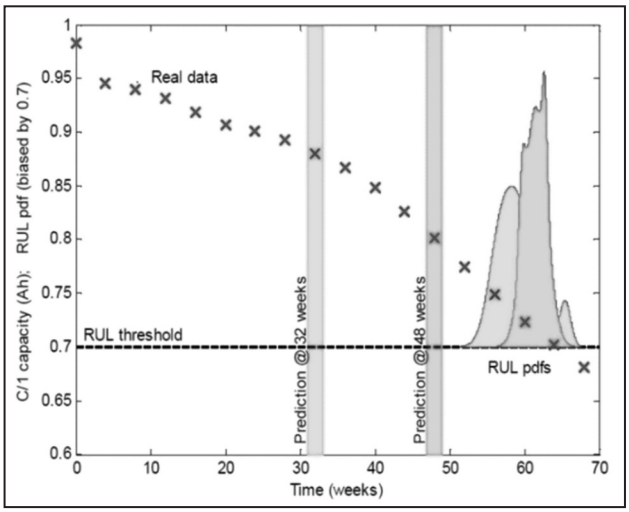


*Figure 12: PF state tracking for diagnostics and state prediction during prognostics from 32 weeks onward for battery capacity [10]*

estimation, thus tuning the system model to fault progression, thereby making it superior to Kalman filters for health management approaches.

## 15. Remaining Useful Life (RUL) Estimation

A degradation parameter is required for predicting (RUL) before final failure occurs. Temperature time series data was collected by the SPOTs from the Lithium-ion battery. Since run-to-failure experiments with these components take considerable amount of time (more than the battery life of the free ranging SPOTs), pre-recorded battery aging data was fed to the monitoring SPOTs through the base station in order to show proof of concept of the integrated PF-based diagnostics-prognostics framework. The state variables of interest are the battery capacity, the electrolyte resistance (RE) and the charge transfer resistance (RCT). But only battery capacity graphs are shown in this paper.

### 15.1. Diagnostics-Prognostics Framework

The predictions are fairly accurate since PF can adapt to the system aging model during the diagnostic routine. Here particle filter with only 20 particles is taken, so as to fit with the computational and memory resources of a single computational element (CE). Using less number of particles somewhat diminishes the ability of the PF to handle uncertainties, but since diagnostics is only concerned with tracking performance (1 step ahead prediction), the PF output is acceptable. Also, PF not only provides the mean prediction trajectories, but also the predicted state pdf. This distribution was compared against the EOL threshold (30% capacity fade, i.e. a battery capacity of 0.7 Ah) to generate the RUL pdf. PF prognosis improves in both accuracy and precision (narrowness of the pdf) from 32 weeks to 48 weeks as more data is made available before prediction.

For state prediction purpose the same PF framework can be used by running only the model-based particle propagation step until the predicted state value crosses some predetermined end-of-life threshold. The predicted trajectory of each particle then generates an estimate of RUL, which can be combined with the associated weights to give the RUL pdf. The process is broken down into an offline learning part, and an online tracking and prediction part. During offline analysis, regression is performed to find representative ageing curves. Exponential growth models, as shown in Eqn. 7, are then fitted on these curves to identify the relevant parameters viz. C (initial value of θ) and λ (the decay parameters) with thermal cycling among the most prevalent accelerated aging methodology in electronics.

$$E(\bar{a}) = y_i - f(x_i, \bar{a}) \tag{7}$$

where θ is an internal model parameter of interest [71].

The state and measurement equations that describe the semiconductor aging model are given below [24]:

$$P(RUL) = Likelihood(FM_i) * \Pr(PDF_i) \tag{8}$$

where the vector **z**, consists of the OFF state exponential time decay constants for the IGBT collector-emitter current (ICE), and matrices **C** and **Λ** contain their aging decay parameters *C* and *λ* values respectively. The **z** and **Λ** vectors are combined to form the state vector **x**. The measurement vector **y** comprises the time decay parameters inferred from measured data. The time index is denoted by *k*. The values of the **C** and **Λ** vectors learned from regression were used to initialize the particle filter. The noise samples $\boldsymbol{\omega}$, $\boldsymbol{\nu}$ and $\boldsymbol{\upsilon}$ are picked from zero mean Gaussian distributions whose standard deviations are derived from the given training data, thus accommodating for the sources of uncertainty in feature extraction, regression modelling and measurement. System importance resampling of the particles is carried out in each iteration, in order to reduce the degeneracy of particle weights.

The system description model developed in the offline process is fed into the online process where the particle filtering prognosis framework is triggered by a diagnostic routine. The algorithm incorporates the model parameter as an additional component of the state vector and thus, performs parameter identification in parallel with state vector, even under the presence of disruptive effects like un-modelled operational conditions (in this case, high temperatures) estimation. Predicted values of the time decay parameters are compared against end-of-life thresholds to derive time of end-of-life (EOL) and RUL estimates.

Overall, the parameter shows an exponential growth rate (negative), indicating an Arrhenius aging process. Near the end, the curve shows some anomalous behaviour since the IGBT approaches the latch-up condition. Originally the Arrhenius equation described the temperature dependence of the rate of a chemical reaction.

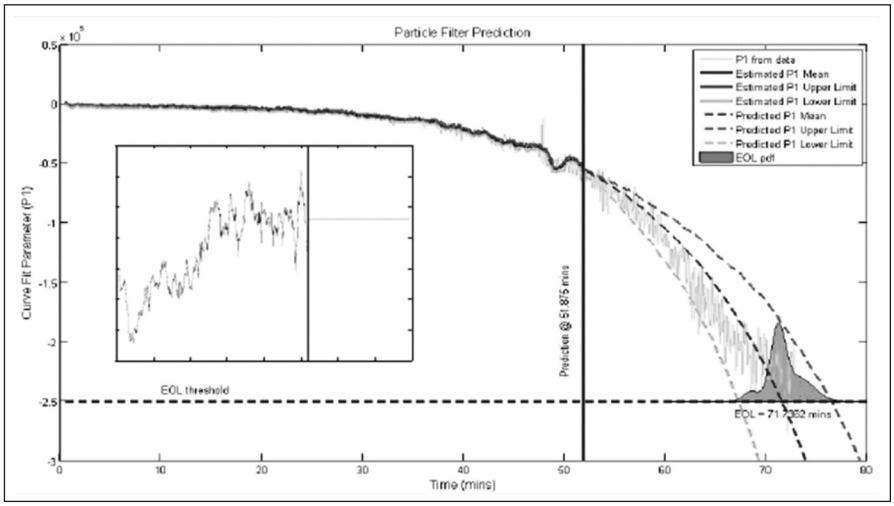


*Figure 13: Filter Tracking and Prediction [24]*

In running the particle filter framework, an exponential growth model for P1was used like the one shown in eqn. 8. Since there was no separate learning and testing datasets, regressed $C$ and $\lambda$ values were not used from the model learning process to jump start the PF algorithm. Instead, 0 and 1 were used as the initial values for P1 and $\lambda$P1.The EOL threshold is chosen as $-2.5 \times 10^5$, which is approximately the value of P1 at the end of its exponential behaviour. Without loss of generality, the prediction time was arbitrarily chosen to be 51.875 minutes.

After the prediction timeline, the mean of the last 100 $\lambda_{P1}$ values is used for the propagation of each particle according to the state transition model (first line in eqn. 8. No additional computed $\lambda_{P1}$ values are used to update the particle weights. The propagated particle values are compared against the EOL threshold to compute the distribution of time at EOL. A mixture of Gaussians is then fitted in a least square sense to these EOL values to plot the magenta EOL pdf as shown in Figure 13. The RUL pdf is simply the prediction time subtracted from the EOL pdf. Inspite of the generic initial particle values, for modeling uncertainties and system noise, the PF performance is very good.

Limitations: Some significant limiting assumptions employed here are: Simple exponential growth models were used to explain the aging behaviour of IGBTs. Although the prediction results are very good, such an approach has limitations when applying the aging parameters and EOL thresholds learnt from one device to another. In order to achieve that, one needs to explicitly derive PoF based aging models, identify their parameters from externally observable device characteristics and then use those models in a PF framework to carry out prognostics. In such a case, aging behavior will be linked to the changes in the internal model parameters which can then be tied to failure mechanisms like hot carrier injection, electromigration etc.

### 15.2 Decision Making

Decision Making can be cast as a classification problem: the classifier makes a hypothesis about the classification of a given data instance into one of predefined categories that represent different decisions. The decision is based on prior training of the classifier, using a set of representative training data, for which the correct decisions are *apriori* known. Availability of an adequate and representative set of training data is of prime importance for a classification algorithm to successfully learn the underlying data distribution. In the absence of adequate training data, resampling techniques can be used for drawing overlapping random subsets of the available data, each of which can be used to train a different classifier, creating the ensemble. Such approaches have also proven to be very effective. Interpretation allows forming an ensemble through algebraic combination rules (majority voting, maximum /minimum/ sum/ product or other combinations of posterior probabilities), fuzzy integral for combination, the Dempster-Shafer based classifier fusion, and more recently, the decision templates like margin theory or Support Vector Machines. Having diversity of the classifiers, and hence it is possible to achieve better performance of the overall system.

Overfitting is usually attributed to memorizing the data, or learning the noise in the data. As a classifier's capacity increases (for example, with the complexity of its architecture), so does its tendency to memorize the training data and/or learn the noise in the data.

Uncertainty which is often present in diagnosis and is inherent to prognosis can be handled using Bayesian network models and Bayesian inference. Multiple sources of evidence in diagnosis and prognosis are coherently integrated, including component usage, environmental conditions of operation as well as component health and health trends [72]. This technique has been applied to diagnosis of very complex transportation and aviation systems and

to prognosis of electromechanical and electronic subsystems in aviation wherein general inference algorithms are employed for Bayesian networks to compute the desired probabilities.

Mechanisms that perform information fusion, uncertainty management, decision generation, evaluation, and optimization as crucial and necessary to the success of an effective PHM decision support system, complementing each other and making a robust decision support system for optimal prognostic decision making are mentioned in [73].

### 15.3 Damage Identification

The developed model-based reasoner in reference [40], applies physical modeling and advanced parametric identification techniques, an evolutionary prognostics fault detection and failure prediction algorithm, for predicting the time-to-failure for each of the critical, competitive failure modes within the system. An advanced probabilistic fusion strategy is also built-in to combine both collaborative and competitive predictions. The model-based reasoner is non-intrusive and operates only on command/ response data from the flight control system. Ultimately, this approach can be transitioned towards an onboard or at-wing application. Figure 14 illustrates a key concept behind model-based diagnostics and prediction. The actual system output response (event and performance variables) is the result of nominal system response plus fault effects and uncertainty. A path of the model-based analysis and identification of faults is to organize this method as an optimization problem to identify the fault effects (and thus identify the fault) that produces the minimum residual between the predicted and actual response. This can be represented mathematically using the equation:

$$P(275hours) = [(0.25)(0.02) + (0.05)(0.50) + (0.70)(0.98)] = 0.716 \quad (9)$$

Global search methods, such as genetic algorithms and simulated annealing, are much better options for on-line model identification. However, similar to simplex methods, genetic algorithms do not always find the global minima. A hybrid approach that combines both genetic algorithms and simulated annealing in order to reduce the number of iterations needed to reach a global solution. The use of a global stochastic search routine may give good results. Probabilistic global search routines have proven to achieve similar accuracy as simulated annealing methods while reaching convergence upon the global solution in far less iterations.

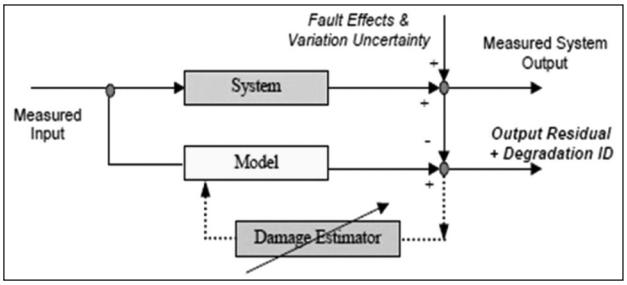


*Figure 14: Model–Based Approach to Damage Identification [40]*

Classification and prognostics are critical steps within any PHM monitoring scheme. Impact's model-based approach employs a classification system for translating the model parameters (known evidence) to a current level of damage for each failure mode. Once faults are detected and the current damage level is assessed, prognostics are implemented to predict the progression of the fault towards failure [40].

The trend-based or evolutionary prognostics approach has proven to be very effective at predicting slow degradation mechanisms and is attractive for system prognostics. This approach relies on gauging the proximity and rate of change of the current component condition (by way of the model parameters) to known fault conditions within N-dimensional parameter (feature) space. This approach requires that sufficient sensor information is available to assess the current condition of the system or subsystem with a relative level of uncertainty in this measurement. Furthermore, the parametric conditions that signify known condition-related faults must be identifiable. The evolutionary prognostics routine works well within the model-based PHM architecture. The developed probabilistic approach uses Euclidean distance to calculate the distance between the (current) measured condition and known fault conditions in parameter space. The fault regions having the shortest Euclidean distance to the current condition are then used to determine the current health. The primary task of diagnostic and damage assessment in real time using input from multiple sources, both sensor-based and model-based are dealt in [74].

### 16.1 Prognostic Fusion Strategy

PHM can be based on a hybrid approach to accomplish specific goals. Various algorithms are developed and each is having some advantage over others in various applications. Fusion or hybridization

of techniques viz. 'Multiple classifier fusion', wherein outputs from several different prognostic algorithms is fused. Resultant output is more accurate and has tighter uncertainty bounds as compared to individual algorithm output. Final decision should be weighted combination of decisions of different theories where weights are conditional probability of the theories given the evidence using Probabilistic Graphical Modeling techniques [54].

There is some inherent uncertainty in material properties and dimensions of the structures in electronic components, electronic system and the environment actually experienced. Since uncertainty is there in the estimation process, confidence level needs to be applied. Thus RUL requires the fusion of models and sensor data to provide an estimate of equipment failure time. The modelling of uncertainty is essential in PHM, since the objective is to estimate a lower bound on time-to-failure at a user selected confidence level.

The application of fusion can be performed at a number of areas within the developed framework. The developed classification scheme can be expanded to include additional classifiers. The results of the independent classifications can then be fused using one of the approaches discussed above for a more robust classification. Likewise, multiple fault-to-failure predictors can be used to assess RUL and fused to produce a single estimate. Other possible applications of fusion include sensor validation and confidence evaluation, to name a few.

A framework for applying such fusion approaches to multiple RUL predictions was considered in reference [40]. As part of the model-based approach, an RUL prediction is returned for each of the competitive failure modes, each having a different likelihood of occurrence. The fusion approach evaluates the probability that a given RUL will be reached given the probability that the correct failure mode has been classified. As illustrated in figure 15, the probability that an RUL value will be reached is a function of all RUL pdfs from each failure mode. Additionally, the probability of reaching an RUL is a function of the likelihood of occurrence for each failure mode. Therefore, the probability that a specified RUL will be reached can be evaluated by the following equation

$$P(RUL) = Likelihood(FM_i) * \Pr(PDF_i) \quad (10)$$

To further illustrate the concept through an example, the probability of reaching 275 hours will be evaluated. For this example, assume the likelihood of gear slip failure is 0.25,the likelihood of bearing seizure is 0.05, and the likelihood of motor failure is 0.70. The probability that the gear slip failure mode will not happen for another 275hours is approximately 0.02, the probability that bearing seizure will not occur for another 275 hours is approximately 0.50, and the probability that motor failure will not occur is approximately 0.98. Evaluating the joint probability that the 275 hours remaining useful life will be reached yields:

$$P(275hours) = [(0.25)(0.02)+(0.05)(0.50)+(0.70)(0.98)] = 0.716 \quad (11)$$

The advantage of using this technique for reporting RUL is that the user has the ability to assess RUL based on a desired risk level. This is manifested and reported through the use of a prognostic vector, rather than a single RUL prediction. Prognostic vectors are arrays of RUL values, returned with the corresponding probability that each RUL value will be reached. Figure 16 illustrates a prognostic output vector, which ultimately allows the user to choose the appropriate risk level and make maintenance decisions accordingly.

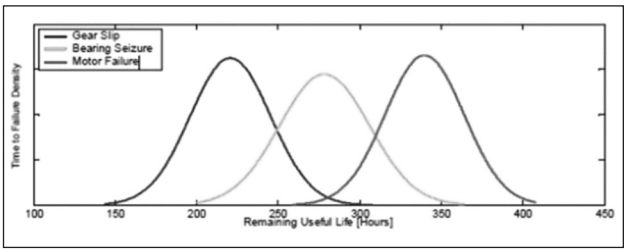


*Figure 15: Distribution of RUL Predictions for Each Competitive Failure Mode [33]*

### 16.1 Advanced Fusion Strategies

Data or knowledge fusion is the process of using collaborative or competitive information to arrive at a more confident inference. It is used in both diagnostic and prognostic processes. There are three main areas where fusion technologies are utilized. At the lowest level, data fusion can be used to combine information from a multi-sensor data array to validate signals and create features [75]. At a higher level, fusion may be used to combine derived features to obtain the best possible diagnostic information. Finally, knowledge or decision fusion is used to incorporate experience-based information such as legacy failure rates or physical model predictions with signal-based information.

There exist many algorithms for fusion including Bayesian and Dempster-Shafer Combination, and Weighted Voting schemes to name a few. (17) Bayesian Inference can be eq (10) used to determine the probability that a diagnosis is correct, given a piece of apriori information. Analytically this process is described as follows [40]:

$$P\left(f_1 / O_n\right) = \frac{P\left(O_n / f_1\right) \cdot P(f_1)}{\sum_{i=1}^{n} P\left(O_n / f_i\right) \cdot P(f_i)} \quad (12)$$

where $P(f1 / On)$ = Probability of fault (f) given a diagnostic output ($O_n$)

$P(On/f1)$= Probability that a diagnostic output($O_n$) is associated with a fault ($f_1$)

$P(f1)$ = Probability of the fault ($f_1$) occurring

The Dempster-Shafer methodology lies on the construction of a set, called the frame of discernment, which contains every possible hypothesis. Every hypothesis has a belief denoted by a mass probability (m). Beliefs are combined with the following equation [40]:

$$Belief = \frac{\sum_{A \cap B = H_n} m_i(A) \cdot m_i(B)}{1 - \sum_{A \cap B = 0} m_i(A) \cdot m_i(B)} \quad (13)$$

## 17. Conclusion and Recommendations

The current state of practice and ongoing research in PHM of electronic products and systems is reviewed in this paper. The paper deals with all the phases in PHM development; starting from failure mechanisms of semiconductor transistors, physics of failure models, monitoring parameters for detecting failure progression, sensors, data preprocessing techniques, identifying important features, handling n-dimensional features and system non-linearities in classifying healthy and faulty states, regression techniques, damage assessment, RUL estimation along with uncertainties handling and the required mathematical techniques to realize these. It also gives methodologies to implement these phases.

The traditional reliability predictions based on handbook methods are inaccurate and misleading. PHM is more suitable for reliability prediction and remaining life assessment, since it considers actual operational and environmental loading conditions. By using physics-based damage models for electronics, obtaining the life cycle data of product, and assessing the uncertainty in RUL prediction (in order to make PHM more realistic) are covered in this paper. From the applications and examples, it is obvious that PHM can be incorporated into various electronics products and systems which can benefit in reducing life cycle costs. In near future, due to the increasing amount of electronics in the world and using COTS devices and the competitive drive toward more reliable products, PHM will be looked upon as a cost-effective solution for reliability of electronic products and systems. The major technological items necessary to construct an PHM system (failure and cost models and modelling tools, prognostic cells, sensors, statistical techniques) are all sufficiently matured to consider PHM. It remains only to put these pieces together into a workable solution and generate a PHM solution having sensors with embedded algorithms that will enable fault detection, diagnostics and remaining life prognostics. The possible applications in nuclear plants considering prognotics at system level, critical components level, etc. which will help in reducing outages and aid in scheduling effective maintenance leading to failure avoidance, high availability, and reduction of life cycle costs are covered. Implementation of PHM technology providing comprehensive and effective prognostic solution, should require minimal sensor retrofitting or hardware modifications, and should be suitable for deployment on wide range of digital electronics applications including integration into digital electronic boards and COTS embedded computer system.

## References


1. Sheppard J. W., Kaufman M. A., and Wilmering T. J., "IEEE Standards for Prognostics and Health Management", IEEE Aerospace and Electronic Systems Magazine, Vol 24 No.9: pp.34-41, 2009.
2. Vichare N. M. and Pecht M. G. , " Prognostics and health management of electronics", IEEE Transactions on Components and Packaging Technologies, Vol. 29, pp. 222-229, 2006.
3. Polikar R. 2006. Ensemble based systems in decision making. IEEE Circuits and Systems Magazine, 6(3): 21-44.
4. Pecht M. , "Prognostics and Health Management of Electronics", Wiley-Interscience, New York, 2008.
5. Smelyanskiy V.N., Luchinsky D.G., Osipov V.V., Timuchin D.A. and Uckun S.,"Development of an on-board failure diagnostics and prognostics system for Solid Rocket Booster", Proceeding of 44rd AIAA/ASME/SAE/ASEE Joint Propulsion Conference and Exhibit, Hartford, CT, 2008.
6. Vichare N., Rodgers P., Eveloy V., and Pecht M., "In-Situ Temperature Measurement of a Notebook Computer – A Case Study in Health and Usage Monitoring of Electronics", IEEE Transactions on Device and Materials Reliability, Vol. 4, No. 4. pp. 658-663, 2004.

7. Ramakrishnan A. and Pecht, M. G., "A life consumption monitoring methodology for electronic systems", IEEE Transactions on Components and Packaging Technologies, 26(3): 625-634, 2003.
8. Mishra S., Pecht M., Smith T., McNee I., and Harris R., " Remaining life prediction of electronic products using life consumption monitoring approach. European Microelectronics Packaging and Interconnection Symposium. IMAPS Europe, pp. 136-142, 2002.
9. Samanta B. and Nataraj, C., " Prognostics of machine condition using soft computing", Robotics and Computer-Integrated Manufacturing, Vol.24, No.6, pp. 816-823, 2008.
10. Saha S., Saha B., Goebel K., and IEEE, "Distributed Prognostics Using Wireless Embedded Devices", International Conference on Prognostics and Health Management (PHM), pp. 457-463, 2008
11. Donald D. Dudenhoeffer, Tuan Tran, Ronald L. Boring, Bruce P. Hallbert, "Joint System Prognostics for Increased Efficiency and Risk Mitigation in Advanced Nuclear Reactor Instrumentation and Control", Workshop Meeting on Advanced Control-System Designs, Idaho National Lab, US, August 2006.
12. Bond Leonard J. and Doctor Steven R. , "From NDE to prognostics: a revolution in asset management for Generation IV Nuclear Power Plants", Pacific Northwest National Laboratory, Richland, WA. Transactions, SMiRT 19, Toronto, 2007.
13. Shetty V., Das D., Pecht M., Hiemstra D.Martin S., "Remaining Life Assessment of Shuttle Remote Manipulator System End Effector", Proceedings of the 22nd Space Simulation Conference, Ellicott City, 2002.
14. Mathew S., Das D., Osterman M., Pecht M., Ferebee R. and Clayton J., "Virtual Remaining Life Assessment of Electronic Hardware Subjected to Shock and Random Vibration Life Cycle Loads", Journal of the IEST, Vol. 50, No. 1, pp.86-97, 2007.
15. Mishra S., Ganesan S., Pecht M., Xie J., "Life consumption Monitoring for Electronics Prognostics", IEEE Aerospace Conference, pp.3455-3467, 2004.
16. Whisnant K., Gross K., and Lingurovska N., "Proactive Fault Monitoring in Enterprise Servers", IEEE International Multi-conference in Computer Science and Computer Engineering, Las Vegas, 2005.
17. Brown D. W., Kalgren P. W., Byington C. S., Orsagh R. F., "Electronic prognostics - A case study using global positioning system (GPS)", Autotestcon, pp. 833-839, 2005.
18. Nasser L. and Curtin M., "Electronics reliability prognosis through material modeling and simulation", IEEE Aerospace Conference, Big Sky, MT, 2006.
19. Bodenhoefer K., Schneider A., Cock T., Brooks A., Sands G., Allman L., Chong S. K., Yang K., Delannoy O., Catanese B., and Mueller K., "Environmental life cycle information management and acquisition - First experiences and results from field trials", Electronics Goes Green 2004 (Plus): Driving Forces for Future Electronics, Proceedings, pp.541-546, 2004.
20. Gu J., Barker D., and Pecht M., "Prognostics implementation of electronics under vibration loading", Microelectronics Reliability, Vol. 47, No.12, pp.1849-1856, 2007.
21. Simons J. W., Shockey D. A., "Prognostics modeling of solder joints in electronic components", IEEE Aerospace Conference, Big Sky, MT, 2006.
22. Rufus F., Jr. Lee S., Thakker A., "Health Monitoring Algorithms for Space Application Batteries", International Conference on Prognostics and Health Management (PHM), pp. 125-132, 2008.
23. Patil N., Celaya J., Das D., Goebel K., and Pecht M., "Precursor Parameter Identification for Insulated Gate Bipolar Transistor (IGBT) Prognostics", IEEE Transactions on Reliability, 58(2): 271-276, 2009.
24. Saha B., Celaya J. R., Wysocki P. F., and Goebel K. F, "Towards prognostics for electronics components", IEEE Aerospace Conference, pp.7 2009.
25. Gu J. Azarian M. H., and Pecht M. G., "Failure prognostics of multilayer ceramic capacitors in temperature-humidity-bias conditions", International Conference on Prognostics and Health Management, pp.7, 2008.
26. Goodman D., Vermeire B., Ralston-Good J., and Graves R., "A board-level prognostic monitor for MOSFET TDDB", IEEE Aerospace Conference (IEEE Cat. No. 05TH8853C): pp.6, 2006..
27. Saha B. and Goebel K., "Uncertainty management for diagnostics and prognostics of batteries using Bayesian techniques", IEEE Aerospace Conference, pp.1-8, 2008.
28. Sandborn P., "A decision support model for determining the applicability of prognostic health management (PHM) approaches to electronic systems", Annual Reliability and Maintainability Symposium (RAMS), Alexandria, VA, 2005.
29. Kalgren PW, Baybutt M ,Ginart A, Minnella C , Roemer MJ, "Application of Prognostic Health Management in Digital Electronic Systems ", IEEE Aerospace Conference, Vol. 1-9 Book Series: IEEE Aerospace Conference Proceedings pp. 3978-3986, 2007.
30. Brown D., Kalgren P. and Roemer M., "Electronic Prognostics - A Case Study Using Switched-Mode Power Supplies (SMPS)", IEEE Instrumentation and Measurement Magazine, August, pp. 20-26, 2007.
31. Gu J., and Pecht M., "Reliability Prognostics of Electronics Products", 8th International Conference on Reliability, Maintainability and Safety, pp: 912 – 919, 2009.
32. Gu J. and Pecht M. 2007. Predicting the reliability of electronic products. Icept: 2007 8th International Conference on Electronics Packaging Technology, Proceedings: 8-15.
33. Caesarendra Wahyu, Widodo Achmad, Yang Bo-Suk, "Combination Of Probability Approach And Support Vector Machine Towards Machine Health Prognostics", Probabilistic Engineering Mechanics 26, pp. 165–173, 2011.
34. Widodo A, Yang BS, 2008. Support vector machine for machine fault diagnosis and prognosis. J Syst Des Dyn 2008;2(1). 12–23.
35. Schwabacher Mark and Goebel Kai, "A Survey of Artificial Intelligence for Prognostics", NASA Ames Research Center, CA 94035, mark.a.schwabacher@nasa.gov; kai.f.goebel@nasa.gov,2010.
36. Goodman Douglas L., "Prognostic Methodology for Deep Submicron Semiconductor Failure Modes", IEEE Transactions on Components and Packaging, Volume 24, Number 1, pp:199-200, 2001.
37. Jarron. P., "Commercial of the shelf for LHS experiments", CMS Cavern electronic, http://nepp.nasa.gov/docuploads/A3A73F3A-28B1-43D5-8D46037AFED21812/Commercial%20of%20the%20shelf%20for%20LHS%20experiments.pdf, 1999.

38. Wilkinson Chris, Humphrey Dave, Vermeire Bert, Houston Jim, "Prognostic and Health Management for Avionics", IEEE Paper Number: 1485, 2004.
39. Jie G., Lau D., and Pecht M., "Health assessment and prognostics of electronic products", 8th International Conference on Reliability, Maintainability and Safety (ICRMS 2009), pp. 912-919, 2009.
40. Byington C. S. and Stoelting P., "A model-based approach to prognostics and health management for flight control actuators", IEEE Aerospace Conference, pp. 3551-3562, 2004.
41. Saha B., Goebel K., and Christophersen J., "Comparison of prognostic algorithms for estimating remaining useful life of batteries", Transactions of the Institute of Measurement and Control, Vol. 31, No.3-4: 293-308, 2009.
42. White Mark and Bernstein Joseph B., "Microelectronics Reliability: Physics-of-Failure Based Modeling and Lifetime Evaluation", University of Maryland, 2008.
43. Segura Jaume and Hawkins Charles F., "CMOS Electronics – How it works, how it fails", Wiley, 2004.
44. Kelkar N., Dasgupta A., Pecht M., Knowles I., Hawley M., and Jennings D. 1997. "Smart' electronic systems for condition-based health management", Quality and Reliability Engineering International, Vol.13, No.1, pp. 3-8.
45. Vichare Nikhil M., Rodgers Peter, Eveloy Valérie and Pecht Michael G., "Environment and Usage Monitoring of Electronic Products for Health Assessment and Product Design", Quality Technology and Quantitative Management Vol. 4, No. 2, pp. 235-250, 2007.
46. Rajsuman Rochit, "Iddq Testing for CMOS VLSI", Proceedings of the IEEE Volume 88, Issue 4, April 2000, pp.544-566, 2000.
47. Variyam Pramodchandran N., "Increasing the IDDQ Test Resolution Using Current Prediction", International Test Conference Proceedings, pp. 217-224, 2000.
48. Wallquist Kenneth M., Righter Alan W., and Hawkins Charles F. A, "General Purpose Iddq Measurement Circuit", International Test Conference, 642-651, 1993.
49. Hashizume Masaki, Yotsuyanagi Hiroyuki, Ichimiya Masahiro, Tamesada Takeomi, Masashi Takeda, "High Speed IDDQ Test and Its Testability for Process Variation", Proceedings of the Ninth Asian Test Symposium, pp 342-.349, 2000.
50. Byington C. S., Watson M. J., and Edwards D., "Data-Driven Neural Network Methodology to Remaining Life Predictions for Aircraft Actuator Components", Proceedings of the IEEE Aerospace Conference, New York IEEE, pp. 646-653, 2004.
51. Vichare Nikhil M., Rodgers Peter And Pecht Michael G., "Methods for Binning and Density Estimation of Load Parameters for Prognostic Health Monitoring", Int J. of Perfomability Engineering, Vol 2, No. 2, pp.149 – 161, 2006.
52. Elissa Bumiller and Dr. Craig Hillman, http://www.dfrsolutions.com/uploads/white-papers/Time-to-Failure_Metallic_Migration.pdf, 2013.
53. RAIC, http:// www.theriac.org/ WARP/display_model.html?model_id=26, 2013.
54. Koller Daphne and Friedman Nir, "Probabilistic Graphical Models: Principles and Techniques", MIT Press, 2009.
55. Saha B., Goebel K., Poll S., and Christopherson J., "An Integrated Approach to Battery Health Monitoringusing Bayesian Regression, Classification and State Estimation", Proceedings of IEEE Autotestcon, Vol 1 And 2, pp.646-653, 2007.
56. Vapnik VN., "An overview of statistical learning theory", IEEE Trans Neural Networks; Vol 10, pp.988–1000, 1999.
57. Christopher Burges J.C., "A Tutorial on Support Vector Machines for Pattern Recognition", Bell Laboratories, Lucent Technologies. Kluwer Academic Publishers, Boston. burges@lucent.com, 2010.
58. Guo M., Xie L., Wang S. Q., Zhang J. M., "Research on an integrated ICA-SVM based framework for fault diagnosis", IEEE International Conference on Systems, Man and Cybernetics (SMC 03), Washington, D.C., 2003.
59. Sarmiento T., Hong S.J., May G.S, "Fault detection in reactive ion etching systems using one-class support vector machines", Advanced Semiconductor Manufacturing Conference and Workshop, Article number 5.9a, pp.140-143, 2005.
60. Taylor John Shawe and Cristianini Nello, "Support Vector Machines and other kernel-based learning methods", Cambridge University Press, 2000.
61. Hanczar Blaise, Hua Jianping, Sima Chao, Weinstein John, Bittner Michael and Dougherty Edward R., "Small-sample precision of ROC-related estimates", Bioinformatics, Vol. 26, No. 6, pp. 822–830, 2010.
62. Evers Ludger and Messow Claudia-Martina, "Sparse kernel methods for high-dimensional survival data", BIOINFORMATICS Vol. 24, No. 14 2008, pages 1632–1638, 2008.
63. Cristianini Nello, "Support Vector and Kernel Machines", http://www.support-vector.net/icml-tutorial.pdf, 2001.
64. Barakat Nahla and Bradley Andrew P., "Rule extraction from support vector machines: A review", Elsevier B.V., Neurocomputing, Vol 74, pp.178–190, 2010.
65. Bishop Christopher M., "Pattern Recognition and Machine Learning", Springer, 2006.
66. Raudys Sarunas J. and Jain Anil K., "Small Sample Size Effects in Statistical Pattern Recognition: Recommendations for Practitioners", IEEE Transactions on Pattern Analysis and Machine Intelligence, Vol. 13, No. 3, pp.252-264, 1991.
67. Chinnam, R.B. and Baruah, P., "A neuro-fuzzy approach for estimating mean residua life in condition-based maintenance systems", Int. J. Materials and Product Technology, Vol 20, Nos. 1-3, pp.166-179, 2004.
68. Sotiris Vasilis A., Tse Peter W., and Pecht Michael G., "Anomaly Detection through a Bayesian Support Vector Machine", IEEE Transactions On Reliability, Vol. 59, No. 2, June 2010, pp. 277-286, 2010.
69. Welling Max, "Support Vector Regression", www.ics.uci.edu/~welling/teaching/KernelsICS273B/SVregression.pdf, 2010.
70. Liu Datong, Wang Shaojun, Peng Yu, Peng Xiyuan, "On-line Adaptive Data-Driven Fault Prognostics of Complex Systems", IEEE Autotestcon 2011: Systems Readiness Technology Conference Book Series: IEEE Autotestcon, pp. 166-173, 2011.
71. Arulampalam M. S., Maskell S., Gordon N., and Clapp T., "A tutorial on particle filters for online nonlinear/non-Gaussian Bayesian tracking", IEEE Transactions on Signal Processing, Vol 50, No.2, pp. 174-188, 2002.
72. Przytula K. Wojtek and Choi Arthur, "Reasoning Framework for Diagnosis and Prognosis", IEEE Aerospace Conference Proceedings, pp.3861-3870, 2007.

73. Iyer N., Goebel K., Bonissone P., "Framework for Post-Prognostic Decision Support", Proceedings of IEEE Aerospace Conference, 11.0903, 2006.
74. Goebel Kai Bonanni, Pierino and Eklund Neil, "Towards an Integrated Reasoner for Bearings Prognostics", Proceedings of IEEE Aerospace Conference, pp.1-11, 2005.
75. Jardine Andrew K.S., Lin Daming and Banjevic Dragan, "A review on machinery diagnostics and prognostics implementing condition-based maintenance", Mechanical Systems and Signal Processing, Vol 20, pp.1483–1510, Elsevier, 2005.
76. James Mark L. and Dubon Lydia P, "An Autonomous Diagnostic and Prognostic Monitoring System for NASA's Deep Space Network", IEEE Aerospace Conference, pp. 403-414, 2000.
77. Vaca-Trigo I. and Meeker W. Q., "A Statistical Model for Linking Field and Laboratory Exposure Results for a Model Coating", Service Life Prediction of Polymeric Materials: Global Perspectives, pp.29-43, 2009.
78. Pecht, M. G. and Vichare, N. M., "Method for analyzing environmental and operational exposures of product for prognostics of product, involves storing parameters of raw data showing irregular changes of product over time while reducing data storage up to preset value", Oxfordian Llc.
79. Mitchell Tom M., "Machine Learning", McGraw-Hill, 1997.
80. Son J.D, Niu Gang , Yang B.S., Hwang D.H., Kang D.S., "Development of smart sensors system for machine fault diagnosis", Expert Systems with Applications, Vol 36, pp.11981–11991, 2009.
81. Heng Aiwina_, Zhang Sheng, Tan Andy C.C., Mathew Joseph, "Rotating machinery prognostics: State of the art, challenges and opportunities", Journal of Mechanical Systems and Signal Processing Elsevier, Vol 23 pp.724–739, 2009.
82. Guo Yu, Graber Armin, McBurney Robert N., Balasubramanian Raji, "Sample size and statistical power considerations in high-dimensionality data settings: a comparative study of classification algorithms", BMC Bioinformatics. http:// www.biomedcentral.com/ 1471-2105/11/447, 2010.

*Life Cycle Reliability and Safety Engineering*
*Vol.2 Issue 4 (2013) 69-75*

# Fuzzy Arithmetic form Credibility Theory

**Rituparna Chutia[1] and Tapan Kumar Chutia[2]**
*Department of Mathematics, Moridhal College, Dhemaji, Assam, India.*
*[1]Email: rituparnachutia7@gmail.com*

## Abstract

***In this article, it has been shown that the credibility distribution of triangular fuzzy variable leads us to find a very simple alternative method of finding the membership function for functions of triangular fuzzy variables. This concept of credibility theory also leads us in finding an alternative method of computing basic arithmetic operations of triangular fuzzy variables and generalised membership function for the root of triangular fuzzy variable. The method has been demonstrated with the help of some examples.***

***Keywords: Credibility distribution, Credibility density function, Credibility measure, Membership function.***

## 1. Introduction

The basic arithmetic operation of fuzzy number has been developed well through the years. Indeed Chou [4, 5] has actually developed a method of finding the membership function of the square root and cube root of a triangular fuzzy number. Although there are many arithmetical operation approaches, none of the approaches presents a generalised method for finding the $n^{th}$ root of the fuzzy number.

Zadeh [7] proposed the concept of possibility measure and thereafter this has been widely used in solving fuzzy problems. The necessity measure is defined as a dual part of possibility measure. However, both possibility measure and necessity measure are not self-dual. In order to define a self-dual measure, Liu and Liu [1] present the concept of credibility measure.

In this paper the triangular fuzzy variable are considered and we try to develop a generalised method for finding the membership function for functions of triangular fuzzy variables, and very well applied in dealing the basic arithmetical operations of triangular fuzzy variables, based on the concept of credibility distribution.

## 2. Preliminaries

### 3.1 Triangular Fuzzy Variable

A fuzzy variable determined by the triplet $\beta = [a, b, c]$ of crisp number with $(a < b < c)$ and whose membership function is given by

$$\mu_\beta(x) = \begin{cases} \dfrac{x-a}{b-a}, if\ a \le x \le b \\ \dfrac{c-x}{c-b}, if\ b \le x \le c \\ 0,\ otherwise \end{cases} \quad (2.1.1)$$

is called a triangular fuzzy variable.

### 3.2. Credibility Measure

Let $\Theta$ be a non-empty set, and $P$ the power set of $\Theta$ and $A \in P$, Liu and Liu [1] defined the credibility measure as

$$Cr\{A\} = \frac{1}{2}(Pos\{A\} + Nec\{A\}) \quad (2.2.1)$$

Furthermore, for any $A \in P$ we have

$$Pos\{A\} = \min(2Cr\{A\}, 1) \quad (2.2.2)$$

Li and Liu [8] defined that a set function $Cr$ is a credibility measure if it holds the following

1. $Cr\{\Theta\} = 1$.
2. $Cr\{A\} \le Cr\{B\}$ whenever $A \subset B$
3. $Cr\{A\} + Cr\{A^C\} = 1$ for any event $A$.
4. $Cr\{\cup_i A_i\} = \sup_i Cr\{A_i\}$ for any events $\{A_i\}$ with $\sup_i Cr\{A_i\} < 0.5$.

Let $\xi$ be a fuzzy variable defined on the credibility space $(\Theta, P, Cr)$. Then its membership function is defined from the credibility measure by

$$\mu_\xi(x) = \min(2Cr\{\xi = x\}, 1) \quad (2.2.3)$$

### 2.3 Credibility Distribution

Liu [2] defined credibility distribution as $\Phi_\xi : R \to [0,1]$ of any fuzzy variable $\xi$ as

$$\Phi_\xi(x) = Cr\ \{\theta \in \Theta : \xi(\theta) \le x\}$$

That is the credibility that the fuzzy variable $\xi$ takes a value less than or equal to $x$. If the fuzzy variable $\xi$ is given by a membership function $\mu$, then its credibility distribution is determined by

$$\Phi_\xi(x) = \frac{1}{2}\{\sup_{y \le x} \mu(y) + 1 - \sup_{y > x} \mu(y)\}, \forall x \in R$$

### 2.4 Credibility Distribution of Triangular Fuzzy Variable

The credibility distribution of a triangular fuzzy variable $\beta = [a,b,c]$ is given by

$$\Phi_\beta(x) = Cr\{\beta \le x\} = \begin{cases} 0, & if\ x < a \\ \dfrac{x-a}{2(b-a)}, & if\ a \le x < b \\ \dfrac{x+c-2b}{2(c-b)}, & if\ b \le x < c \\ 1, & if\ x \ge c \end{cases} \quad (2.4.1)$$

### 2.5 Credibility Density Function

The credibility density function defined by Liu [3] as $\phi_\xi : R \to [0,\infty)$ of any fuzzy variable $\xi$ is a function such that

$$\Phi_\xi(x) = \int_{-\infty}^{x} \phi(y)\,dy,\ \forall x \in R.$$

### 2.6 Credibility Density Function of Triangular Fuzzy Variable,

The credibility density function of a triangular fuzzy variable $\beta = [a,b,c]$ is given by

$$\phi_\beta(x) = \begin{cases} f(x) = \dfrac{1}{2(b-a)}, if\ a \le x \le b \\ g(x) = \dfrac{1}{2(c-b)}, if\ b \le x \le c \\ 0, \quad otherwise \end{cases} \quad (2.6.1)$$

### 3. The Membership Function for Functions of Triangular Fuzzy Variable

Let $X = [a,b,c], (a,b,c > 0)$, be a triangular fuzzy variable. Let $F(X) = [F(a), F(b), F(c)]$, be the fuzzy variable of the function $F(X)$. Suppose the membership function of *X* is given by (2.1.1). The credibility distribution function is as given in (2.4.1) and the credibility density function is as given in (2.6.1).

Let $y = F(x)$ or, $x = \phi(y)$ or

$\left|\dfrac{dx}{dy}\right| = \dfrac{d}{dy}(\phi(y)) = m(y)$ say. Replacing *x* by $\phi(y)$ in $f(x)$ and $g(x)$, we obtain $f(x) = \phi_1(y)$ and $g(x) = \phi_2(y)$, say. Then the credibility distribution function of $F(X)$ is

$$\begin{cases} 0, & if\ x < F(a) \\ \Phi_1(x) = \int_{F(a)}^{x} \phi_1(y) m(y)\,dy, & if\ F(a) \le x < F(b) \\ \Phi_2(x) = 1 + \int_{F(c)}^{x} \phi_2(y) m(y)\,dy, & if\ F(b) \le x < F(c) \\ 1, & if\ x \ge F(c) \end{cases}$$

Thus the membership function of the fuzzy variable $F(X)$ is given by

$$\mu_{F(X)}(x) = \begin{cases} 2\Phi_1(x), & if\ F(a) \le x < F(b) \\ 2(1-\Phi_2(x)), & if\ F(b) \le x < F(c) \\ 0, & otherwise \end{cases}$$

### 3.1 Inverse of a Triangular Fuzzy Variable

Consider a triangular fuzzy variable $X = [a,b,c], (a,b,c > 0)$, with membership function given in (2.1.1) and let $X^{-1} = [c^{-1}, b^{-1}, a^{-1}]$. The credibility distribution function and the credibility density function are as given in (2.4.1) and (2.6.1) respectively.

Let $y = \dfrac{1}{x}$ so that. The credibility distribution of $X^{-1}$ is

distribution of $X^{-1}$ is

$$\Phi_{X^{-1}}(x) = \begin{cases} 0, & if\ x < c^{-1} \\ \int_{c^{-1}}^{x} \dfrac{1}{2(c-b)}\left(\dfrac{1}{y^2}\right)dy, & if\ c^{-1} \le x < b^{-1} \\ 1 + \int_{a^{-1}}^{x} \dfrac{1}{2(b-a)}\left(\dfrac{1}{y^2}\right)dy, & if\ b^{-1} \le x < a^{-1} \\ 1, & if\ x \ge a^{-1} \end{cases}$$

The membership function of $X^{-1}$ is

$$\mu_{X^{-1}}(x) = \begin{cases} \dfrac{cx-1}{x(c-b)} & if\ c^{-1} \le x < b^{-1} \\ \dfrac{1-ax}{x(b-a)}, & if\ b^{-1} \le x < a^{-1} \\ 0, & otherwise \end{cases}$$

### 3.2 Negative of a Triangular Fuzzy Variable

Consider a triangular fuzzy variable $X=[a,b,c],(a,b,c>0)$, with membership function as given in (2.1.1) and let $-X=[-c,-b,-a]$. The credibility distribution function and the credibility density function are as given in (2.4.1) and (2.6.1) respectively.

Let $y=-x$, so that $\left|\frac{dx}{dy}\right|=1$. The credibility distribution of $-X$ is

distribution of $-X$ is

$$\Phi_{-X}(x)=\begin{cases}0, & if\ x<-c\\ \frac{x+c}{2(c-b)}, & if -c\le x<-b\\ \frac{x-a+2b}{2(b-a)}, & if -b\le x<-a\\ 1, & if\ x\ge -a\end{cases}$$

Then the membership function of $-X$ is

$$\mu_{(-X)}(x)=\begin{cases}\frac{x+c}{c-b}, if -c\le x\le -b\\ \frac{x+a}{a-b}, if -b\le x\le -a\\ 0,\ otherwise\end{cases}$$

### 4.3 Square Root of a Triangular Fuzzy Variable

Consider a triangular fuzzy variable $X=[a,b,c],(a,b,c>0)$, with membership function is as given in (2.1.1), and let $\sqrt{X}=[\sqrt{a},\sqrt{b},\sqrt{c}]$. Accordingly the credibility distribution and the credibility density function are as given in (2.4.1) and (2.6.1) respectively.

Let $y=\sqrt{x}$ so that $\left|\frac{dx}{dy}\right|=2y$. The credibility distribution function for $\sqrt{X}$, is

$$\Phi_{\sqrt{X}}(x)=\begin{cases}0, & if\ x<\sqrt{a}\\ \frac{x^2-a}{2(b-a)}, & if\ \sqrt{a}\le x<\sqrt{b}\\ \frac{x^2+c-2b}{2(c-b)}, & if\ \sqrt{b}\le x<\sqrt{c}\\ 1, & if\ x\ge\sqrt{c}\end{cases}$$

Then the membership function of the fuzzy variable $\sqrt{X}$ is

$$\mu_{\sqrt{X}}(x)=\begin{cases}\frac{x^2-a}{b-a}, if\ \sqrt{a}\le x\le\sqrt{b}\\ \frac{c-x^2}{c-b}, if\ \sqrt{b}\le x\le\sqrt{c}\\ 0,\ otherwise\end{cases}$$

### 3.4 $n^{th}$ Root of a Triangular Fuzzy Variable

Consider a triangular fuzzy variable $X=[a,b,c],(a,b,c>0)$, with membership function as given in (2.1.1), and let $\sqrt[n]{X}=[\sqrt[n]{a},\sqrt[n]{b},\sqrt[n]{c}]$. Accordingly the credibility distribution and the credibility density function are as given in (2.4.1) and (2.6.1) respectively.

Let $y=\sqrt[n]{x}$ so that $\left|\frac{dx}{dy}\right|=ny^{n-1}$. The credibility distribution for $\sqrt[n]{X}$ is

$$\Phi_{\sqrt[n]{X}}(x)=\begin{cases}0, & if\ x<\sqrt[n]{a}\\ \frac{x^n-a}{2(b-a)}, & if\ \sqrt[n]{a}\le x<\sqrt[n]{b}\\ \frac{x^n+c-2b}{2(c-b)}, & if\ \sqrt[n]{b}\le x<\sqrt[n]{c}\\ 1, & if\ x\ge\sqrt[n]{c}\end{cases}$$

Then the membership function of $n^{th}$ root of the fuzzy variable *X* is

$$\mu_{\sqrt[n]{X}}(x)=\begin{cases}\frac{x^n-a}{b-a}, if\ \sqrt[n]{a}\le x<\sqrt[n]{b}\\ \frac{c-x^n}{c-b}, if\ \sqrt[n]{a}\le x<\sqrt[n]{b}\\ 0,\ otherwise\end{cases}$$

## 4. Arithmetic of Triangular Fuzzy Variables

### 4.1 Addition of Fuzzy Variable

Consider the fuzzy variables $X=[a,b,c]$ and $Y=[p,q,r]$. Suppose $Z=X+Y=[a+p, b+q,c+r]$ be the fuzzy number of $X+Y$. Let the membership function of $X$ and $Y$ be $\mu_X(x)$ and $\mu_Y(y)$, where,

$$\mu_X(x)=\begin{cases}L(x), if\ a\le x\le b\\ R(x), if\ b\le x\le c\\ 0,\ otherwise\end{cases} \quad (4.1.1)$$

$$\mu_Y(y)=\begin{cases}L(y), if\ p\le y\le q\\ R(y), if\ q\le y\le r\\ 0,\ otherwise\end{cases} \quad (4.1.2)$$

Let the credibility distribution of the triangular fuzzy variables (4.1.1) and (4.1.2) are

$$\Phi_X(x)=\begin{cases}0, & if\ x<a\\ \Phi_1(x), & if\ a\le x<b\\ \Phi_2(x), & if\ b\le x<c\\ 1, & if\ x\ge c\end{cases} \quad (4.1.3)$$

$$\Phi_Y(y)=\begin{cases}0, & if\ y<p\\ \Phi_1(y), & if\ p\le y<q\\ \Phi_2(y), & if\ q\le y<r\\ 1, & if\ y\ge c\end{cases} \quad (4.1.4)$$

Let the credibility density function of the credibility distribution function (4.1.3) is

$$\phi_X(x)=\begin{cases}f(x), & if\ a\le x<b\\ g(x), & if\ b\le x<c\end{cases} \quad (4.1.5)$$

We start with equating $\Phi_1(x)$ with $\Phi_1(y)$ and $\Phi_2(x)$ with $\Phi_2(y)$. And so, we obtain $y=\psi_1(x)$ and $y=\psi_2(x)$ respectively. Let $z=x+y$, so we have $z=x+\psi_1(x)$ and $z=x+\psi_2(x)$, so that $x=\omega_1(z)$ and $x=\omega_2(z)$, say. The credibility density function (4.1.5) should be transformed in terms of the function of *z* by replacing *x* by $\omega_1(z)$ and $\omega_2(z)$ in $f(x)$ and $g(x)$, so that $f(x)=\chi_1(z)$ and $g(x)=\chi_2(z)$, say.

Now let, $\left|\frac{dx}{dz}\right|=\left|\frac{d}{dz}(\omega_1(z))\right|=m_1(z)$, and. $\left|\frac{dx}{dz}\right|=\left|\frac{d}{dz}(\omega_2(z))\right|=m_2(z)$

The credibility distribution function of $X+Y$ is

$$\Phi_{X+Y}(x)=\begin{cases}0, & if\ x<a+p\\ \int_{a+p}^{x}\chi_1(z)m_1(z)dz, & if\ a+p\le x<b+q\\ 1+\int_{c+r}^{x}\chi_2(z)m_2(z)dz, & if\ b+q\le x<c+r\\ 1, & if\ x\ge c+r\end{cases}$$

Thus the membership function of addition of the fuzzy variables can be easily found from the credibility distribution function $\Phi_{X+Y}(x)$.

### 4.2 Subtraction of Fuzzy Variable

Consider the triangular fuzzy variables $X=[a,b,c]$ and $Y=[p,q,r]$. Suppose $Z=X-Y$, then the membership function of $Z=X-Y$ is given by $Z=X+(-Y)$.

### 4.3 Multiplication of Fuzzy Variables

Consider the triangular fuzzy variables

$X=[a,b,c],(a,b,c>0)$

and

$Y=[p,q,r],(p,q,r>0)$.

Suppose $Z=X.Y=[a.p,b.q,c.r]$ be the fuzzy variable of $X.Y$. Let the membership function of $X$ and $Y$ be $\mu_X(x)$ and $\mu_Y(y)$ as mentioned in (4.1.1) and (4.1.2) respectively. Let the credibility distribution of (4.1.1) and (4.1.2) are as mentioned in (4.1.3) and (4.1.4) respectively. Let the credibility density function of the credibility distribution function (4.1.3) is (4.1.5).

We start with equating $\Phi_1(x)$ with $\Phi_1(y)$ and $\Phi_2(x)$ with $\Phi_2(y)$. And so, we obtain $y=\psi_1(x)$ and $y=\psi_2(x)$ respectively. Let $z=x.y$, so we have $z=x\psi_1(x)$ and $z=x\psi_2(x)$, so that $x=\omega_1(z)$ and $x=\omega_2(z)$, say. The credibility density function (4.1.5) should be transformed in terms of the function of *z* by replacing *x* by $\omega_1(z)$ and $\omega_2(z)$ in $f(x)$ and $g(x)$, so that $f(x)=\chi_1(z)$ and $g(x)=\chi_2(z)$, say.

Now let, $\left|\frac{dx}{dz}\right|=\left|\frac{d}{dz}(\omega_1(z))\right|=m_1(z)$ and. $\left|\frac{dx}{dz}\right|=\left|\frac{d}{dz}(\omega_2(z))\right|=m_2(z)$

The credibility distribution function of $X.Y$, is given by

$$\Phi_{X.Y}(x)=\begin{cases}0, & if\ x<a.p\\ \int_{a.p}^{x}\chi_1(z)m_1(z)dz, & if\ a.p\le x<b.q\\ 1+\int_{c..r}^{x}\chi_2(z)m_2(z)dz & if\ b.q\le x<c.r\\ 1, & if\ x\ge c.r\end{cases}$$

Thus the membership function of multiplication of the fuzzy variables can be easily found from the credibility distribution function $\Phi_{X.Y}(x)$.

### 4.4 Division of Fuzzy Variables

Consider the triangular fuzzy variables

$X=[a,b,c],(a,b,c>0)$

and

$Y=[p,q,r],(p,q,r>0)$.

Suppose $Z=\frac{X}{Y}$ then membership function of $Z=\frac{X}{Y}$ is given by $Z=X.Y^{-1}$.

## 5. Numerical Examples

**Example**

Consider two triangular fuzzy variables $X=[12,16,28]$ and $Y=[5,6,8]$ with membership function as given below, and let. $Z=\frac{X}{Y}=\left[\frac{3}{2},\frac{8}{3},\frac{28}{5}\right]$.

$$\mu_X(x)=\begin{cases}\frac{x-12}{4}, & if\ 12\le x\le 16\\ \frac{84-3x}{36}, & if\ 16\le x\le 28\\ 0, & otherwise\end{cases}$$

$$\mu_Y(y)=\begin{cases}y-5, & if\ 5\le y\le 6\\ \frac{8-y}{2}, & if\ 6\le y\le 8\\ 0, & otherwise\end{cases}$$

The credibility distribution function and credibility density function of $\mu_X(x)$ are as below respectively.

$$\Phi_X(x)=\begin{cases}0, & if\ x<12\\ \frac{x-12}{8}, & if\ 12\le x<16\\ \frac{x-4}{24}, & if\ 16\le x<28\\ 1, & if\ x\ge 28\end{cases}$$

$$\phi_X(z)=\begin{cases}\chi_1(z)=\frac{1}{8}, & if\ 12\le z<16\\ \chi_2(z)=\frac{1}{24}, & if\ 16\le z<28\end{cases}$$

The credibility distribution function of $Y^{-1}$ is found to be

$$\Phi_{Y^{-1}}(y)=\begin{cases}0, & if\ y<8^{-1}\\ \frac{8y-1}{4y}, & if\ 8^{-1}\le y<6^{-1}\\ \frac{7y-1}{2y}, & if\ 6^{-1}\le y<5^{-1}\\ 1, & if\ y\ge 5^{-1}\end{cases}$$

Now equating the credibility distribution functions of $X$ and $Y^{-1}$, we have

$\left|\frac{dx}{dz}\right|=\frac{56}{(z+2)^2}=m_1(z)$ and similarly.

$\left|\frac{dx}{dz}\right|=\frac{1056}{(z+12)^2}=m_2(z)$ Thus the credibility distribution function of $Z=X.Y^{-1}$ is of the form

$$\Phi_{X.Y^{-1}}(x)=\begin{cases}0, & if\ x<3/2\\ \frac{2x-3}{x+2}, & if\ 3/2\le x<8/3\\ \frac{7x-4}{2(x+12)}, & if\ 8/3\le x<28/5\\ 1, & if\ x\ge 28/5\end{cases}$$

Thus the membership function of the fuzzy variable $X.Y^{-1}$ is,

$$\mu_{X.Y^{-1}}(x)=\begin{cases}\frac{4x-6}{x+2}, & if\ 3/2\le x\le 8/3\\ \frac{28-5x}{x+12}, & if\ 8/3\le x\le 28/5\\ 0, & otherwise\end{cases}$$

**Example**

Consider two triangular fuzzy variables $X=[7,14,19]$ and $Y=[3,5,10]$ with membership function as given below, and let.
$Z=X-Y=[-3,9,16]$.

$$\mu_X(x)=\begin{cases}\frac{x-7}{7}, & if\ 7\le x\le 14\\ \frac{19-x}{5}, & if\ 14\le x\le 19\\ 0, & otherwise\end{cases}$$

$$\mu_Y(y)=\begin{cases}\frac{y-3}{2}, & if\ 3\le y\le 5\\ \frac{10-y}{2}, & if\ 5\le y\le 10\\ 0, & otherwise\end{cases}$$

The credibility distribution function and credibility density function of $\mu_X(x)$ are as below respectively.

$$\Phi_X(x)=\begin{cases}0, & if\ x<7\\ \frac{x-7}{8}, & if\ 7\le x<14\\ \frac{x-9}{10}, & if\ 14\le x<19\\ 1, & if\ x\ge 19\end{cases}$$

$$\phi_X(z)=\begin{cases}\chi_1(z)=\frac{1}{8}, & if\ 7\le z<14\\ \chi_2(z)=\frac{1}{10}, & if\ 14\le z<19\end{cases}$$

The credibility distribution function of $-Y$ is found to be

$$\Phi_{-Y}(y)=\begin{cases}0, & if\ \ y<-10\\ \dfrac{y-10}{10}, & if\ \ -10\le y<-5\\ \dfrac{y+7}{4}, & if\ \ -5\le y<-3\\ 1, & if\ \ y\ge -3\end{cases}$$

Now equating the credibility distribution functions of $X$ and $-Y$, we have

$\left|\dfrac{dx}{dz}\right|=\dfrac{7}{12}=m_1(z)$ and similarly.

$\left|\dfrac{dx}{dz}\right|=\dfrac{5}{7}=m_2(z)$ Thus the credibility distribution function of $Z=X+(-Y)$ is of the form

$$\Phi_{X+(-Y)}(x)=\begin{cases}0, & if\ \ x<-3\\ \dfrac{x+3}{24}, & if\ \ -3\le x<9\\ \dfrac{x-2}{14}, & if\ \ 9\le x<16\\ 1, & if\ \ x\ge 16\end{cases}$$

Thus the membership function of the fuzzy variable $X+(-Y)$ is

$$\mu_{X+(-Y)}(x)=\begin{cases}\dfrac{x+3}{12}, & if\ \ -3\le x\le 9\\ \dfrac{16-x}{7}, & if\ \ 9\le x\le 16\\ 0, & otherwise\end{cases}$$

**Example**

Consider two triangular fuzzy variables $X=[2,3,5]$ and $Y=[3,5,6]$ with membership function as given below, and let

$Z=X.Y=[6,15,30]$

$$\mu_X(x)=\begin{cases}x-2, & if\ \ 2\le x\le 3\\ \dfrac{5-x}{2}, & if\ \ 3\le x\le 5\\ 0, & otherwise\end{cases}$$

$$\mu_Y(y)=\begin{cases}\dfrac{y-3}{2}, & if\ \ 3\le y\le 5\\ 6-y, & if\ \ 5\le y\le 6\\ 0, & otherwise\end{cases}$$

The credibility distribution functions of $\mu_X(x)$ and $\mu_Y(y)$ are as below respectively.

$$\Phi_X(x)=\begin{cases}0, & if\ \ x<2\\ \dfrac{x-2}{2}, & if\ \ 2\le x<3\\ \dfrac{x-1}{4}, & if\ \ 3\le x<5\\ 1, & if\ \ x\ge 5\end{cases}$$

$$\Phi_Y(y)=\begin{cases}0, & if\ \ y<3\\ \dfrac{y-3}{4}, & if\ \ 3\le y<5\\ \dfrac{y-4}{2}, & if\ \ 5\le y<6\\ 1, & if\ \ y\ge 6\end{cases}$$

The credibility density function of the credibility distribution function $\Phi_X(x)$

$$\phi_X(z)=\begin{cases}\chi_1(z)=\dfrac{1}{2}, & if\ \ 2\le z<3\\ \chi_2(z)=\dfrac{1}{4}, & if\ \ 3\le z<5\end{cases}$$

Now equating the credibility distribution functions of $X$ and $Y$, we have

$\left|\dfrac{dx}{dz}\right|=\dfrac{1}{\sqrt{1+8z}}=m_1(z)$ and similarly.

$\left|\dfrac{dx}{dz}\right|=\dfrac{2}{\sqrt{49+8z}}=m_2(z)$ Thus the credibility distribution function of $Z=X.Y$ is of the form

$$\Phi_{X.Y}(x)=\begin{cases}0, & if\ \ x<6\\ \dfrac{-7+\sqrt{1+8x}}{8}, & if\ \ 6\le x<15\\ \dfrac{\sqrt{49+8x}-9}{8}, & if\ \ 15\le x<30\\ 1, & if\ \ x\ge 30\end{cases}$$

Thus the membership function of the fuzzy variable $X.Y$ is

$$\mu_{X.Y}(x)=\begin{cases}\dfrac{-7+\sqrt{1+8x}}{4}, & if\ \ 6\le x\le 15\\ \dfrac{\sqrt{49+8x}-17}{4}, & if\ \ 15\le x\le 30\\ 0, & otherwise\end{cases}$$

These examples have been quoted from the book by Bojadziev and Bojadziev [6], the result tallies with it, where it has been solved by the method of $\alpha$ -cuts.

## 6. Conclusion

Here we have tried to develop an alternative method of finding the membership function for functions of triangular fuzzy variable from the concept of credibility theory. A new method for computation of basic arithmetical operations of fuzzy variable is forwarded. This method validity has been tested evaluating some examples which were quoted from [6], where they were solved by the method of alpha-cuts and are compared with the results obtained here. The square root of triangular fuzzy variable found by our proposed method tallies with the one defined by Chou [2]. A generalised membership function for the $n^{th}$ root of triangular fuzzy variable has been forwarded. The method can be applied in solving equations with fuzzy coefficients. Further the proposed method can be applied to the uncertainty analysis of dispersion models and engineering problems which can be taken for further research.

## 7. Acknowledgement

The authors would like to offer their thanks and gratitude to Dr. D. Datta, Distinguished Scientist, BARC, Mumbai, India for his comments and suggestion which helped in improving the manuscript both from the point of quality and clarity.

## References

1. B. Liu and Y. K. Liu, "Expected Value of Fuzzy Variable and Fuzzy Expected Value Models", IEEE Transactions on Fuzzy Systems, Vol. 10, No. 4, 2002, pp. 445-450.
2. B. Liu, "Theory and Practice of Uncertain Programming", Physica-Verlag, Heidelberg, 2002.
3. B. Liu, "Uncertainty Theory", 3rd Edition, 2008, http://orsc.edu.cn/liu/ut.pdf
4. Chien-Chang Chou, "Cube Roots of Triangular Fuzzy Number and its Application to the Fuzzy System", Journal of Beijing Jiaotong University. Vol. 33, Nos. 2, 2009, pp. 40-43.
5. Chien-Chang Chou, "The Square Roots of Triangular Fuzzy Number", ICIC Express Letters. Vol. 3, Nos. 2, 2009, pp. 207-212.
6. G. Bojadziev and M. Bojadziev, Fuzzy Sets, Fuzzy Logic, Applications. World Scientific Publishing Co. Pte. Ltd, Singapore, 1995.
7. L. Zadeh, "Fuzzy Sets as a basis for a theory of Possibility", Fuzzy Sets and Systems, Vol. 1, 1978, pp-3-28.
8. X. Li, and B. Liu, "A Sufficient and Necessary Condition for Credibility Measures", Int. Journal of Uncertainty, Fuzziness & Knowledge-Based Systems, Vol. 14, No. 5, 2006, pp-527-535.

# SRESA JOURNAL SUBSCRIPTION FORM

## Subscriber Information (Individual)

| Title | First Name | Middle Name | Last Name |
|---|---|---|---|
| _____ | _____ | _____ | _____ |

| Street Address Line 1 | Street Address line 2 |
|---|---|
| _____ | _____ |

| City | State/Province | Postal Code | Country |
|---|---|---|---|
| _____ | _____ | _____ | _____ |

| Work Phone | Home Phone | E-mail address |
|---|---|---|
| _____ | _____ | _____ |

## Subscriber Information (Institution)

Name of Institution/ Library _____

Name and Designation of Authority for Correspondence _____

Address of the Institution/Library _____

## Subscription Rates

| | Subscription Quantity | Rate | Total |
|---|---|---|---|
| Annual Subscription (in India) | _____ | Rs. 15, 000 | _____ |
| (Abroad) | _____ | $ 500 | _____ |
| | _____ | | _____ |
| | _____ | | _____ |

**Payment mode (please mark)**

Cheque ☐ Credit Card ☐ Master Card ☐ Visa ☐ Online Banking ☐ Cash ☐ De mand Draft ☐

Credit card Number _____

Credit Card Holders Name _____

Credit Card Holde _____

*SRESA's International Journal of*

# Life Cycle Reliability and Safety Engineering

## Contents

Vol.2 Issue No.4 October–December 2013 ISSN – 2250 0820

**Guest Editorial** ..... iv

**A Comparison of Model-Form Uncertainty Quantification Techniques for Thermal-Structural Modeling**
*C. Corey Fischer and Ramana V. Grandhi* ..... 1

**Long-term Assessment of Health Risk under Uncertain Environment of Contaminated Sites using Spatiotemporal Modelling**
*Abhirup Bandyopadhyay and Samarjit Kar* ..... 15

**Reliability Evaluation of Weibull and Exponentiated Weibull Distribution Estimates for Wind Speed Data through Uncertainty Analysis**
*D. Datta and Debanshee Datta* ..... 28

**Review on Prognostics and Health Management of Digital Systems and its Application to Nuclear Plants**
*S.V. Shrikhande, P.V. Varde and D. Datta* ..... 35

**Fuzzy Arithmetic form Credibility Theory**
*Rituparna Chutia[1] and Tapan Kumar Chutia* ..... 69